METAL-ORGANIC FRAMEWORK AND COVALENT ORGANIC FRAMEWORK MEMBRANES FOR MOLECULAR SEPARATIONS

by

Zhiqin Qiang

A Dissertation Submitted in

Partial Fulfillment of the

Requirements for the Degree of

Doctor of Philosophy

in Engineering

at

The University of Wisconsin-Milwaukee

May 2024

ABSTRACT

METAL-ORGANIC FRAMEWORK AND COVALENT ORGANIC FRAMEWORK MEMBRANES FOR MOLECULAR SEPARATIONS

by

Zhiqin Qiang

The University of Wisconsin-Milwaukee, 2024
Under the Supervision of Professor Xiaoli Ma

Olefin/paraffin separation as a typical example of gas separation has attracted a lot of research interest because of the high demand for high-purity olefins in the petrochemical industry. However, the physical and chemical similarities of olefins and paraffins make them difficult to separate. It is also critical to separate organic liquid mixtures in the petroleum industry since the consumption of organic solvents is increasing as industries develop, and the problem of recovering and reusing organic solvents is becoming more prevalent. Distillation is the most commonly used separation technology in the industry, but it is an energy-intensive process. As an alternative separation process, membrane technology has become a reliable, energy-efficient, and techno-economically attractive option for separation and purification, especially in chemical and petrochemical industries. Over the past decade, metal-organic frameworks (MOFs) and covalent organic frameworks (COFs) have emerged as appealing materials for molecular separation due to their porous structure and interconnected transport channels.

Zeolitic imidazolate frameworks (ZIF) are a subclass of MOFs. ZIF membranes featuring small aperture sizes have shown promising performance for olefin/paraffin separation. However, the fabrication of thin, defect-free polycrystalline ZIF membranes is still challenging. Therefore,

one objective of this research is to prepare high-quality polycrystalline ZIF membranes on low-cost macroporous ceramic supports with high olefin/paraffin selectivities using vapor-phase processing, which combines atomic layer deposition (ALD) and ligand vapor treatment. The second objective is to investigate the properties of the resultant ZIF membranes for separating 1,3-butadiene from C4 hydrocarbon mixtures that include 1,3-butadiene, butenes, and butanes.

COFs, a novel class of crystalline porous polymers, have attracted increasing interest due to their unique characteristics, abundant open sites, and interpenetrating channels and cages. Three-dimensional COFs (3D COFs) usually have the characteristics of interpenetration, so their effective pore size can be reduced, thereby achieving more effective separation compared to two-dimensional COFs (2D COFs). It was also reported that COFs are stable in organic solvents owing to the robust covalent linkages (e.g., imine, hydrazine, and ketoenamine) in the frameworks, making them promising porous materials for the preparation of organic solvent nanofiltration (OSN) membranes. Thus, another objective of this research is to prepare 3D COF membranes (e.g., COF-300) that can effectively remove various dyes in organic solvents (e.g., Rose Bengal, Methyl Orange) and to investigate the relationships between interfacial synthesis, membrane structure, and OSN performance.

This dissertation entails (1) the synthesis and characterization of ZIF membranes by a vapor-phase seeding method and the study of their olefin/paraffin separation properties, (2) the fabrication of ZIF membranes by all-vapor-phase ligand-induced permselectivation (LIPS) method and secondary growth method for 1,3-butadiene separation from C4 hydrocarbons, (3) the review on the fabrication methods and application fields of 3D COF membranes, and (4) the synthesis

and characterization of 3D COF membranes using interfacial polymerization (IP) method and preliminary mechanistic investigation of the solvent transport properties.

TABLE OF CONTENTS

LIST OF FIGURES

LIST OF TABLES

ACKNOWLEDGMENTS

As I complete my Ph.D. journey, I want to express my deep gratitude to my advisor, Dr. Xiaoli Ma, for his unwavering support and encouragement throughout my life in the United States. Dr. Ma not only provided me with a broad perspective to guide my research, but also gave me detailed instructions for conducting experiments. The knowledge and experience I have gained under his guidance will undoubtedly shape my future endeavors and contribute to my lifelong learning.

I would also like to thank Dr. Nidal H Abu-Zahra, Dr. Benjamin C Church, Dr. Yin Wang, and Dr. Laodong Guo for their invaluable contributions as members of my dissertation committee, which greatly enhanced the quality of my research. I am especially grateful to Dr. Heather Owen, Dr. Steven Hardcastle, and the entities within the School of Freshwater Sciences, Department of Biological Sciences, Advanced Analysis Facility, Water Technology Accelerator, and UWM Innovation Accelerator for Advanced and Applied Analytical Chemistry at UWM for their indispensable assistance in my research.

I would like to express my heartfelt appreciation to my friends and labmates in Dr. Ma's research group and the Department of Materials Science & Engineering, including Dr. Junwei Wang, Rahul Sampat Khandge, Miguel Angel Jaimes, Zihao Yi, Ho Kuan Yu, Hanlun Gao, and Dr. Xiaopeng Min from Dr. Yin Wang's research group. The shared experiences, both challenging and rewarding, have truly enriched my academic journey.

I am also grateful for the financial support I have received from the Research Growth Initiative (RGI) Program at the University of Wisconsin-Milwaukee (UWM), Department of Defense (DoD)

Strategic Environmental Research and Development Program, ACS PRF Research Grant Program, and the College of Engineering and Applied Science.

Special acknowledgment goes to the Clean Energy Clean Water program at UWM for supporting my internship at A.O. Smith Corporation. This invaluable opportunity has broadened my practical understanding and allowed me to witness firsthand the intersection of academic knowledge and real-world applications. I am grateful to the dedicated professionals at A.O. Smith Corporation, especially Senior Staff Engineer Haifeng Zhang, whose mentorship has been instrumental in shaping my perspective.

Lastly, and most importantly, I want to express my heartfelt thanks to everyone who has supported me throughout my journey. I am deeply grateful for all the love, care, and encouragement that I have received from my family and friends, without whom this achievement would not have been possible. A special and enduring thanks go to my husband, Zihao Yi, who has consistently provided unwavering support and taken care of me throughout the four years and beyond. His steadfast encouragement has been my pillar, and I am profoundly appreciative of his enduring commitment.

Best wishes to all!

Zhiqin Qiang

University of Wisconsin-Milwaukee

May 2024

Chapter 1 Introduction and Research Objectives

1.1 Olefin/Paraffin Separation

Olefins have long been one of the most important chemical raw materials because of the broad application of their downstream products, such as polyethylene, polypropylene, and poly(vinyl chloride) [1]. Among them, ethylene and propylene account for more than 50% of the global consumption of basic chemicals used in industries such as packaging, construction, textiles, consumer products, transportation, etc [2]. In 2021, ethylene and propylene consumption totaled about 172 million tons and 130 million tons, respectively [2]. The downstream of the olefin industry requires high-purity (≥ 95 mol%) olefins, so highly efficient olefin/paraffin separation is in high demand in the petrochemical industry. However, it is challenging to separate olefins from paraffin with the same carbon number because of the similarities in physical and chemical properties, such as boiling point: C_2H_4 (-102.4℃), C_2H_6 (-88.5 ℃), C_3H_6 (-47.7 ℃), and C_3H_8 (-42.2 ℃) [3, 4].

Cryogenic distillation, which demands low temperature and high pressure, is an energy-insensitive process currently used for olefin/paraffin separation [5]. Adsorption and absorption are two alternative separation techniques that are potentially more energy-efficient than distillation. Compared to adsorption, membrane process does not require desorption to regenerate the adsorbent or obtain purified olefins, a step that comes at an unavoidable energy expense [6, 7]. Membrane technology, an environmentally friendly process, has the potential to save up to 90% energy when used as an alternative to the distillation method for olefin/paraffin separations [8]. The benefits of using membranes for gas separation also include the possibility of process

intensification, which significantly reduces production costs, equipment size, energy consumption, and waste generation [9].

A variety of membrane materials, such as polymer membranes, facilitated transport membranes, and carbon molecular sieve (CMS) membranes, have been investigated for olefin/paraffin separation [10, 11]. Although polymeric membranes are dominating the market for the separation of industrial non-condensable gases, they have shown a trade-off between permeability and selectivity for olefin/paraffin separations and experienced the plasticization issue under the high-pressure feed of hydrocarbons [12, 13]. Facilitated transport membranes have higher olefin selectivity than polymeric membranes because of the preferential interactions between olefins and carriers [14]. However, the long-term stability of carrier agents still hinders the commercialization of facilitated transport membranes [15]. Microporous inorganic membranes, such as CMS membranes, zeolites, and metal-organic frameworks (MOF), have the potential to overcome the permeability vs. selectivity trade-off relationship of currently available polymeric membranes due to their well-defined and controllable pore structure [16, 17].

1.2 ZIF Membranes for Olefin/Paraffin Separation

Metal-organic frameworks (MOF) possess a high porosity and interconnected transport channels constructed by metal ions/clusters and organic ligands. Zeolitic imidazolate frameworks (ZIFs), a subclass of MOFs, are composed of transition-metal ions bridged by imidazolate linkers in a manner similar to the Si-O bond in zeolites. They have emerged as promising candidates for gas separation, particularly for separating similar-sized molecules, such as xylene isomers and olefin/paraffin gas pairs [6, 7, 18]. Among the ZIFs discovered, ZIF-8, first reported by Chen et al.[19] and Yaghi et al.[20], is composed of Zn(II) and 2-methylimidazole ligands, which form a

zeolite-like structure with tetrahedral cages of approximately 11.6 Å in diameter, as shown in **Figure 1.1**. The unique properties of ZIF-8, such as its thermal and chemical stability, high surface area, sub-nanometer pore size, enhanced stability compared to other MOFs, as well as the low cost of the easily accessible raw materials used for synthesis, make it a promising material for a range of applications including gas storage and separation [21, 22], catalysis [23], drug delivery [24], and sensing [25].

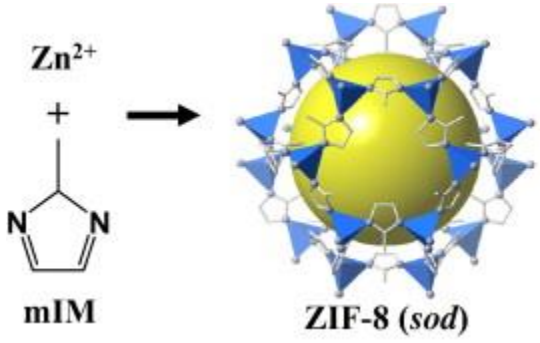

Figure 1.1 Crystal structure of ZIF-8: Zn (polyhedral), N (sphere), and C (line) (reproduced from ref. [26] with permission from Elsevier, Copyright 2015).

The pore size of ZIF-8 was first determined by XRD in 2006 to be 3.4 Å [20], but Li et al. revealed that both propylene (van der Waals diameters 4.03 Å) and propane (van der Waals diameters 4.16 Å) could enter the pores of ZIF-8, indicating the potential for the separation of propylene/propane [27]. Some computational and experimental studies have also confirmed this unexpected molecular sieve property, implying that the effective aperture size of ZIF-8 should be in the range of 4.0-4.2 Å [28-30]. Lai and co-workers first reported the exceptional propylene/propane separation performance of continuous polycrystalline ZIF-8 membranes, which exhibited a propylene permeability of 200 barrers and propylene/propane separation factors of up to 50 [31, 32]. Other ZIF-8 membranes with a propylene/propane selectivity of about 40 and 55

have been synthesized using microwave-assisted seeding and in situ methods, respectively [33].The separation factor of ZIF-8 membranes was then improved to around 90 after a carefully optimized activation process and defect elimination [34]. However, increasing selectivity is often accompanied by a decrease in permeance because a relatively thick membrane is required to minimize defects, which inevitably reduces membrane permeance. Recently, Ma et al. and Lai et al. developed several novel methods for fabricating ZIF-8 membranes with excellent C_3H_6/C_3H_8 separation (selectivity above 100) and high C_3H_6 permeance (higher than 170 GPU), including atomic layer deposition (ALD) and aqueously cathodic deposition (ACD) [16, 35]. Hence, developing novel ZIF-8 membrane fabrication methods remains critical for the improvement of separation performance and the scale-up of ZIF membranes for industrial implementation.

1.3 Organic Solvent Separation

The consumption of organic solvents is on the rise with the continued growth of industries, and the issue of organic solvent recovery and reuse is gaining prominence [36]. Organic solvents have long played a pivotal role in the pharmaceutical, oil, and chemical industries, particularly in the production of drugs, edible oils, and chemical products [37, 38]. However, the prevailing approach for separating these products from solvents involves energy-intensive phase-changing processes like distillation and evaporation [8, 39]. Hence, there is a critical need for innovative technologies that can surpass these conventional separation methods. Moreover, the significant disparity in molecular sizes between solutes and solvents, with solutes typically being over ten times larger [40], allows for a size exclusion mechanism. Membranes can exploit this mechanism to selectively reject solutes while permitting solvents to pass through, resulting in solute enrichment and solvent purification. Just as in gas separation, one of the primary challenges in

OSN research lies in the discovery and/or engineering of membrane materials that offer both high solvent permeability and solute rejection. Additionally, membranes used in OSN must exhibit chemical and structural stability in organic solvent environments, conditions that pose a formidable challenge for conventional polymer membranes.

1.4 COF Membranes for Organic Solvent Separation

Covalent organic frameworks (COFs) have emerged as a new class of crystalline porous materials, encompassing both two-dimensional (2D) and three-dimensional (3D) structures. These frameworks are constructed by linking organic building blocks through covalent bonds, attracting extensive interest in various fields. The versatility of COFs, rooted in their structural diversity, expansive surface area, tunable pore size, and exceptional thermal stability, has led to their application in the development of membranes. These COF membranes may offer a solution to the trade-off between selectivity and permeability. It was found that COFs are stable in organic solvents and suitable for use as materials for preparing OSN membranes.

In contrast to 2D COFs, 3D COFs represented by COF-300 with a small pore size of less than 1 nm are fully covalent and more sensitive to the synthesis conditions [41]. The interpenetrations of 3D COFs lead to shrunk channels, allowing them to have highly porous structures and smaller pore sizes. This distinctive attribute holds great potential for OSN, where the separation of small molecular weight solutes and solvents is a critical challenge. It is worth noting that some 2D and 3D COFs membranes can be synthesized on some polymeric or low-cost substrates by the facile and scalable interfacial polymerization method in a short reaction time, which greatly reduces costs and increases the possibility of commercialization compared to other membrane materials [42-46].

It is essential to highlight that while 2D COF membranes with a molecular weight cutoff (MWCO) in the range of 800-1200 g/mol have garnered considerable attention in the context of organic solvent nanofiltration (OSN) [47, 48], research on 3D COF-based OSN membranes is still in its nascent stages. In this context, the distinctive features of 3D COF membranes present an exciting avenue for further exploration and research.

1.5 Research Objectives and Outline

In summary, the reliable fabrication of ZIF membranes on low-cost macroporous supports with minimal defects and high separation performance remains challenging when using solution-based membrane fabrication methods. Additionally, the use of solvents makes the membrane fabrication process more expensive and unfriendly to the environment. Currently, only a handful of ZIF-8 membranes have been successfully produced using the less costly vapor-phase synthesis method, and even fewer have demonstrated the combination of high permeance, superior separation factor, and good reproducibility concurrently. To date, vapor-phase synthesis has not been extended to macroporous ceramic supports, which could lower the membrane cost. Therefore, there is a need to develop more efficient and reliable synthesis methods to produce low-cost macroporous supported-ZIF membranes that exhibit enhanced performance.

Moreover, the exploration of membranes for the purification of 1,3-butadiene is a relatively underexplored area, with only a limited number of studies primarily focusing on polymer-based membranes. These membranes exhibited relatively low selectivities due to the similar molecular sizes and physical properties of C4 compounds. There is a significant gap in the literature as membranes capable of effectively separating 1,3-butadiene from complex, practically relevant multi-component mixtures resembling C4 crude compositions have not been reported. Hence,

employing ZIF-8 membranes for the purification of 1,3-butadiene from complex C4 hydrocarbon mixtures represents a novel and environmentally friendly approach. This innovative method holds promise for addressing the challenges associated with achieving efficient and eco-friendly 1,3-butadiene purification from complex industrial feedstocks.

3D COFs represent a promising group of emerging membrane materials due to their desirable structural features, including tunable pore size, high surface area, and good chemical stability. Compared to conventional polymer membranes, 3D COF membranes have been shown to be more stable in solvents, suggesting their potential for use in organic solvent nanofiltration (OSN) processes. Despite the high potential, the study of 3D COF membranes for OSN is still in its early stages, and further research is needed to fully understand their structure-properties relationships.

The overall objective of this research is to synthesize a series of MOF and COF membranes with high performance for gas separation and liquid separation applications and understand the membrane synthesis-structure-separation property relationships. Our objectives encompass the creation of high-performance ZIF membranes on macroporous ceramic supports, facilitating the efficient separation of olefins and paraffins, while unraveling the influence of atomic layer deposition (ALD) on gas permeance and separation factor. Simultaneously, we seek to synthesize a group of 3D COF membranes through interfacial polymerization, designed for the removal of diverse dyes from organic solvents. This phase involves a comprehensive exploration of crucial synthetic parameters to enhance the membrane's performance in organic solvent nanofiltration (OSN) and to gain insights into the underlying solvent transport mechanisms.

To meet these research objectives, our work is organized into four tasks, as outlined below:

Task 1: Fabrication of zeolitic imidazolate framework membranes on macroporous ceramic supports based on vapor phase synthesis for the olefin and paraffin separation (Chapter 2). In this chapter, we focused on the synthesis and characterization of ZIF membranes prepared on macroporous ceramic supports via the vapor-phase seeding method. The impact of ALD cycle numbers and pulse times on the separation performance of olefin and paraffin was investigated. Furthermore, the synthesis of various ZIF membranes with ZIF-8 seed layers produced through the vapor-phase seeding approach was conducted. We systematically investigated the pulse time of precursors and ALD temperature, aiming to optimize the performance of these membranes for enhanced gas separation capabilities. In addition, the vapor-phase processing was improved and optimized to achieve the formation of ZIF membranes on macroporous supports without the need for secondary growth.

Task 2: ZIF membranes for the effective separation of 1,3-butadiene from C4 mixtures (1,3-butadiene, 1-butene, n-butane, and isobutene) (Chapter 3). Task 2 focused on the investigation of the C4 gas separation performance using different ZIF membranes synthesized under various methods, such as secondary growth and ligand-induced permselectivation (LIPS) methods. The C4 separation performance was thoroughly examined, comparing the effectiveness of membranes synthesized under different methods. To gain insights into the separation mechanism, gas permeation models were employed to calculate the diffusivities of C4 hydrocarbons through the membranes. Furthermore, the chapter explored the impact of varying compositions of C4 hydrocarbon mixtures and various operating conditions on membrane performance and stability.

Task 3: 3D COFs and membranes: structure, fabrication methods, and applications (Chapter 4). Task 3 provided a comprehensive literature review on the fabrication methods and

applications of 3D COF membranes. This encompassed an exploration of various aspects, including the structure of these membranes, fabrication methods, and their diverse application fields. The review discussed different types of 3D COF membranes, such as pure 3D COF membranes, 3D COF-based mixed matrix membranes (MMMs), and free-standing COF films. Furthermore, it delved into the wide-ranging applications of 3D COF-based membranes, specifically in organic solvent nanofiltration, gas separation, water filtration, and fuel cells.

Task 4: 3D covalent organic framework membranes: interfacial synthesis and organic solvent nanofiltration properties (Chapter 5). Task 4 is dedicated to the exploration of 3D covalent organic framework (COF) membranes with a specific focus on their development and characterization for achieving high organic solvent nanofiltration (OSN) permeance. These membranes were synthesized using the interfacial polymerization (IP) method. The impact of various factors, including solvents, catalysts, reaction concentration, and time, on both the structural characteristics of the membranes and their performance in organic solvent nanofiltration were evaluated. Through a systematic investigation, we aim to understand the relationships between synthesis parameters and membrane properties and optimize the interfacial synthesis process for enhanced OSN performance. This task serves as a crucial step towards advancing the understanding and practical application of 3D COF membranes in organic solvent nanofiltration.

Chapter 2 Synthesis of Zeolitic Imidazolate Framework Membranes on Macroporous Support by A Vapor-phase Seeding Method for C_3H_6/C_3H_8 Separation

Results of this chapter have been partially published in Qiang, Z.; Yi, Z.; Wang, J.-W.; Khandge, R.S.; Ma, X. 2023. Fabrication of Polycrystalline Zeolitic Imidazolate Framework Membranes by a Vapor-Phase Seeding Method. *Membranes*, 13, 782.

Abstract

Polycrystalline zeolitic imidazolate framework (ZIF) membranes have demonstrated molecular sieving capability for separating molecules of similar sizes. However, their reliable fabrication continues to pose challenges for their scale-up for industrial applications. Here, we report a vapor-phase seeding approach that combines atomic layer deposition (ALD) and ligand vapor treatment to synthesize ZIF membranes with high propylene/propane separation performance. In this method, ALD was used to deposit a uniform and conformal ZnO coating on the support surface, followed by treatment using 2-methylimidazole vapor to convert ZnO to ZIF-8, forming the seed layer. A subsequent near-room temperature secondary growth was employed to grow the seed layer into a continuous membrane. ZIF-8 membranes made on macroporous α-alumina support by this method consistently exhibited propylene permeances above 1×10^{-8} mol Pa^{-1} m^{-2} s^{-1} and propylene/propane separation factor higher than 50. Using mesoporous TiO_2 as the support allowed for fewer ALD cycles and shorter reactant pulse times, resulting in ZIF-8 membranes with a propylene permeance of ~4×10^{-8} mol Pa^{-1} m^{-2} s^{-1} and a propylene/propane

separation factor of up to 152. Moreover, we demonstrated the effectiveness of the vapor-phase seeding method in producing membranes of other ZIF structures, including ZIF-67 and ZIF-90.

2.1 Introduction

The energy-intensive cryogenic distillation technology is currently used in the olefin and paraffin separation processes, which are among the most critical separation processes in the petrochemical industry [6]. Adsorptive separation has also been developed as a more energy-efficient alternative to the olefins and paraffin separation, but it is still challenging to separate olefin and paraffin pairs with the same number of carbon atoms and similar properties. Metal-organic frameworks (MOFs) with a highly ordered porous structure, ultrahigh surface area, and tunable crystallographic micropore size have been used in these separation processes [49, 50]. Bülow et al. first demonstrated that HKUST-1 could be used to separate ethylene and ethane mixtures in the low-pressure range [51]. Chang and co-workers showed that HKUST-1 was useful in the separation of propylene and propane in 2010 [52]. Nowadays, membrane-based separation is thought to be an attractive option for energy-efficient operation compared to the other processes, but only specific MOFs were successfully made into membranes due to the rigorous synthesis conditions and the possible stability issues.

Zeolitic imidazolate frameworks (ZIFs) with a well-ordered porous structure and good stability are some of the most promising MOFs for membrane gas separation. They can be prepared from a diverse range of solvents, including water, methanol, and dimethylformamide (DMF). ZIFs can be used as adsorbents to separate olefins and paraffin as well. For example, ZIF-7 was the first microporous solid to exhibit selective adsorption of ethane over ethylene, validated by Gascon et al. in 2010 [53]. It was proposed that the separation performance of ZIF-7 can be attributed to a

gate-opening effect in which specific threshold pressures control the uptake and release of different gas molecules. Besides, for the first time, $Zn(2\text{-cim})_2$, $Zn(2\text{-bim})_2$, and ZIF-8 were explored by Li and co-workers to separate propylene and propane [27]. Single-component diffusion studies suggest that the kinetic separation of propylene and propane should be feasible with these MOFs based on the observed significant difference in their diffusion rates.

Polycrystalline ZIF membranes are commonly referred to as inorganic membranes because their structures, synthesis, and gas transport properties are similar to those of inorganic zeolites [54, 55]. Among the various ZIF candidates, ZIF-8 has received tremendous attention for C_3H_6/C_3H_8 separation due to its well-fitted effective apertures of 4.0-4.2 Å, and the predicted C_3H_6/C_3H_8 ideal selectivity of ZIF-8 was around 130 based on the propylene and propane diffusivities calculated by Zhang and co-workers [28]. Lai and their co-worker first reported the ~2.0 μm thick ZIF-8 membranes with an average propylene/propane separation factor greater than 30 and a C_3H_6 permeance above 80 GPU [32]. Later, ZIF-67 and Co-Zn-ZIF-8 membranes were developed for the separation of propylene and propane [56-60].

The first ZIF-8 membrane with excellent hydrogen separation properties was reported by Caro et al. in 2009, and their membrane was synthesized using the microwave heating method [61]. So far, there have been a number of known methods for the synthesis of ZIF membranes. Based on whether seeds are used, they can generally be categorized into two groups: the seed-free or in-situ method and the seeded growth or secondary growth method. The seed-free approach includes conventional hydrothermal or solvothermal synthesis [62], microwave synthesis [61, 63], counter-diffusion [64], electrospray deposition [65-67] and so on. The original in-situ method is the first and most used method among researchers to prepare membranes as the preparation step is less

complicated. However, it is challenging to control the microstructures of membranes, and the membranes made by this method are relatively thick [68]. Compared with the in-situ method, the secondary method can provide better control over membrane microstructures such as crystal orientation, crystal size, grain boundary structures, etc [55, 69]. For this approach, a homogeneous seed layer is critical for obtaining a high-quality membrane. At present, there are numerous methods have been developed, like manual rubbing [70], spin-coating or dip-coating [57, 71-73], thermal seeding [74], and microwave seeding [33, 56, 58, 70, 75].

Solvent-free vapor phase synthesis is another innovative route for fabricating ZIF membranes on porous supports. This procedure typically involves the deposition of a metal source and a ligand vapor treatment to transform the metal deposition into a ZIF structure [76]. Li et al. reported the fabrication of an ultrathin ZIF-8 membrane using a gel-vapor deposition method, which has higher gas permeance than membranes made by conventional approaches [77]. In another work, atomic layer deposition (ALD) was used to deposit ZnO, which was converted to ZIF-8 membrane after solvothermal treatment [78]. Using an all-vapor-phase method, Ma et al. were able to synthesize ZIF-8 membrane with excellent propylene/propane selectivity and high propylene permeance [16]. However, this approach has only been used to prepare ZIF-8 films/membranes, and it is challenging to produce other polycrystalline ZIF membranes with this methodology. In addition, this approach required the use of mesoporous alumina support and has not been extended to the low-cost macroporous supports.

In this chapter, we developed a vapor-phase seeding approach to create a conformal and compact ZIF-8 seeds layer that can be easily grown into a continuous membrane via near-room temperature secondary growth. In the seeding step, ZnO was deposited onto the support using ALD

and then converted into ZIF-8 seeds through exposure to 2-mIm vapors. Subsequent secondary growth of these seeds led to the formation of ZIF-8 membranes with excellent propylene/propane separation performances. Additionally, we systematically investigated the impact of ALD cycle number and precursor pulse time on the structure and properties of ZIF-8 membranes. Our results show that the vapor-phase seeding approach is highly effective on both macroporous and mesoporous ceramic supports, and it can also be employed to fabricate other ZIF membranes.

2.2 Experimental Section

2.2.1 Raw materials

Alumina powders (Baikalox 1.0CR, average particle size of ~0.5 μm) from Baikowski International Corporation were used to prepare the macroporous α-alumina supports. Nitric acid (1.0 N standardized solution, Alfa Aesar), zinc nitrate hexahydrate ($Zn(NO_3)_2 \cdot 6H_2O$, 98%, Sigma-Aldrich), 2-methylimidazole ($C_4H_6N_2$, 99%, Sigma-Aldrich), cobalt nitrate hexahydrate ($Co(NO_3)_2 \cdot 6H_2O$, ACS reagent, ≥98%, Sigma-Aldrich), imidazole-2-carboxaldehyde ($C_4H_4N_2O$, >98%, TGI), methanol (CH_3OH, ACS reagent, ≥99.8%, Sigma-Aldrich) dimethylformamide (C_3H_7NO, 99.9%, Alfa Aesar), and deionized water (DI water) were used to prepare ZIF membranes. All chemicals were used as received without further purification.

2.2.2 Preparation of macroporous and mesoporous ceramic supports

Macroporous α-alumina supports with a diameter of 22 mm were prepared by a casting-sintering method reported in the literature [16]. The supports were polished with silicon carbide paper (MicroCut Plain, 1200 grit size), dried at 250 °C for 10 h, and stored in a desiccator for later use. The mesoporous ceramic support consists of a mesoporous TiO_2 thin film on top of the

macroporous α-alumina support. The TiO_2 layer was prepared using the sol-gel method reported in the literature [79]. Briefly, 0.25 M TiO_2 sol was prepared by first dissolving 74 ml of titanium tetra-isopropoxide in 500 ml of isopropanol, and slowly adding the mixture to 450 ml of water while vigorously stirring for 1-2 h. Next, the titania precipitate was washed with water to remove the remaining alcohols, diluted with one liter of water, and peptized by adding 72 ml of 1 M HNO_3 under reflux conditions at 75 °C. The TiO_2 sol was mixed with 3 wt% poly(vinyl alcohol) solution at a volume ratio of 20:13 to obtain a coating solution, which was used to coat a thin layer of TiO_2 onto the surface of α-alumina support using the dip-coating method. The resulting asymmetric support was left to dry overnight at room temperature and then sintered at 450 °C for 3 h. The coating-sintering process was repeated to enhance the quality of the TiO_2 membrane.

2.2.3 Fabrication of ZIF-8 membranes

One type of ZIF-8 membranes were fabricated using the vapor-phase seeding and secondary growth methods (**Figure 2.1**). The vapor-phase seeding consists of two steps: atomic layer deposition (ALD) and ligand vapor treatment. GEMStar XT-S/D™ Benchtop Thermal ALD was used to deposit zinc oxide (ZnO) on the porous supports at a deposition temperature of 125 ℃. The supports were placed horizontally in the center of the ALD chamber, and the system was evacuated for 30 min. During ALD, the gaseous reactants, diethylzinc (DEZ) used as the precursor and H_2O as the oxidant, were alternately introduced into the reaction cham-ber. A typical ALD cycle consists of a 15 ms pulse of DEZ, 1 s exposure, 19 s purge with N2, 15 ms pulse of H_2O, 1 s exposure, and 19 s purge with N_2. The numbers of deposition cycles (10, 20, 30, and 40 cycles) were varied to control the amount of ZnO deposits. The deposition temperature was maintained at 125 °C under all conditions. To transform ZnO into ZIF-8 seeds, The ZnO-modified support was

vertically held above 2-methylimidazole (0.2 g) powders at a distance of around 4 cm in a PTFE container and then heated to 125 °C for one day. The 2-methylimidazole vapors were generated to react with ZnO, forming ZIF-8. A temperature of 125 °C was chosen as the treatment temperature because of the effective conversion of ZnO to ZIF-8 under this condition [16, 17]. The as-synthesized seeded support was directly used in the next step without further treatment.

The secondary growth method was employed to grow the ZIF-8 seeds into a continuous membrane. The ZIF-8 seeded support was placed vertically in a solution containing 2.27 g 2-mIm and 0.11 g Zn $(NO_3)_2 \cdot 6H_2O$ dissolved in 40 ml of deionized (DI) water. The growth was carried out at 30 ℃ for 6 h. After the synthesis, the membrane was rinsed with methanol, soaked in 40 ml methanol for 12 h, and dried at room temperature for 24 h before gas permeation measurement and structure characterizations.

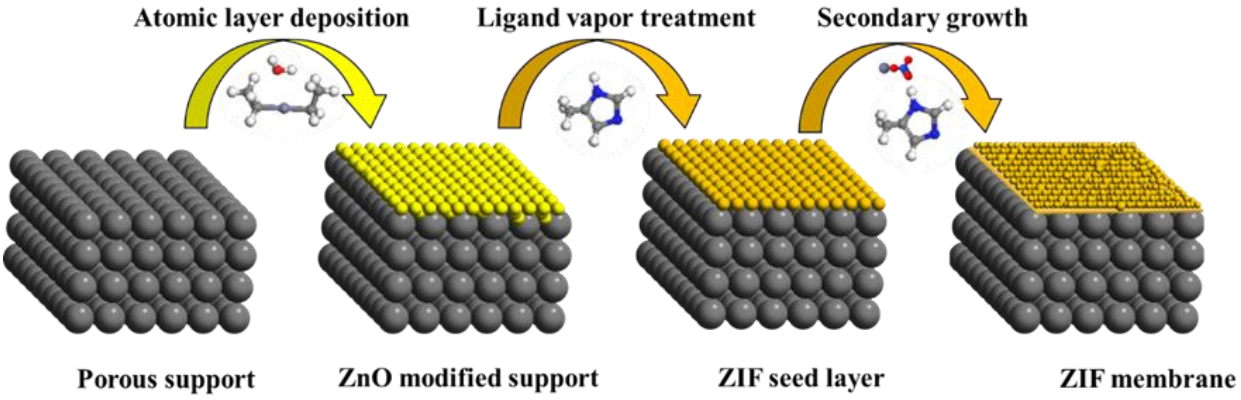

Figure 2.1 A schematic illustration depicting the process for fabricating ZIF membranes using vapor-phase seeding and secondary growth.

Another type of ZIF-8 membrane was prepared by the all-vapor-phase ligand-induced permselectivation method (LIPS) [16]. This method involves two distinct steps: atomic layer deposition (ALD) and ligand vapor treatment. In this study, the GEMStar XT-S/D™ Benchtop

Thermal ALD was used to deposit zinc oxide (ZnO) on porous substrates at varying temperatures (100, 125, and 180°C). During the ALD process, alternating pulses of diethylzinc (DEZ) and H_2O precursors were introduced into the reaction chamber. Typically, the ALD cycle involved a 50 ms pulse of DEZ followed by a 100 ms pulse of H_2O. After each precursor pulse, there was a 1 s exposure period and a 5 s purge with N_2. The number of deposition cycles (10, 20, 30, and 40 cycles) and precursor pulse time (15, 30, 50, and 100 ms) were varied to regulate the amount of ZnO deposition.

After ALD, ZnO-modified support was transferred to a Teflon liner with 0.2 g of 2-methylimidazole (2-mIm) powders at the bottom. The support was positioned vertically above the 2-mIm bed at a distance of approximately 4 cm. The Teflon liner was heated to 125 ℃ for 24 hours to convert the ZnO into ZIF. The vacuum oven was pre-heated at 125 ℃ for 2 hours. Following growth, the membrane was directly transferred to the vacuum oven to do heat treatment and remove any residual 2-mIm present within the α-alumina support pores.

2.2.4 Fabrication of ZIF-67 and ZIF-90 membranes

ZIF membranes with chemical composition and structure different from those of ZIF-8 were synthesized by epitaxial growth. The ZIF-8 seeded support prepared by the vapor-phase seeding method was placed in a solution containing the precursors for the corresponding ZIF and underwent solvothermal synthesis at 30 ℃ for 6 h. For ZIF-67 membrane synthesis, the epitaxial growth solution contains 0.108 g $Co(NO_3)_2 \cdot 6H_2O$ and 2.27 g 2-mIm dissolved in 40 ml DI water. The solution used to grow the ZIF-90 membrane was prepared by mixing a 60 ml DMF solution that contains 849 mg imidazole-2-carboxaldehyde and 20 ml methanol that contains 970 mg

$Zn(NO_3)_2 \cdot 6H_2O$ [80]. The synthesized ZIF membranes underwent the same cleaning and drying procedures as the ZIF-8 membrane.

2.2.5 Gas permeation/sparation experiments

The gas permeances of the support and membranes were measured on a home-built constant volume variable pressure apparatus. The membrane was sealed in a stainless-steel permeation cell. The system was evacuated 2 h prior to the gas permeation measurement. The feed pressure was held constant at 1 atm. The permeate side was initially under vacuum, and the pressure increase in the permeate side during gas permeation measurement was used to calculate the gas permeance. For He and N_2 single gas, the ideal selectivity was determined by the ratio of their single-component permeances. For mixture gas separation, an equimolar C_3H_6/C_3H_8 mixture with a total flow rate of 60 mL/min was provided on the feed side, and the permeate side was swept with 60 mL/min Ar gas. The gas composition was measured by gas chromatography (Thermo Scientific TRACE 1300 GC) with a flame ionization detector (FID). The separation factor was calculated from the molar ratio of C_3H_6/C_3H_8 on the permeate side divided by their molar ratio on the feed side using the following equation:

$$a_{ij} = \frac{y_i/y_j}{x_i/x_j} \tag{2.1}$$

Where x_i and x_j represent the molar fraction of propylene and propane in the feed, respectively, and y_i and y_j are their corresponding fractions in the permeate.

2.2.6 Characterizations

Scanning electron microscope (SEM) images were collected on a Hitachi S4800 field emission SEM coupled with energy dispersive X-ray analysis (EDS). Samples were coated with 5 nm thick iridium in the Emitech K575X Sputter coater (Emitech Ltd., Ashford, Kent, UK) before SEM analysis. X-ray diffraction patterns (XRD) of supports and membranes were obtained using a Bruker D8 Discover A25 diffractometer (Bruker Corporation, Billerica, MA, USA) equipped with a Cu Kα X-ray radiation source (40 kV and 40 mA, $\lambda = 0.154$ nm).

2.3 Results and Discussion

2.3.1 Microstructure evolvement during membrane fabrication

In the vapor-phase seeding process, the surface of the α-alumina support was first coated with ZnO using ALD. Then the ZnO deposits were transformed into a layer of ZIF-8 seeds by undergoing a vapor-phase treatment with sublimated 2-mIm vapors. Subsequently, secondary growth was used to grow the seed layer into a continuous membrane. **Figures 2.2-3** present the XRD patterns and SEM images of the support and membrane at each step. As shown in **Figure 2.2**, the ZnO deposited from ALD appears to be amorphous due to the relatively low deposition temperature (125 ºC) and the low number of ALD cycles (<50 cycles) used in this study. XRD peaks associated with the ZIF-8 phase were observed in the seeded support, confirming the successful conversion of ZnO to ZIF-8 under the mild ligand vapor treatment condition. The increase in peak intensity in the membrane suggests continued growth of ZIF-8 seeds during the solvothermal synthesis at near room temperature (30 ℃).

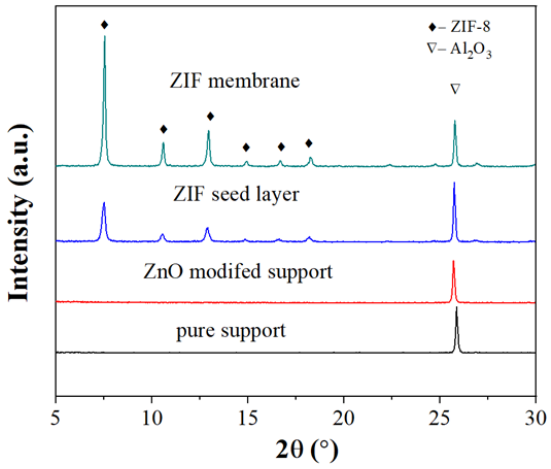

Figure 2.2 XRD patterns of pure α-alumina support, ZnO modified support, ZIF-8 seed layer after ligand vapor treatment, and ZIF-8 membrane after secondary growth.

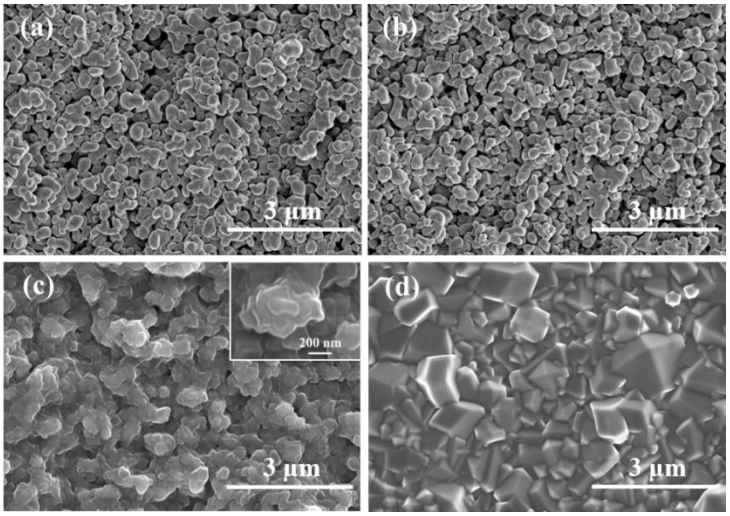

Figure 2.3 SEM images of samples. (a) pure support, (b) support modified with 20 cycles ZnO ALD, (c) ZIF-8 seed layer after ligand vapor treatment, (d) and ZIF-8 membrane. Insert in (c) shows the higher-magnification image of seeds.

SEM was employed to reveal the morphological changes that occurred during membrane synthesis. As shown in **Figure 2.3a**, the α-alumina support contains macropores of several hundred

nanometers. After coating the support with ZnO via ALD, no morphological changes were detected by high-resolution SEM (**Figure 2.3b**). Following ligand vapor treatment, ZIF-8 nanocrystals with an average particle size smaller than 100 nm appeared on the support (**Figure 2.3c**). It is worth noting that the transformation from ZnO to ZIF-8 is accompanied by a ~17 times volume increase due to the different densities of these two materials [81]. This expansive conversion led to a closely packed or even partially inter-grown ZIF-8 seed layer with small inter-particle voids. These voids were easily eliminated by the continued growth of the ZIF-8 seeds during the near-room temperature secondary growth step. As shown in **Figure 2.3d**, the resulting ZIF-8 membrane is of high quality and continuous without any visible voids or defects.

The ZnO ALD-modified support was further characterized by EDS, which confirmed the presence of Zn (**Figure 2.4a**). Cross-section EDS analysis unveiled a penetration depth of ~9 μm for the ZnO deposition within the α-alumina support after 40 cycles ALD (**Figure 2.4b** and **Figure 2.5**). FTIR and XPS results revealed the presence of Zn–O bonds (**Figure 2.6**). These observations, coupled with the XRD results, suggest the amorphous nature of the ZnO deposits.

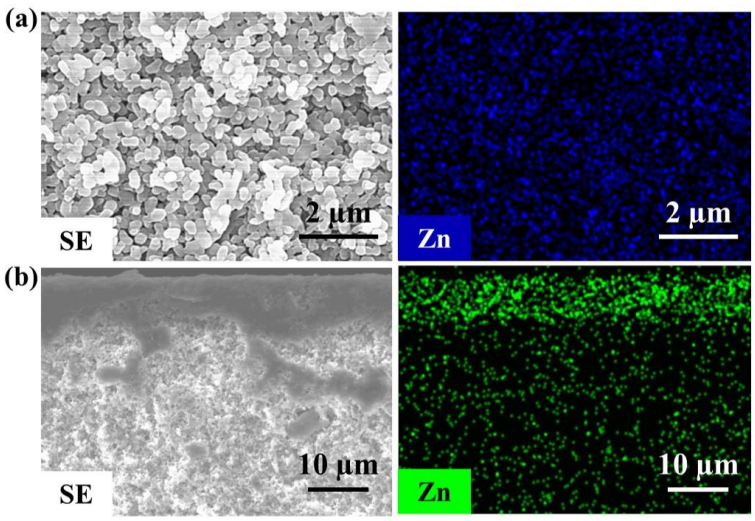

Figure 2.4 EDS analysis of ZnO ALD modified support (a) top view and (b) side view.

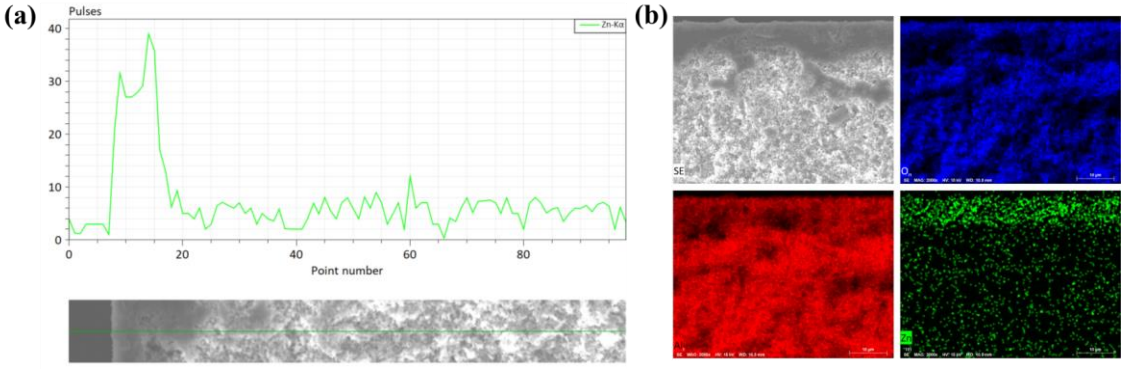

Figure 2.5 EDS analysis of support modified with ZnO ALD (a) line scan and (b) mapping.

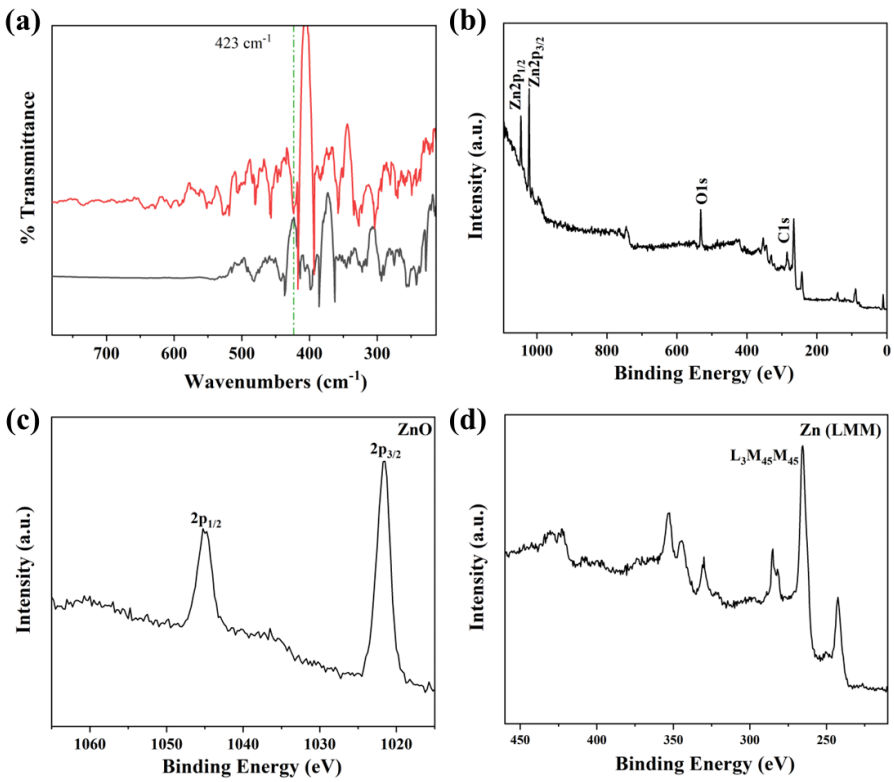

Figure 2.6 (a) FT-IR analysis of support modified with ZnO ALD, (b) XPS survey spectra for ZnO ALD modified support ranging from 1100 to 0 eV, highlighted XPS spectra for (c) Zn 2p and (d) Zn (LMMM).

2.3.2 Effect of ALD cycle number

A systematic investigation was conducted to understand the impact of critical ALD parameters, such as cycle number and precursor pulse time, on the structure and gas permeation properties of ZIF-8 membranes. The ligand vapor treatment and secondary growth conditions were kept unchanged while varying the ALD parameters.

We first varied the number of ALD cycles from 10 to 20, 30, and 40, using a pulse time of 15 ms for DEZ and water precursors. **Figure 2.7a** presents the XRD patterns of the ZIF-8 seed layers

prepared with different ALD cycle numbers. As the number of ALD cycles increased, the intensity of ZIF-8 characteristic peaks increased slightly. Top-view SEM images in **Figure 2.7b** show uniform ZIF-8 seeds covering the entire surface of α-alumina support under all conditions. With an increase in ALD cycles, the seed layer appeared denser with the ZIF-8 nanoparticles becoming slightly larger, consistent with the increased intensities in XRD peaks. The single gas permeance of the ALD-modified support was also evaluated. The He/N_2 ideal selectivity of seeded supports matched that predicted from the Knudsen diffusion, and the gas permeances decreased with increasing ALD cycle numbers (**Figure 2.8**). The apparent reduction in gas permeances at 40 cycles could be attributed to the increased penetration depth of ZnO ALD inside the support (**Figure 2.5**). Moreover, the seeded supports showed no C3 selectivity.

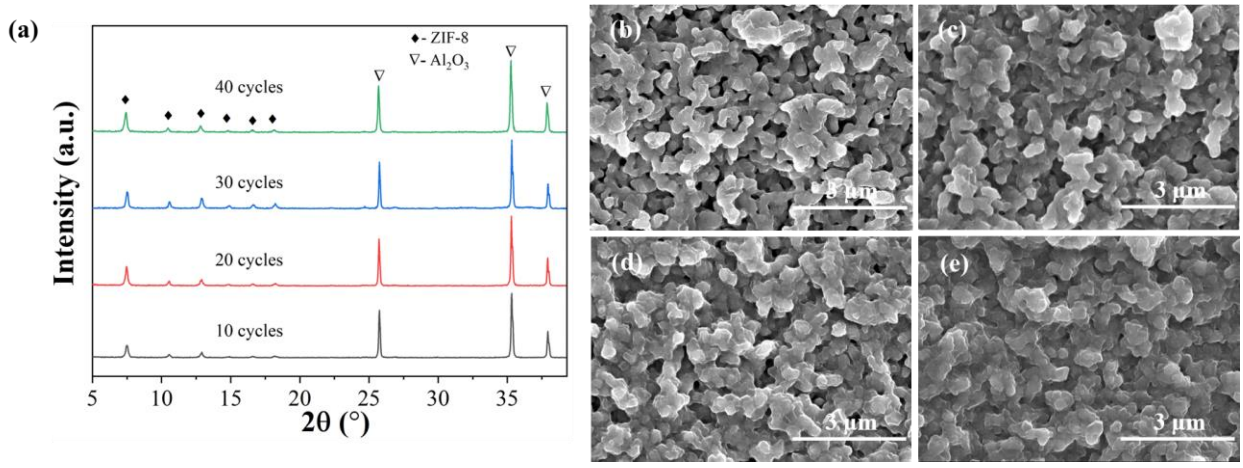

Figure 2.7 XRD patterns (a) and SEM images (b–e) of ZIF-8 seed layers prepared using different numbers of ALD cycles (10, 20, 30, and 40 cycles).

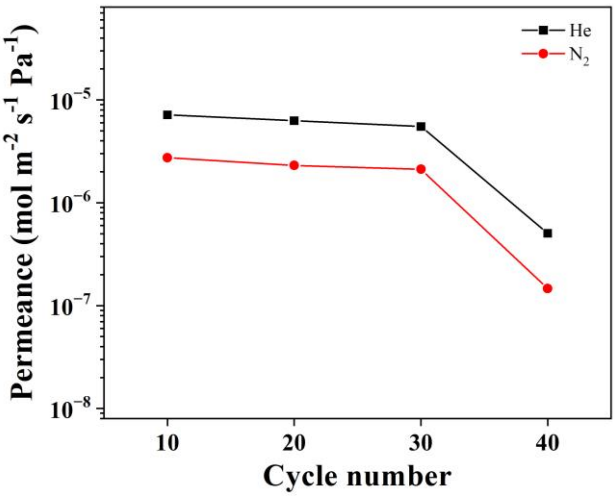

Figure 2.8 He and N_2 single-component permeances of ZIF-8 seed layer as a function of the number of ALD cycles (10, 20, 30, and 40 cycles).

ZIF-8 membranes synthesized from these different seed layers were characterized with XRD, SEM, and propylene/propane mixed gas permeation measurements. Top-view SEM images (**Figure 2.9**) show that all membranes are highly continuous, without apparent pinholes or defects. However, cross-sectional SEM images revealed an increase in membrane thickness with cycle numbers. Specifically, the thickness was less than 1 μm at 10 cycles, approximately 1.5 μm at 20 cycles, and 1.5-2 μm at 30 and 40 cycles. ZIF-8 membranes exhibited much stronger XRD peaks than seed layers, with peak intensity increasing with ALD cycle numbers (**Figure 2.10**), consistent with the observation from SEM. The membranes exhibited much stronger ZIF-8 XRD peaks than seed layers, and the peak intensity increased with the number of ALD cycles.

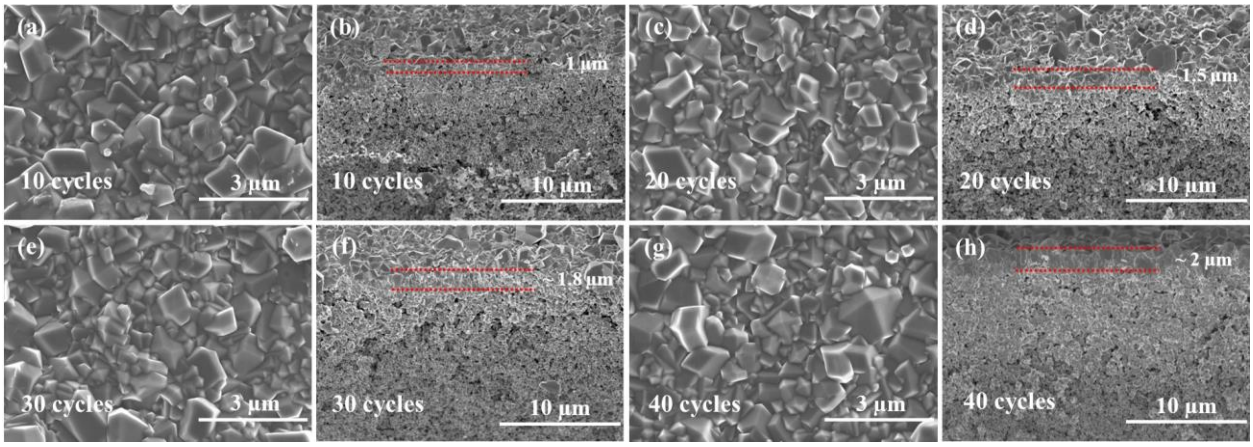

Figure 2.9 SEM images of ZIF-8 membranes made under different ZnO ALD cycles: (a,b) 10 cycles, (c,d) 20 cycles, (e,f) 30 cycles, and (g,h) 40 cycles.

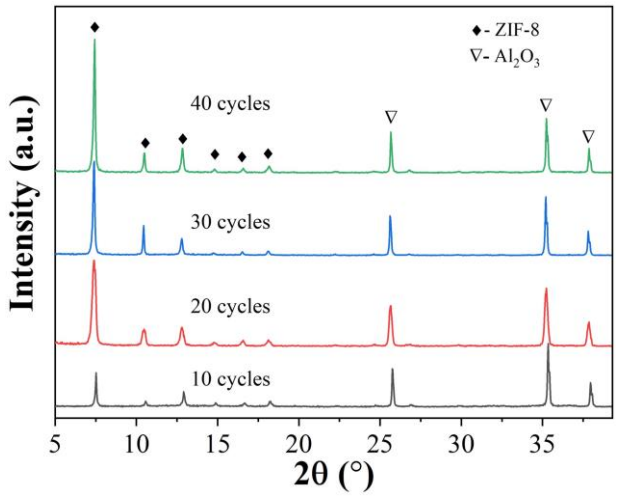

Figure 2.10 XRD patterns of ZIF-8 membranes made under different ZnO ALD cycles.

These different thicknesses resulted in varying C3 separation properties. Specifically, propylene permeance decreased, but the C3 separation factor increased with the ALD cycle number (**Figure 2.11**). At a 40-cycle ALD, the separation factor reached 55.5 with a propylene permeance of 1.1×10^{-8} mol Pa^{-1} m^{-2} s^{-1}. On the other hand, it is worth noting that the propylene permeance was not linearly proportional to the inverse of membrane thickness. For instance,

compared to the membrane prepared with 10 cycles, the membrane produced using 40 cycles had a propylene permeance that was approximately four times lower despite being only around 100% thicker. This difference can be explained by the different amounts of defects in the membranes and the additional transport resistance caused by ZIFs formed inside the support pores (**Figure 2.12**). Overall, these results showed that increasing the ALD cycle number led to more closely packed seeds, which resulted in membranes with enhanced separation factors and good gas permeances.

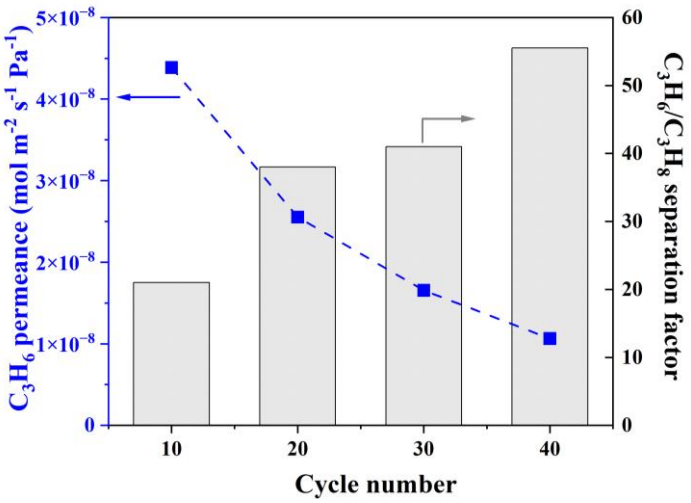

Figure 2.11 C3 separation performances of ZIF-8 membranes made under different numbers of ALD cycles.

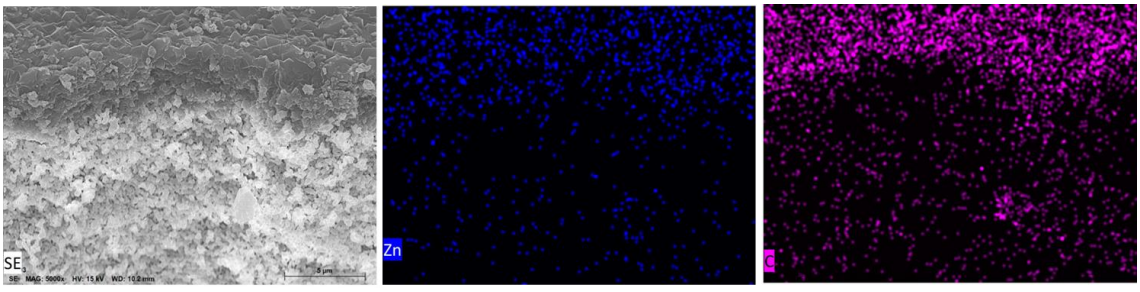

Figure 2.12 EDS analysis of ZIF-8 membrane.

2.3.3 Effect of ALD pulse time

Next, we investigated the effect of pulse time for ALD precursors on the formation and properties of the ZIF-8 seed layers and membranes. The pulse time duration controls the quantity of precursors introduced to the ALD reactor during each cycle, which directly impacts the diffusion of precursors into the support pores and the subsequent formation of ZnO inside the support. To investigate this effect, a group of supports was coated with ZnO ALD using a fixed cycle number of 20 but with different pulse times (15, 30, and 50 ms) for the DEZ and water precursors. The ZnO ALD-modified supports were subjected to the same ligand vapor treatment and secondary growth described earlier. The XRD patterns and SEM images (**Figures 2.13a and 2.14**) showed no apparent differences between the ZIF-8 seed layers prepared. However, the peak intensity of the ZIF-8 membrane (**Figure 2.13b**) became stronger with the increase in pulse time, suggesting an increase in membrane thickness. Top-view SEM images (**Figure 2.115**) revealed the formation of continuous ZIF-8 membranes with well-intergrown crystals in all three conditions. Cross-sectional SEM images (**Figure 2.15**) confirmed that longer pulse time led to thicker membranes. Furthermore, as the pulse time increased, a greater amount of ZIF-8 particles was observed beneath the membrane layer and within the α-alumina support pores. This suggests that prolonging the precursor pulse time facilitates the deposition of ZnO and the subsequent formation of ZIF-8 phase inside the support, which is expected to increase gas transport resistance.

Gas permeation results revealed that an increase in the precursor pulse time led to a decrease in propylene permeance (**Figure 2.13c**). However, this decrease was not linearly proportional to the inverse of membrane thickness. For instance, compared to the membrane prepared with a 15 ms pulse time, the membrane produced using 50 ms had a propylene permeance that was

approximately ten times lower, despite being only around 50% thicker. This difference can be attributed to the additional transport resistance caused by the ZIF-8 formed inside the support pores in the 50 ms-membrane. Nevertheless, all membranes exhibited a mixed-gas propylene/propane separation factor above 40, with the optimum value of ~55 achieved at 30 ms. These results demonstrate that varying the pulse time is an effective way to adjust the propylene/propane separation performance of ZIF-8 membranes. Decreasing the pulse time can minimize ZIF growth within the support, thereby enhancing gas permeance, whereas a longer pulse time creates more selective membranes.

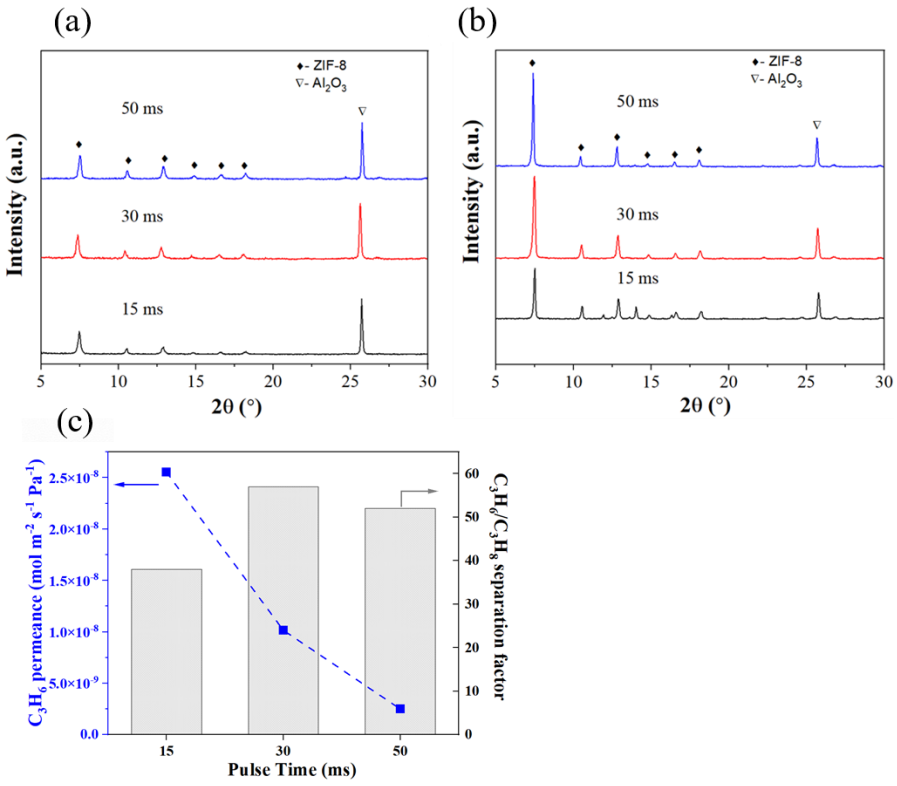

Figure 2.13 Effect of ALD pulse time (15, 30 and 50 ms). (a) XRD patterns of ZIF-8 seed layer, (b) XRD patterns for ZIF-8 membrane, and (c) propylene permeances and C_3H_6/C_3H_8 selectivity of ZIF-8 membranes under different pulse time.

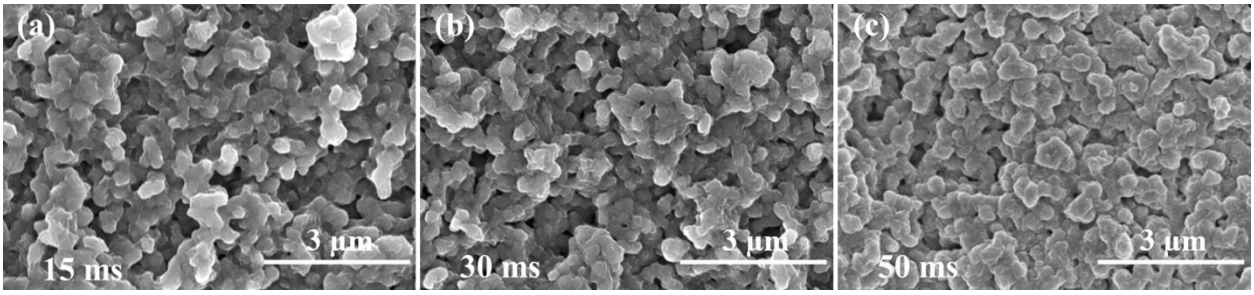

Figure 2.14 Surface SEM images of ZIF-8 seeds under different ALD pulse time: (a) 15ms, (b) 30 ms and (c) 50 ms.

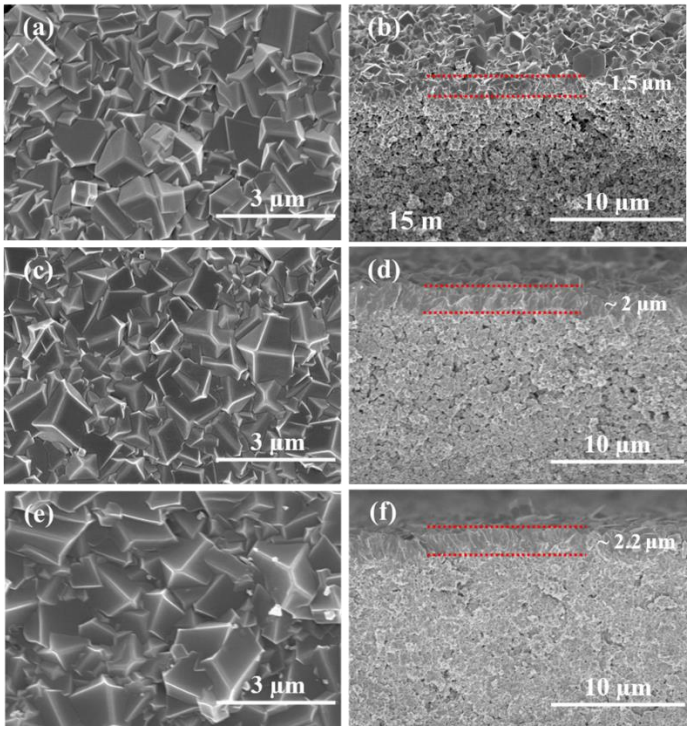

Figure 2.15 Top-view and cross-sectioncross-sectional SEM images of ZIF-8 membranes prepared with different pulse times: (a and b) 15 ms, (c and d) 30 ms, and (e and f) 50 ms.

2.3.4 ZIF-8 membrane fabricated on mesoporous TiO_2 supports

Furthermore, we demonstrated the feasibility of using the vapor phase seeding technique on mesoporous ceramic supports, such as sol-gel derived TiO_2 coated α-alumina support. The TiO_2 layer contains mesopores in the 5-10 nm range, as shown in **Figure 2.16**. A short pulse time of 15 ms and a low cycle number of 10 were utilized to deposit a small amount of ZnO, which reduced the pore size of TiO_2 without entirely blocking the mesopores (**Figure 2.17a**). The subsequent ligand vapor treatment successfully transformed the ZnO to ZIF-8 seeds (**Figure 2.17b** and **Figure 2.18**), which appeared denser than those on the α-alumina support. After secondary growth, the ZIF-8 membrane exhibited high continuity and crystallinity with a thickness of ~1.5 μm (**Figs. 2.17c** and **2.17d**). In contrast to the macroporous α-alumina support, we did not observe any ZIFs inside the support pores, indicating that the mesoporous TiO_2 layer effectively prevented ALD vapor precursors from infiltrating the support and creating ZnO deposits in the interior of the support. Consequently, ZIF membrane growth occurred primarily on the support surface rather than within the support, which is beneficial for enhancing gas permeance. As a result, the membrane demonstrated superior separation performance, with a propylene permeance of $\sim 4\times10^{-8}$ mol Pa^{-1} m^{-2} s^{-1} and a propylene/propane separation factor of up to 152. These findings highlight the advantages of using mesoporous TiO_2 supports for fabricating defect-free and thin ZIF-8 membranes with enhanced separation performance.

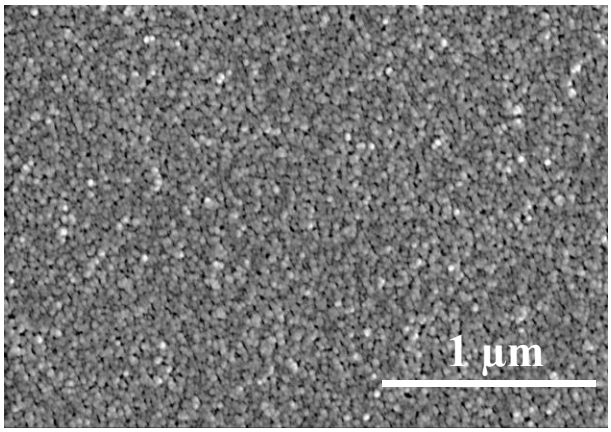

Figure 2.16 SEM image of TiO_2 support.

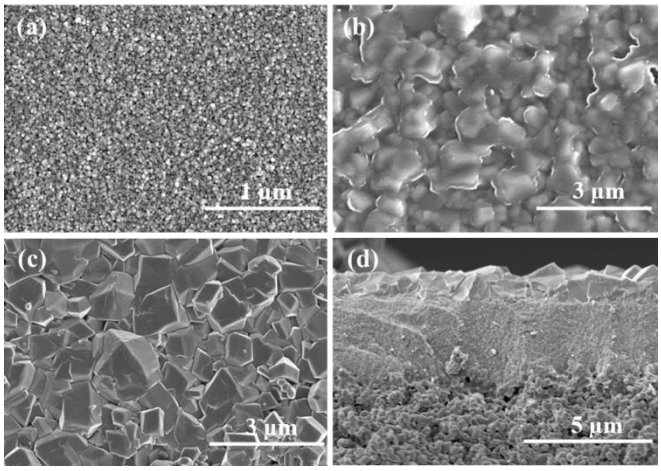

Figure 2.17 Top-view SEM images of (a) TiO_2 support modified with ZnO ALD and (b) ZIF-8 seed layer. (c) Top-view and (d) cross-sectional SEM images of ZIF-8 membrane prepared on TiO_2 support.

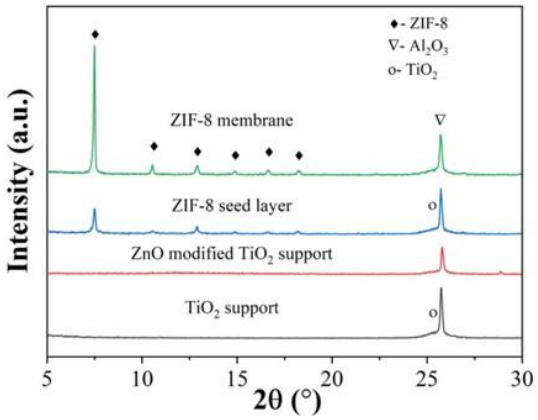

Figure 2.18 XRD patterns of pure TiO_2 support, ZnO modified TiO_2 support ZIF seed layer on TiO_2 support and ZIF membrane TiO_2 support after secondary growth (from bottom to top).

We synthesized additional membranes to evaluate the reproducibility of the vapor-phase seeding method. As shown in Table 1, these ZIF-8 membranes exhibited propylene permeance ranging from 8×10^{-9} to 2.5×10^{-8} mol Pa^{-1} m^{-2} s^{-1}. Moreover, they exhibited a propylene/propane separation factor surpassing 45, with one membrane reaching a high separation factor of 102.

Table 2.1 Permeances and propylene/propane separation factors of ZIF-8 membranes fabricated by vapor-phase seeding method.

Membranes	**Propylene Permeance ($\times 10^{-10}$ mol m^{-2} s^{-1} Pa^{-1})**	**Separation Factor**
M1	202.91	64
M2	235.25	48
M3	246.99	45
M4	79.17	52
M5	241.1	102

The effect of feed pressure, feed composition, and temperature on membrane performance was also investigated (**Figure 2.19**). The membrane exhibited good performance across the varied permeation conditions studied. As feed pressure, temperature, or propylene fraction in the feed increased, separation factors exhibited a slight decline, consistent with trends reported in the literature [16, 82, 83].

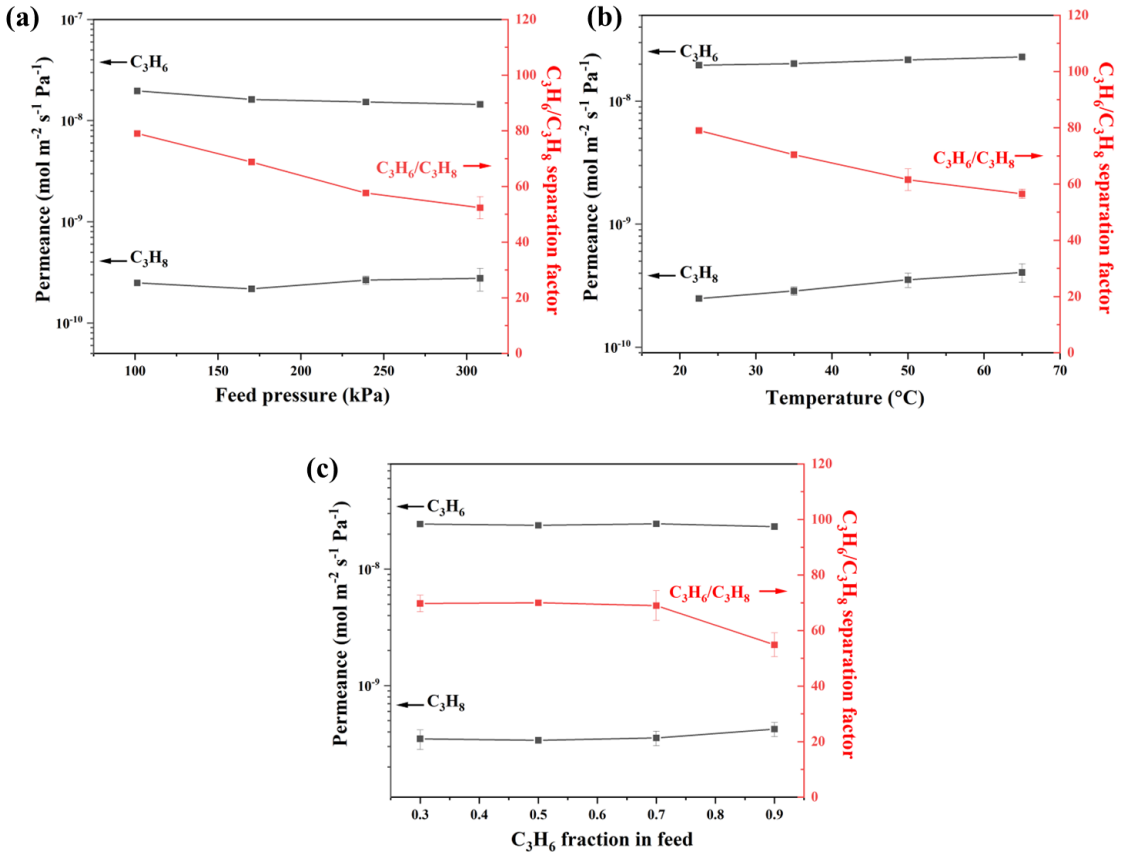

Figure 2.19 The binary C_3H_6/C_3H_8 separation performance of the ZIF-8 membrane as a function of (a) feed pressure, (b) temperature, and (c) C_3H_6 fraction in feed.

Compared to recently reported polycrystalline ZIF-8 membranes prepared on macroporous α-alumina supports (**Figure 2.20**), the overall performance of our membranes ranks at the higher end

in terms of the mixed-gas separation factor and propylene permeance. These results have demonstrated that vapor-phase seeding is a reliable and reproducible method for fabricating high-quality ZIF-8 membranes on low-cost macroporous supports.

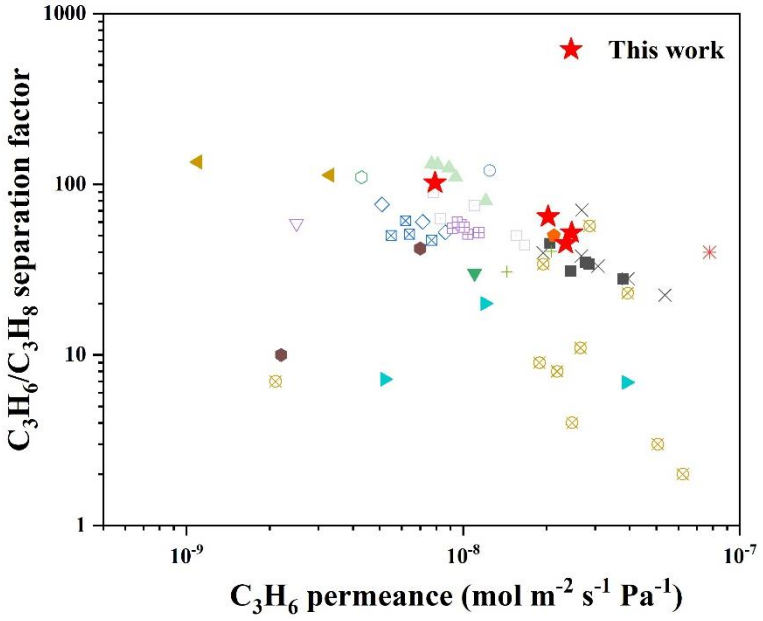

Figure 2.20 Comparison of the C_3H_6/C_3H_8 separation performance of the ZIF-8 membranes in this work with data reported in the literature [32-34, 56, 59, 62, 82, 84-95].

2.3.5 Synthesis of ZIF-67 and ZIF-90 membranes by vapor-phasing seeding

To demonstrate the broad applicability of our vapor seeding method, we conducted preliminary investigations into the synthesis of polycrystalline membranes featuring other ZIF structures, namely ZIF-67 and ZIF-90. These membranes were prepared by using a ZIF-8 seed layer created through the vapor phase seeding approach and then employing epitaxial growth with solutions containing the precursors for the desired ZIF structures. Intriguingly, despite using a ZIF-

8 seed layer, XRD analysis (**Figure 2.21a**) confirmed that the target ZIF-67 and ZIF-90 phases were successfully formed in the membranes after the heteroepitaxial secondary growth step. Top-view SEM images (**Figure 2.21b and c**) showed that both membranes exhibited a high level of continuity and integrity. EDS analysis (**Figure 2.22**) revealed the presence of cobalt elements in the ZIF-67 membrane. Furthermore, the ZIF-67 membrane displayed good propylene/propane separation performance, with a propylene permeance and a propylene/propane separation factor of ~78.

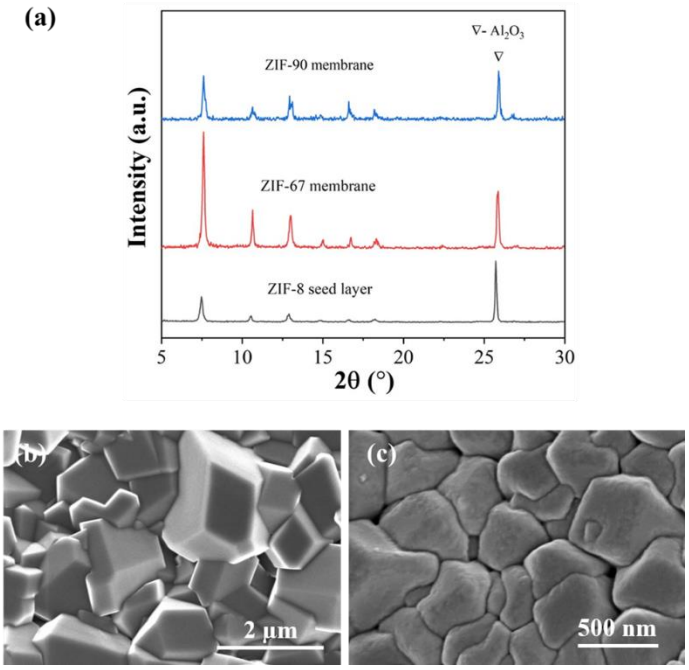

Figure 2.21 (a) XRD patterns of ZIF-67 and ZIF-90 membranes. Top-view SEM images of (a) ZIF-67 membrane and (b) ZIF-90 membrane.

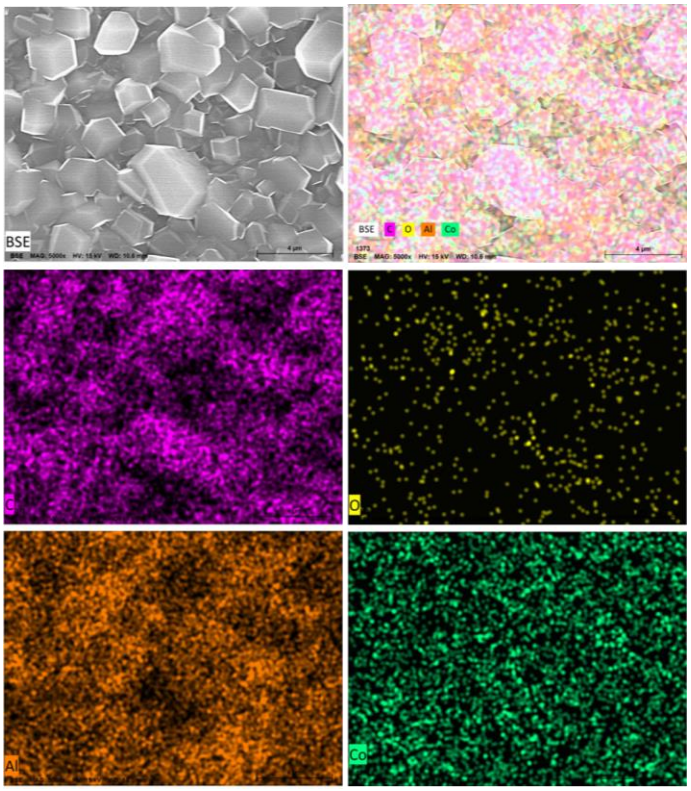

Figure 2.22 EDS of ZIF-67 membrane prepared on Al_2O_3 support.

2.3.6 ZIF-8 membrane fabricated on macroporous support by all-vapor-phase processing

To investigate the feasibility of all-vapor-phase processing of ZIF-8 membrane on macroporous α-alumina support, we concentrated on optimizing conditions for ALD, ligand vapor treatment, and post-synthetic heat treatment. First, the ALD pulse time was examined based on previous data, with reports suggesting that an increase in pulse time could enhance the density of ZnO, ensuring full coverage of the support to reduce defects. As depicted in **Figure 2.23a**, the pulse times for diethylzinc (DEZ) and water (H_2O) were varied while being held at a fixed 1:1 ratio. It is evident that, with an increase in pulse time from 15 to 50 ms, the membrane permeance experienced a significant decrease, while the C_3H_6/C_3H_8 separation factor exhibited an increase.

When both the DEZ and H_2O pulse times were extended to 50 ms, the C_3H_6 permeance reached approximately ~3×10^{-9} mol Pa^{-1} m^{-2} s^{-1}, with the separation factor peaking at 70. Continuing to increase the DEZ and H_2O pulse times led to a subsequent increase in permeance. However, this prolonged increase ultimately resulted in minimal separation between C_3H_6 and C_3H_8, which might be attributed to membrane defects arising from the thick thickness of the deposited ZnO.

To examine the impact of H_2O pulse time on the membrane performance for C_3H_6/C_3H_8 separation, the H_2O pulse time was varied while maintaining a constant 50 ms for DEZ. As depicted in **Figure 2.23b**, the C_3H_6 permeance exhibited minimal variation or remained relatively constant with changes in the H_2O pulse time. However, a noteworthy observation was made at 100 ms H_2O pulse time, where the C_3H_6/C_3H_8 separation factor reached an impressive value of 100. This suggests a critical threshold in H_2O pulse time, indicating a significant influence on the membrane selectivity for C_3H_6/C_3H_8 separation. Considering both gas permeance and separation factor, the conditions of a 50 ms DEZ pulse time and a 100 ms H_2O pulse time were identified as optimal for the ALD process in fabricating ZIF membranes. These results demonstrated the critical role of reactant pulse times in regulating the C_3H_6/C_3H_8 selectivity.

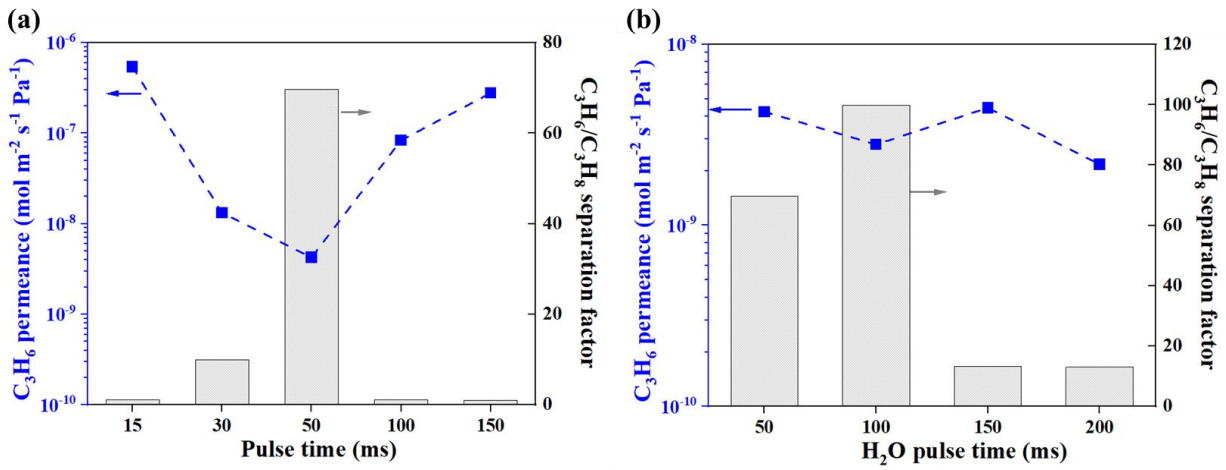

Figure 2.23 Effect of ALD pulse time. (a) Maintain consistent adjustments in DEZ and H_2O pulse times, (b)fix the DEZ pulse time at 50ms while varying H_2O pulse time from 50 ms to 200 ms.

After determining the optimal ALD pulse time, our investigation extended to explore the influence of ALD temperature on the properties of the membranes. As illustrated in Figure 2.24, we fabricated membranes using various ALD temperatures while maintaining the temperature for ligand vapor treatment unchanged at 125 °C. The diffraction patterns of the resulting membranes consistently exhibited ZIF-8 characteristic peaks at $2\theta = 7.4°$.

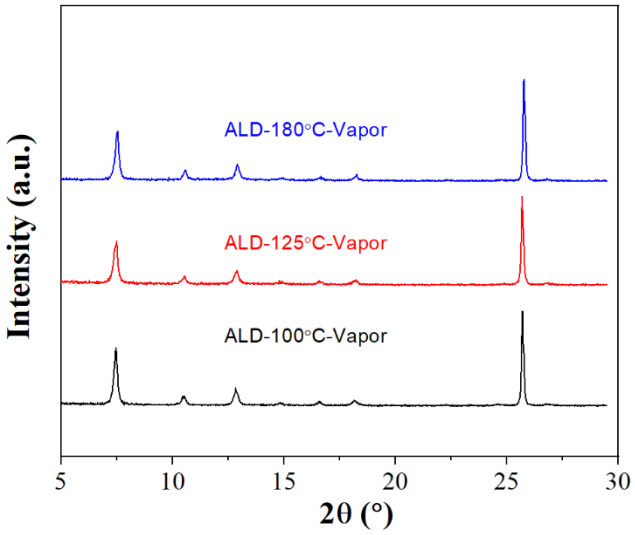

Figure 2.24 XRD patterns of ZIF membranes under different ALD temperatures.

The SEM images in **Figure 2.25** confirmed the formation of the ZIF phase on support. The morphologies of these membranes were similar to those of the ZIF-8 seed layer discussed in the previous section. However, the current ZIF membranes exhibited higher continuity and had fewer voids than the ZIF seed layer made by the vapor-phase seeding method. Furthermore, it is clear that the quality of ZIF membranes synthesized at the ALD temperature of 125℃ is better than that of membranes synthesized at 100℃ and 180℃ ALD temperatures. These findings suggest that the ALD temperature is a critical factor that influences the quality of the resulting ZIF membranes.

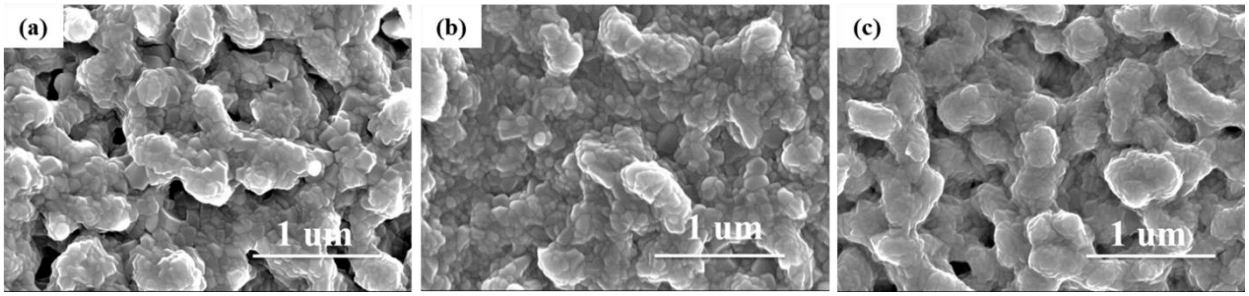

Figure 2.25 SEM images of ZIF membranes. (a) ZIF-8 membrane at 100℃ ALD temperature, (b) ZIF-8 membrane at 125℃ and (c) ZIF-8 membrane at 180℃.

The gas performance of the membranes was evaluated, and the results were presented in Table 2.2. The results indicate that the membranes synthesized at ALD temperatures of 125 ℃ exhibited significantly higher selectivity towards propylene and propane in comparison to the membranes synthesized at an ALD temperature of 100 ℃ and 180 ℃ . We also found that post-synthetic heat treatment under vacuum was an essential process for achieving high separation factor. When compared to membranes synthesized through the combination of vapor treatment and secondary growth methods, it is evident that the membrane separation factor achieved in the all-vapor-phase process is higher while the gas permeance is lower. Future work is needed to enhance the permeance.

Table 2.2 Gas performance of ZIF membranes prepared by all-vapor-phase synthesis method.

ALD temperature		**100℃**	**125℃**	**180℃**
Permeance	He	1.7E-07	1.0E-08	6.0E-08
	N_2	4.0E-08	2.2E-08	1.6E-08

	Propylene	4.3E-09	2.1E-09	8.0E-09
	Propane	6.3E-10	2.6E-11	6.6E-09
Separation factor	**He/N_2**	**4.3**	**4.6**	**3.7**
	Propylene/Propane	6.9	**78.9**	1.2

2.4 Conclusion

In conclusion, our study demonstrates the effectiveness of the vapor phase seeding approach, which relies on ALD and ligand vapor treatment, in creating uniform and compact ZIF-8 seeds that can be readily grown into high-performing ZIF-8 membranes. The ALD cycle number and precursor pulse time were found to influence membrane microstructure strongly, and varying these parameters can be used to tune the membrane performance. Moreover, the vapor seeding approach can produce thin, high-quality ZIF-8 membranes on mesoporous TiO_2 support, achieving superior performance with a propylene/propane separation factor of up to 152. Additionally, we have demonstrated the versatility of this approach by combining it with epitaxial growth to synthesize polycrystalline ZIF membranes with different structures, including ZIF-67 and ZIF-90. Moreover, it was discovered that a ZIF-8 membrane exhibiting a high separation factor can be synthesized directly on a macroporous support through all-vapor-phase synthesis, eliminating the need for solution-based secondary growth. This achievement involves extending the reactant pulse time and incorporating a post-synthetic heat treatment under vacuum. Our findings highlight the potential

of vapor-phase processing as a robust and versatile method for the fabrication of high-quality ZIF membranes for gas separation applications. A relatively high temperature (~125 °C) was used in our work for the ALD and ligand vapor treatment steps, necessitating the utilization of thermally stable support. Further improving the vapor-phase seeding method to lower the processing temperature would be highly beneficial, potentially enabling membrane fabrication on more cost-effective supports, such as polymer substrates. In addition, extending the vapor-seeding approach to supports with a tubular or hollow fiber geometry is vital for the scale-up of ZIF membranes.

Chapter 3 Unexpected High Performance of ZIF-8 Membranes for 1,3-butadiene Purification

Results of this chapter have been published in Wang, J.-W.; Qiang, Z.; Ma, X. 2023. Unexpected high performance of ZIF-8 membranes for 1, 3-butadiene purification[J]. *Journal of Membrane Science Letters*, 3(2): 100066.

Abstract

The purification of 1,3-butadiene from C_4 hydrocarbon mixtures currently relies on energy-intensive extractive distillation. In this study, we employed ZIF membranes for this challenging separation for the first time, unveiling their superior capability in isolating 1,3-butadiene from other C_4 hydrocarbons with similar sizes, including 1-butene, isobutene, and n-butane. This strong sieving effect was evident from two types of ZIF-8 membranes: one with low crystallinity fabricated via the all-vapor-phase ligand-induced permselectivation (LIPS) method and another with high crystallinity synthesized through the seeded growth method. The gas permeances decreased with increasing kinetic diameters, following the order of 1,3-butadiene (4.31 Å) > 1-butene (4.46 Å) > n-butane (4.687 Å) > isobutene (4.84 Å). The LIPS-ZIF-8 membrane exhibited a high 1,3-butadiene permeance of approximately 1.43×10^{-7} mol/m^2 s Pa (~430 GPU) and ideal separation factors of 18, 56, and 134 for 1,3-butadiene over 1-butene, n-butane, and isobutene, respectively. In separating four-component C_4 mixtures, these membranes could enrich 1,3-butadiene content from 50% in the feed to 96–98% in the permeate through a single separation step. This unprecedented performance is attributed to differences in C_4 diffusivities that span several orders of magnitude.

3.1 Introduction

1,3-butadiene (C_4H_6) is an essential industrial chemical utilized to produce synthetic rubbers and elastomers [96]. Approximately 95% of its production results from the by-product of ethylene production through steam cracking [97, 98]. This process generates C_4 hydrocarbon crude streams containing approximately 30–60% 1,3-butadiene, 10–20% 1-butene (1-C_4H_8), 10–30% isobutene (i-C_4H_8), and 3–10% butane (C_4H_{10}) [99, 100]. Separating 1,3-butadiene from these complex mixtures relies mainly on extractive distillation, which involves multiple distillation steps and substantial solvent usage [101, 102].

Introducing more efficient separation techniques could reduce energy consumption, costs, and the environmental impact of 1,3-butadiene purification [103, 104]. One such technique that has been extensively studied is adsorption using porous materials like zeolites [105, 106] and metal-organic frameworks (MOFs) [107-109]. Another promising approach is membrane separation, which has shown great potential in ethylene/ethane (C_2H_4/C_2H_6) and propylene/propane (C_3H_6/C_3H_8) separations [8, 32, 110, 111]. However, only a handful of studies explored membranes for 1,3-butadiene purification, primarily involving polymer [10, 112, 113], facilitated[114], and mixed matrix membranes [115, 116]. These membranes exhibited relatively low selectivities for 1,3-butadiene/1-butene and 1,3-butadiene/isobutene mixtures due to their similar physical properties. Additionally, prior studies were focused on binary gas mixtures, and membranes capable of purifying 1,3-butadiene from practically relevant multi-component mixtures resembling C_4 crude compositions have not been reported.

Among C_4 hydrocarbons, 1,3-butadiene possesses the smallest kinetic diameter. This suggests it can theoretically be separated using molecular sieve membranes with an appropriate pore size.

One potential membrane material is ZIF-8 because its effective pore size for molecular sieving (4.0–4.2 Å) is close to the kinetic diameter of 1,3-butadiene. Although ZIF-8 and other continuous MOF membranes have been well-studied for H_2/CO_2 [117-119], CO_2/CH_4 [120, 121], CO_2/N_2 [122-125], C_2H_4/C_2H_6 [126, 127], and C_3H_6/C_3H_8 separations [93, 128, 129], their use for C_4 separation remains unexplored. In this chapter, we revealed the unexpectedly high efficacy of two types of ZIF-8 membranes for separating 1,3-butadiene from C_4 mono-olefins and paraffin, even though the kinetic diameters of these compounds differ by less than one ångström. This strong sieving ability enabled the production of high-purity 1,3-butadiene (96–98%) from complex four-component C_4 mixtures via a single-step membrane separation. A mathematical gas permeation model was used to estimate the C_4 diffusivities to understand the origin of high membrane selectivity.

3.2 Experimental Section

3.2.1 Raw materials

High-purity alumina powder CR6 (Baikalox 1.0CR) from Baikowski International Corporation and nitric acid 1.0 N standardized solution (HNO_3, Alfa Aesar) were the main raw materials for the lab-made ceramic supports. Zinc nitrate hexahydrate ($Zn(NO_3)_2 \cdot 6H_2O$, 98%, Sigma-Aldrich), 2-methylimidazole (2-mIm, $C_4H_6N_2$, 99%, Sigma-Aldrich), methanol and DI water were used to prepare ZIF membranes. All chemicals were commercially obtained and used without further processing.

3.2.2 Fabrication of porous Al_2O_3 support

Laboratory-made porous α-alumina supports were employed as the substrate for the ZIF membrane development, the preparation of the lab-made supports was depicted in Chapter 2. The mesoporous support was prepared by coating a γ-Al_2O_3 layer on the surface of α- Al_2O_3 support. A boehmite sol was prepared through the hydrolysis of aluminum-tri-sec-butoxide in water under reflux at 90 °C. The concentration of the boehmite sols was fixed at 0.5 M and 0.25 M. These sols were then mixed with a 3 wt% PVA aqueous solution in a volume ratio of 20:13. After vortexing for 10 min, sonicating for 30 min, and degassing for 30 min, the γ-Al_2O_3 sol was left undisturbed under static conditions for at least 24 h. The γ-Al_2O_3 sols were coated on the top surface of the α-Al_2O_3 support using the dip coating. Initially, the sol prepared with 0.5 M boehmite sol was used, followed by heat treatment at 450 °C for 3 hours. Subsequently, the dip coating and heat treatment process was repeated using the sol prepared with 0.25 M boehmite sol.

3.2.3 Synthesis of ZIF-8 membranes

The first type of ZIF-8 membrane was prepared by the ligand-induced permselectivation method [16]. First, ZnO was deposited onto the Al_2O_3 supports using atomic layer deposition (ALD) with diethylzinc and water as vapor-phase reactants. Subsequently, the ZnO-modified support was placed vertically in a Teflon liner with approximately 0.2 g of 2-methylimidazole powders at the bottom. The liner was sealed in an autoclave and heated to 125 °C for 24 h. After the conversion of the deposited ZnO to ZIF-8, the membrane was activated in a vacuum oven at 100 °C for 24 h.

The second type of ZIF-8 membrane was prepared through a combination of vapor-phase seeding and solution-based secondary growth, as we recently reported [130]. Initially, ALD was used to deposit ZnO on macroporous α-Al_2O_3 supports at 125 °C. To create the ZIF-8 seeds layer,

the ZnO-modified support was exposed to 2-methylimidazole vapors at 125 °C for 24 h. Subsequently, the ZIF-8-seeded support was immersed vertically in a solution consisting of 2.27 g 2-methylimidazole and 0.11 g Zn $(NO_3)_2 \cdot 6H_2O$ dissolved in 40 mL of deionized water at 30 °C for 6 h. After synthesis, the membrane was rinsed with methanol and air-dried for 24 hours before conducting gas permeation tests and structure characterizations.

3.2.4 Synthesis of ZIF-8 crystals

The ZIF-8 crystals used in the adsorption experiment were synthesized through the solvothermal synthesis method. Solution A was prepared by dissolving 3.528 g Zn $(NO_3)_2 \cdot 6H_2O$ in 40 ml of methanol. Solution B was prepared by dissolving 1.944 g 2-methylimidazole and 0.807 g sodium formate in 40 ml of methanol. Solution B was slowly added to solution A under stirring. The molar ratio of $Zn(NO_3)_2$/2-methylimidazole/sodium formate/methanol in the solution was 1:2:1:166.5. The solution was heated to 90℃ for 24 h in an autoclave. The resulting ZIF-8 powders were collected, washed extensively with methanol, and dried at room temperature under vacuum.

3.2.5 Characterizations

The X-ray diffraction patterns (XRD) of supports and membranes were obtained using a Bruker D8 Discover A25 diffractometer equipped with a Cu Kα X-ray radiation source (40 kV and 40 mA, λ=0.154 nm). Scanning electron microscope (SEM) images were collected on Hitachi S4800 field emission SEM coupled with energy dispersive X-ray analysis (EDS), operating at 15 kV. Samples were coated with 5 nm thick iridium in the Emitech K575X Sputter before SEM analysis.

3.2.6 Gas permeation measurement

Single gas permeation was measured using the apparatus shown in **Figure 3.1a**. Feed gas pressure was controlled by the pressure regulator and the flow controller, and the membrane permeation temperature was maintained using a water batch. Single gas permeance was determined by measuring the rate of pressure change on the permeate side. For two-component and four-component gas mixture separation measurements (**Figure 3.1b**), the feed gas composition was regulated using a flow meter. Argon was used as the sweep gas to carry the permeated gases to gas chromatography (GC) for composition analysis.

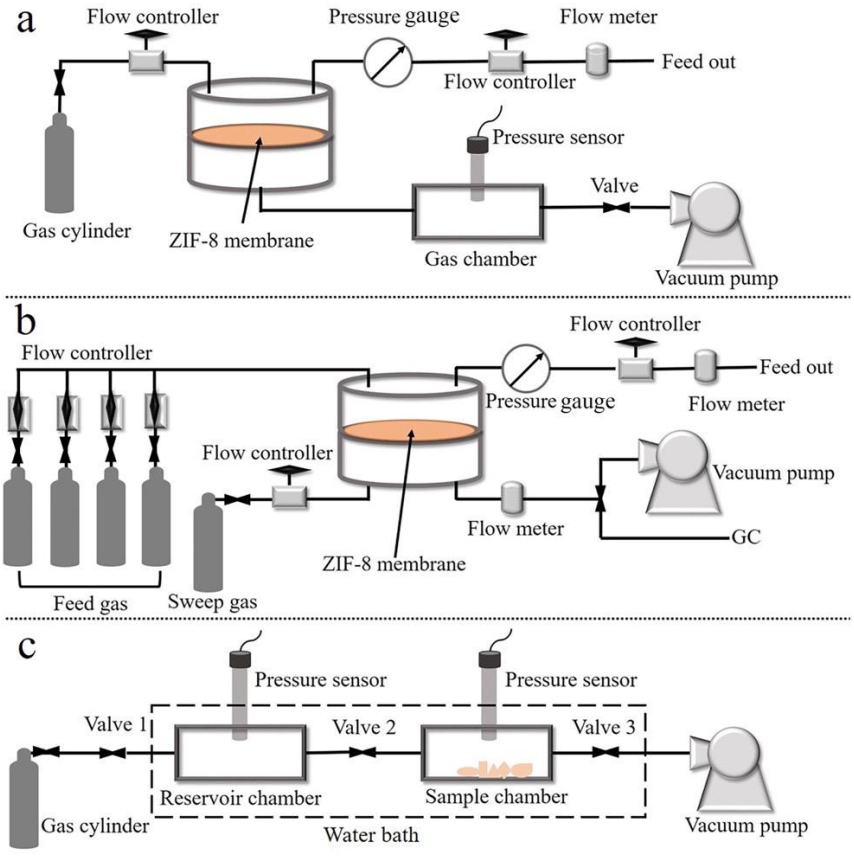

Figure 3.1 Schematic diagram of apparatus for the measurement of (a) single gas permeation, (b) mixed gas permeation and separation, and (c) adsorption isotherm of 1,3-butadiene on ZIF-8 crystals.

3.2.7 Adsorption isotherm measurement

The adsorption isotherm of 1,3-butadiene in ZIF-8 was measured using a dual-volume pressure decay apparatus using ZIF-8 microcrystals prepared by solvothermal synthesis (**Figure 3.1c**). The ZIF-8 crystals, wrapped in Al foil, were activated at 150 ^{o}C under vacuum overnight and subsequently transferred to the sample chamber. The system was then evacuated overnight. The temperature was maintained at 35 ^{o}C using a water bath. 1,3-butadiene was introduced to the sample chamber, and the subsequent pressure drop was monitored and used to deduce the volume of gas adsorbed by the ZIF-8 crystals. The resultant adsorption isotherm curve was fitted using the Langmuir model (Eq. (3.1)):

$$\mathrm{C(p)} = \frac{C_s bp}{1+bp} \tag{3.1}$$

where p is the equilibrium pressure (bar), $C(p)$ is the amount adsorbed (mmol/g), C_s is the adsorption capacity (mmol/g), and b is the affinity constant (1/bar).

3.2.8 Estimation of diffusivities

A gas permeation model developed for microporous membranes in conjunction with adsorption data was employed to calculate the C_4 diffusivities through the ZIF-8 membrane. With the permeate side under approximately zero pressure, the mathematical expression of this model is given by Eq. (3.2) [82, 131]:

$$F = \frac{\phi \rho C_S D_c}{P_f L} ln\left(1 + bP_f\right) \tag{3.2}$$

In which ϕ is defined as the ratio of porosity (ε) and tortuosity (τ) of ZIF-8, ρ is density, L is membrane thickness, and D_c is the calculated diffusivity. From the equation, plots of $F \times P_f$ against

$ln(1+bP_f)$ can be linearly correlated. The slope, $\phi\rho C_s D_c/L$, can subsequently be used to calculate the diffusivity.

3.3 Results and discussion

3.3.1 Structure characterization

The first membrane, designated as LIPS-ZIF-8, was fabricated on a mesoporous γ-alumina support by the all-vapor-phase LIPS method. This membrane displayed weak ZIF-8 XRD peaks and featured nanoparticles lacking distinct crystal facets on the support surface, suggesting a low crystallinity of the formed ZIFs (**Figure 3.2**). Determining the membrane thickness from the cross-section SEM image proved challenging due to the presence of amorphous-like ZIFs on the support surface and within the γ-alumina layer. These observations are consistent with those reported by Ma, Tsapatsis, and co-workers [16]. The second membrane, referred to as SG-ZIF-8, was prepared on a macroporous α-alumina support using seeded growth method, which combined vapor-phase seeding to generate ZIF-8 nanoparticles on the surface of alumina grains and a solution-based secondary growth to grow these seeds into a continuous membrane layer. The resulting membrane exhibited strong XRD peaks characteristic of ZIF-8, along with highly intergrown crystals forming a membrane layer with a thickness of approximately 1.8 μm (**Figure 3.2**).

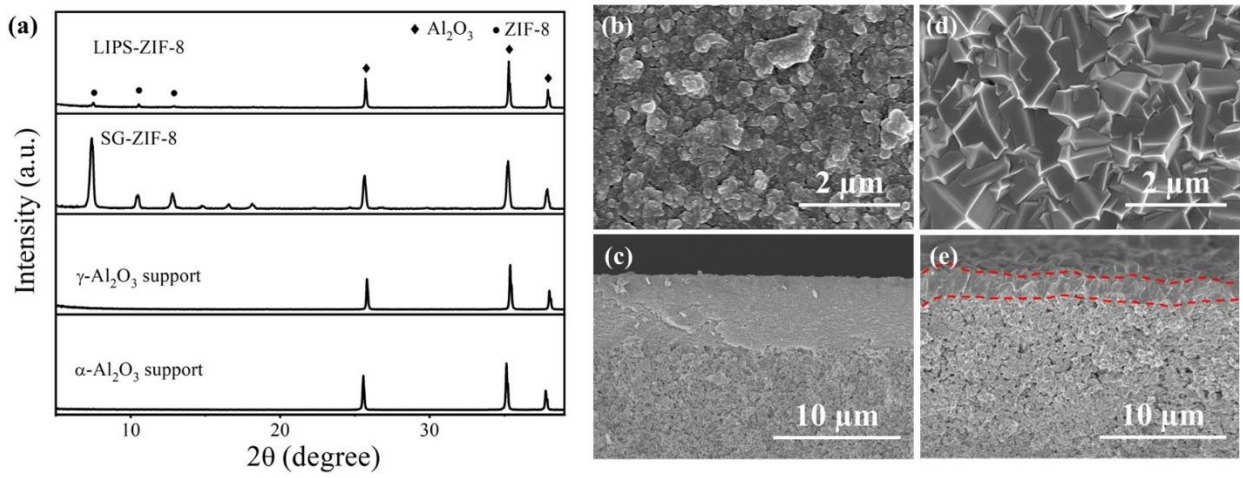

Figure 3.2 (a) XRD patterns of supports and membranes. (b, c) SEM images of LIPS-ZIF-8 membrane. (d, e) SEM images of SG-ZIF-8 membrane.

3.3.2 C_4 hydrocarbon single gas permeation

Figure 3.3a displays the C_4 single gas permeances through the LIPS-ZIF-8 membrane. The observed trend shows a decrease in permeance as the kinetic diameter increases, following the order of 1,3-butadiene (4.31 Å) > 1-butene (4.46 Å) > n-butane (4.687 Å) > isobutene (4.84 Å). There is a sharp cut-off in permeance between 1,3-butadiene and the other hydrocarbons. The LIPS-ZIF-8 membrane showed a high permeance of ~1.43×10^{-7} mol/m^2 s Pa (~430 GPU) for 1,3-butadiene, which was 10–100 times higher than that of the other gases. These considerable differences in permeances translated to ideal separation factors of 18, 56, and 134 for 1,3-butadiene over 1-butene, n-butane, and isobutene, respectively (**Table 3.1**). Similar trends in C_4 permeances were observed in the SG-ZIF-8 membrane, which displayed higher separation factors (**Figure 3.3b** and **Table 3.1**). Given the sub-ångström differences in the kinetic diameters of C_4 molecules, these findings are unexpected, highlighting the exceptional molecular sieving capability of ZIF membranes based on size and shape. Moreover, the high permeance of 1,3-butadiene, despite its

kinetic diameter exceeding the crystallographic aperture size of ZIF-8 (3.4 Å), provides evidence for ligand motion and aperture flexibility induced by the interaction with 1,3-butadiene molecules.

The effect of feed pressure on permeances was subsequently studied. Given the low vapor pressure of C_4 at room temperature, the highest achievable pressure during permeation testing was typically below 275 kPa. All C_4 permeances exhibited a slight decrease as the feed pressure increased (**Figure 3.3c**), which could be attributed to the nonlinearity of the Langmuir adsorption isotherms for these gases on ZIF-8 [28, 132]. The ideal separation factors remained consistent across the tested pressure range (**Figure 3.3d**), indicating the excellent stability of the membrane structure when exposed to C_4 hydrocarbons at different pressures.

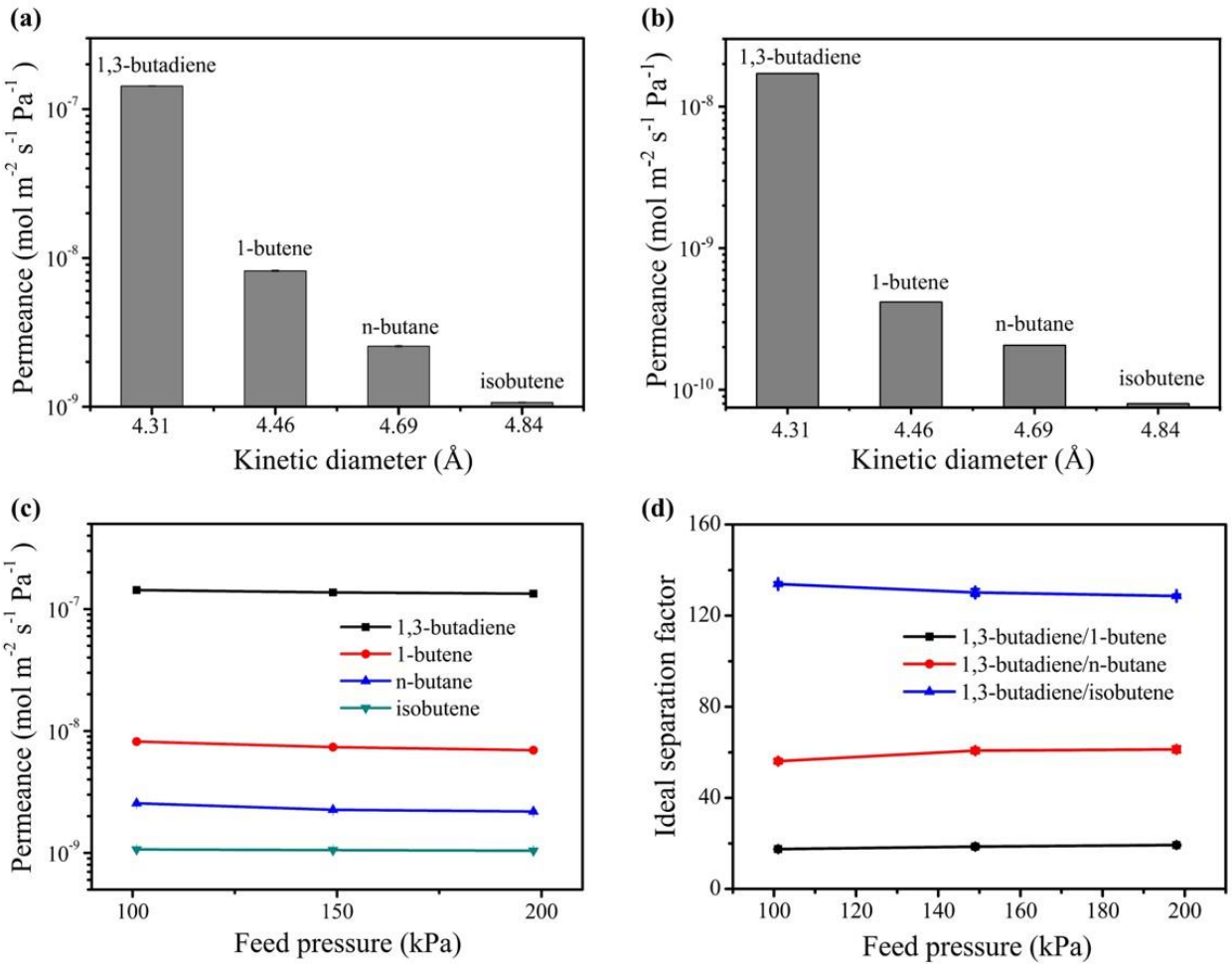

Figure 3.3 Single gas permeances of C_4 hydrocarbons through (a) LIPS-ZIF-8 and (b) SG-ZIF-8 membranes. Pressure dependence of (c) single gas permeances and (d) ideal separation factors of LIPS-ZIF-8 membrane.

Table 3.1 Ideal separation factors for the ZIF-8 membranes synthesized in this study.

Membrane	1,3-butadiene/ 1-butene	1,3-butadiene/ n-butane	1,3-butadiene/ isobutene
LIPS-ZIF-8	18	56	134

SG-ZIF-8	43	87	223

3.3.3 Membrane performance for C4 mixtures separation

The LIPS membrane's efficacy in separating 1,3-butadiene from C_4 mixtures was first assessed using three binary mixtures: 1,3-butadiene/1-butene, 1,3-butadiene/isobutene, and 1,3-butadiene/n-butane (**Figs. 3.4a, 3.4b, and 3.5**). A high 1,3-butadiene permeance between 1-2×10^{-7} mol/m^2 s Pa (~300–600 GPU) and good mixture separation factors were achieved. In all cases, the separation factors were slightly lower than the ideal separation factors obtained from single gas permeances. This could be attributed to increased aperture flexibility from the presence of 1,3-butadiene, which slightly impacts the sieving effect and might also be due to competitive adsorption and diffusion in mixed gas permeation. The separation factors achieved by our membranes are much higher than those reported for other membrane systems (**Table 3.2**).

For a more complex test, we used a four-component C_4 hydrocarbon mixture with a composition of 50%:20%:20%:10% (denoted as 5:2:2:1) for 1,3-butadiene/1-butene/isobutene/n-butane as the feed, which was used in literature to replicate practically relevant C_4 mixtures [99, 100]. Notably, the LIPS-ZIF-8 membrane was highly effective in separating 1,3-butadiene from this intricate mixture across various feed pressures, with 1,3-butadiene permeance similar to that measured from binary gas permeation (**Figure 3.4c**). Through a one-step membrane separation, the 1,3-butadiene content was enriched from 50% in the feed to ~97.05% in the permeate at 1 bar feed pressure (**Figure 3.4d**). Considering the variability in C_4 mixture composition during steam cracking, the LIPS membrane was further tested with three different C_4 formulations and it was proved effective in all instances (**Figure 3.6**). In addition, the SG-ZIF-8 membrane was assessed

with a 5:2:2:1 mixture, and it could enhance the 1,3-butadiene content to 97.7% in the permeate (**Figure 3.7**). These results have demonstrated the effectiveness of ZIF-8 membranes in purifying 1,3-butadiene from practically relevant complex mixtures, a performance that no other membranes have achieved.

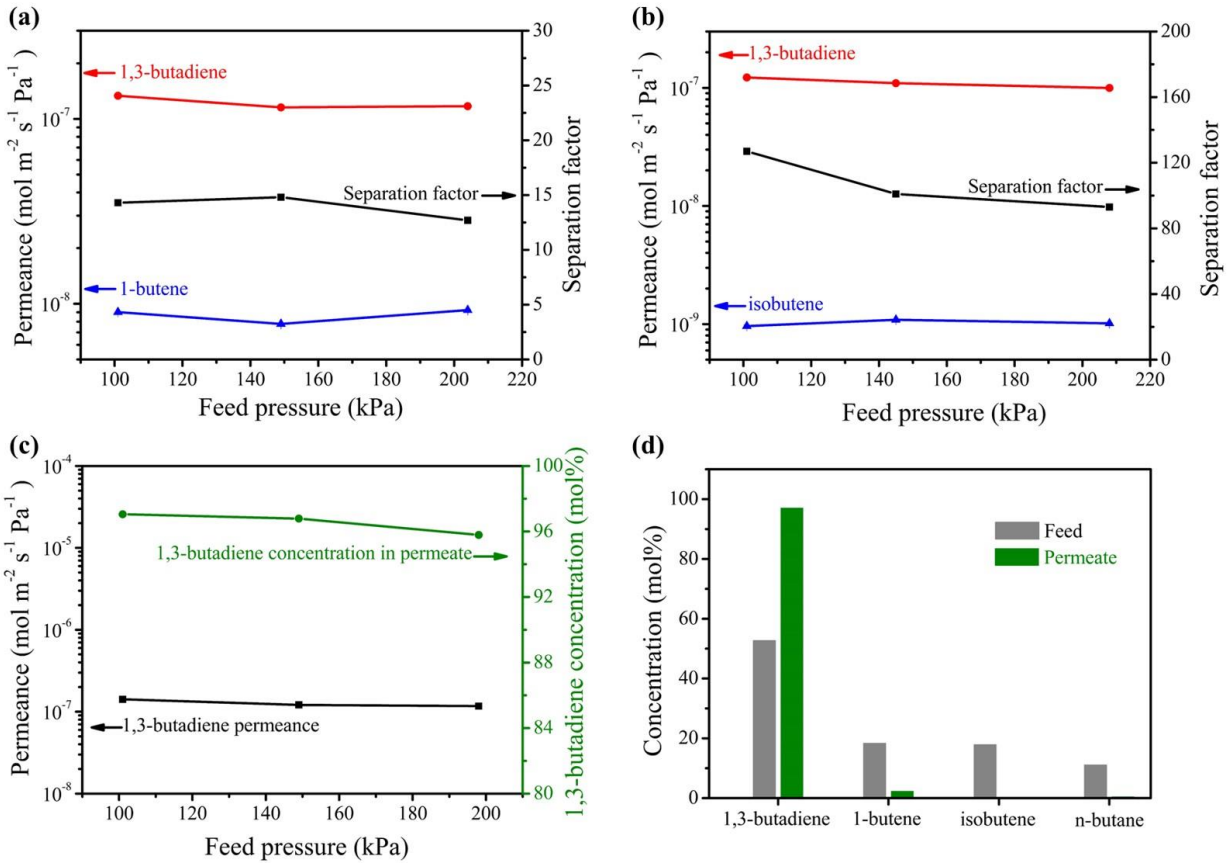

Figure 3.4 Performance of LIPS-ZIF-8 membrane for separating (a) 1,3-butadiene/1-butene and (b) 1,3-butadiene/isobutene binary mixtures. (c) Performance for separating 5:2:2:1 1,3-butadiene/1-butene/isobutene/n-butane mixture and (d) concentrations of each gas on the feed and permeate sides.

Table 3.2 1,3-butadiene separation performances of membranes reported in literature. Only binary mixed gas separation performances were reported in the literature.

Membrane	Feed gas	1,3-Butadiene permeance mol/(m^2 s Pa)	Selectivity	Ref
Zwitterionic silver complex polyester composite membranes	1,3-butadiene/1-butene	/	2.3	[114]
	1,3-butadiene/isobutene	/	4.1	
6FDA/BPDA-DDBT hollow fiber	1,3-butadiene/n-butane	2.48× 10^{-9}	69	[10]
PEBAX2533	1,3-butadiene/n-butane	1.42× 10^{-9}	3.1	[112]
	1,3-butadiene/isobutane		7.5	
	1,3-butadiene/1-butene		2.4	
	1,3-butadiene/isobutene		2.8	
	1,3-butadiene/n-butane	3.68× 10^{-10}	8.7	

PolyActive1500PE GT77PBT23	1,3-butadiene/isobutane		18.8	
	1,3-butadiene/1-butene		3.6	
	1,3-butadiene/isobutene		4.2	
PolyActive4000PE GT77PBT23	1,3-butadiene/n-butane	4.82×10^{-11}	7.3	
	1,3-butadiene/isobutane		19.4	
	1,3-butadiene/1-butene		3.7	
	1,3-butadiene/isobutene		4.5	
Carbonized hollow fiber membranes	1,3-butadiene/n-butane	2.68×10^{-8}	50	[133]
Silver salt/Nafion blend membrane	1,3-butadiene/1-butene	4.8×10^{-10}	1.4	[134]
ZIF-8 membrane	1,3-butadiene/1-butene	1.43×10^{-7}	18	This work
	1,3-butadiene/n-butane		56	
	1,3-butadiene/isobutene		134	

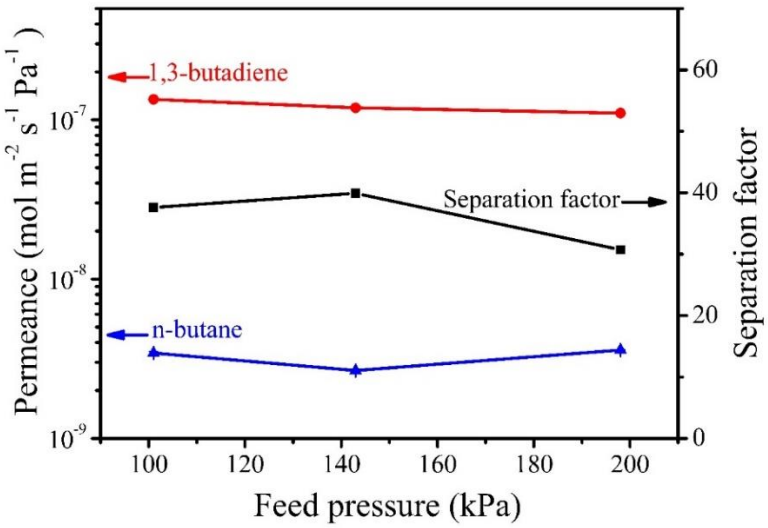

Figure 3.5 Performance of LIPS-ZIF-8 membrane for separating 1,3-butadiene/n-butane binary mixture.

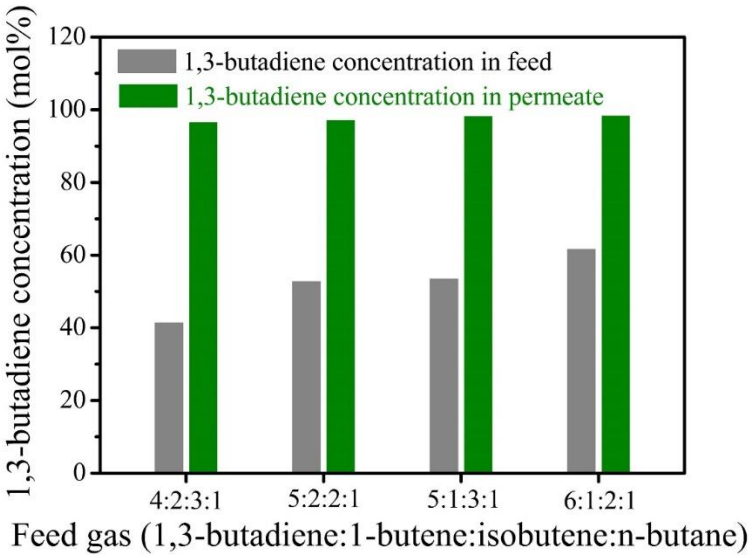

Figure 3.6 Performance of LIPS-ZIF-8 membrane for separating four-component 1,3-butadiene/1-butene/isobutene/n-butane mixtures with a composition of 4:2:3:1, 5:2:2:1, 5:1:3:1 and 6:1:2:1.

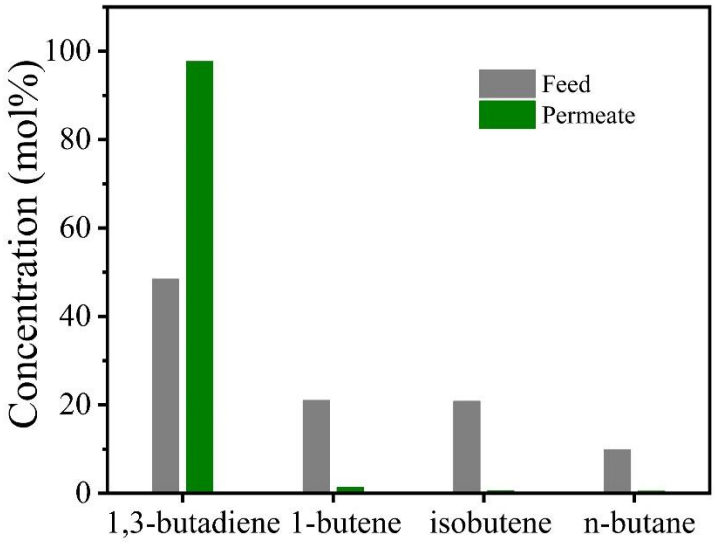

Figure 3.7 Performance of SG-ZIF-8 membrane for separating a four-component 1,3-butadiene/1-butene/isobutene/n-butane mixtures with a composition of 5:2:2:1. The gray and green columns show the concentrations of each gas on the feed and permeate sides, respectively.

3.3.4 Estimation of C4 diffusivities

The objective of this section was to elucidate the separation mechanism. Previous studies have demonstrated that ZIF-8 crystals exhibited comparable adsorption equilibrium properties for C_4 molecules [28, 108], suggesting that the primary reason for the superior membrane performance could be differences in diffusivity. Koros et al. calculated the transport diffusivities of 1-butene, isobutene, and n-butane in ZIF-8 crystals using kinetic uptake rate experiments; however, their study did not encompass 1,3-butadiene [28]. The 1,3-butadiene diffusivity in ZIF-8 was only investigated through molecular simulation in another study [132]. Herein, we employed a consistent method to estimate C_4 diffusivities through the ZIF-8 membrane by analyzing the gas permeance data using a gas permeation model (Eq. (3.2)) [82, 131]. Lin and co-workers

demonstrated that this model is reliable for obtaining diffusivities for gas molecules, such as propylene and propane, through ZIF-8 membranes [82].

The crystalline SG-ZIF-8 membrane was selected for the estimation because its thickness (~1.8 μm) can be reliably determined from the side-view SEM image. **Figure 3.8** illustrates the pressure dependence of C_4 single gas permeances through the SG-ZIF-8 membrane at 35 °C and the plots of $F \times P_f$ against $ln(1 + bP_f)$. Linear fitting provided the slope ($\phi\rho C_s D_c/L$) values (**Table 3.3**). Porosity (ε, 58.8%), density (ρ, 0.95 g/cm^3), and tortuosity (τ, 0.338) of ZIF-8, and C_s and b values for 1-butene, n-butane, and isobutene were extracted from the literature [28, 82]. In the case of 1,3-butadiene, which lacked available data in existing literature, we determined C_s and b by fitting the adsorption isotherm using the Langmuir model (**Figure 3.9** and **Table 3.3**). Substituting these values into the slope expression, the calculated results showed a drastic decrease in C_4 diffusivity with increasing kinetic diameters. In particular, 1,3-butadiene diffusivity (9.44×10^{-9} cm^2/s) was several orders of magnitude higher than the others. These results have concluded that the significant difference in diffusivities is the principal factor contributing to the high membrane performance.

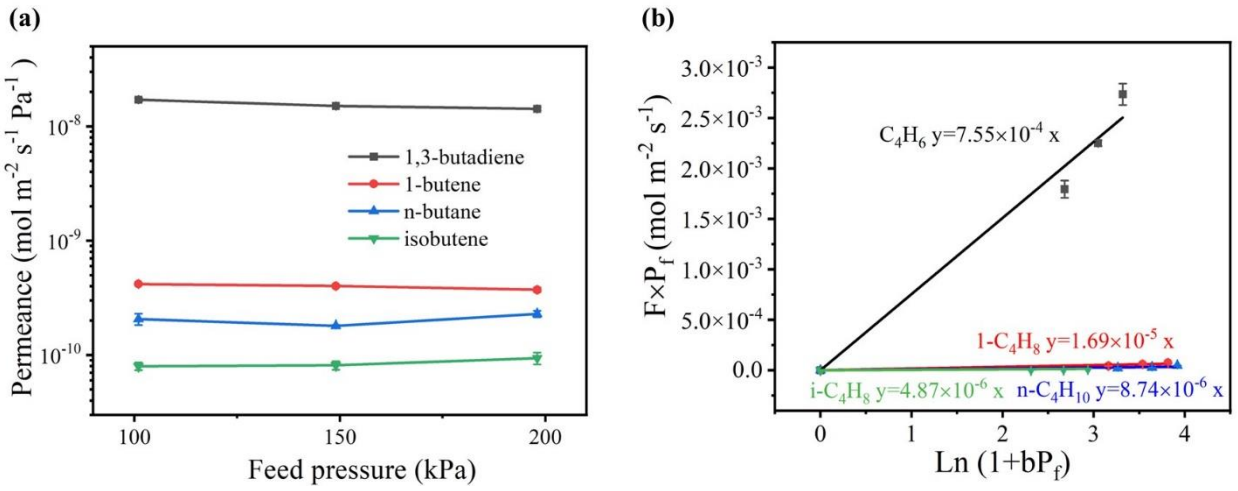

Figure 3.8 (a) C_4 single gas permeances at 35 °C and (b) $F \times P_f$ versus $\ln(1+bP_f)$ for the SG-ZIF-8 membrane.

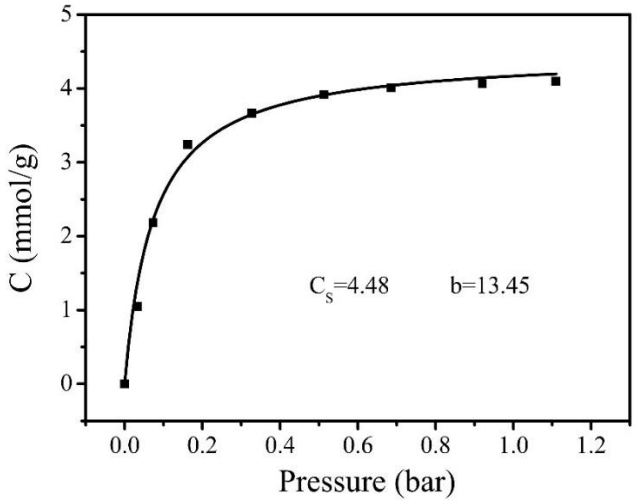

Figure 3.9 Adsorption isotherm of 1,3-butadiene on ZIF-8 crystals.

The high transport diffusivity of 1,3-butadiene may be linked to several factors: (1) 1,3-butadiene predominantly adopts the trans conformation, characterized by a relatively thin and elongated shape with smaller molecular dimensions (**Table 3.4**), facilitating its diffusion through

the slit-like ZIF pore channels; (2) compared to other C_4 molecules, 1,3-butadiene possesses a larger quadrupole moment (-5.5 DÅ) (**Table 3.4**) [108], possibly leading to stronger interactions with the ZIF-8 framework; and (3) 1,3-butadiene might induce greater ligand rotation within ZIF-8, resulting in increased aperture flexibility.

Table 3.3 Isotherm parameters and calculated diffusivities of C_4 gases through the SG-ZIF-8 membrane at 35 ºC.

C_4 gas	C_S (mmol/g)	b (1/bar)	$\phi\rho C_S D_c/L$ (mol/m^2 s)	D_c (cm^2/s)
1,3-butadiene (C_4H_6)	4.48	13.45	7.55×10^{-4}	9.44×10^{-9}
1-butene (1-C_4H_8)	4.28[a]	22.4[a]	1.69×10^{-5}	2.21×10^{-10}
n-butane (n-C_4H_{10})	3.91[a]	24.9[a]	8.74×10^{-6}	1.25×10^{-10}
isobutene (i-C_4H_8)	5.08[a]	9.0[a]	4.87×10^{-6}	5.38×10^{-11}

[a] Values from Zhang et al. [28].

Table 3.4 Physical properties of C_4 hydrocarbon molecules [100, 108].

C_4 hydrocarbons	Kinetic diameter (Å)	Molecular dimensions (Å^3)	Quadrupole moment (DÅ)
trans-1,3-butadiene	4.31	7.9×5.2×3.4	-5.469
cis-1,3-butadiene		7.6×5.4×3.6	

trans-1-butene	4.46	7.9×5.4×5.3	-1.876
cis-1-butene		7.6×5.5×4.2	
isobutene	4.84	6.8×5.8×4.2	-2.006
trans-n-butane	4.687	8.1×4.6×4.2	0.433
cis-n-butane		7.6×5.6×5.2	

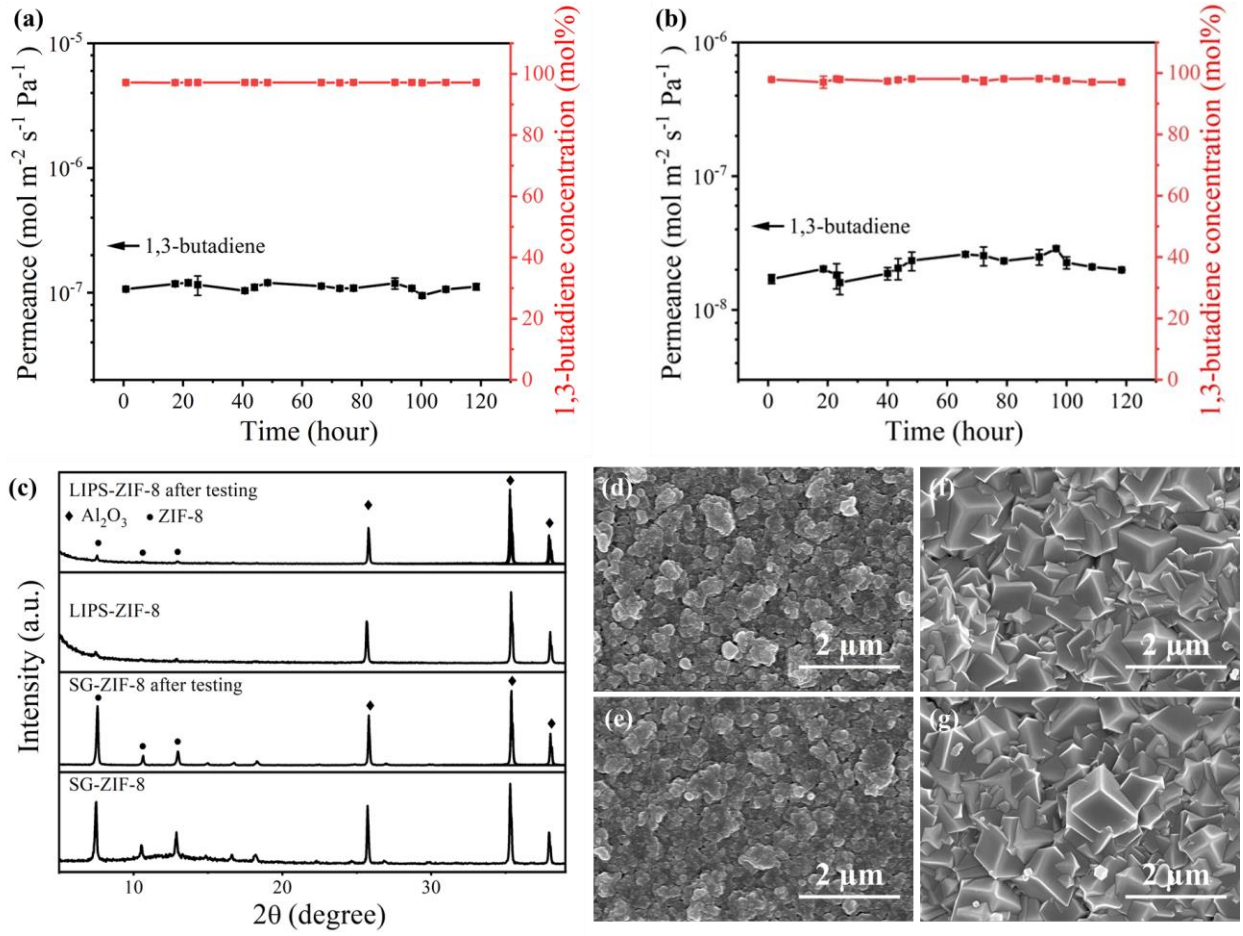

Figure 3.10 Long-term stability performance (a) LIPS-ZIF-8, (b) SG-ZIF-8 membrane, (c) XRD patterns and (d-g) SEM images for both membranes before and after long-term operation.

In addition, we have conducted a series of experiments to assess the long-term stability of our membranes when exposed to a C4 hydrocarbon mixture in a ratio of 5:2:2:1. The stability of membrane performance has been shown in **Figure 3.10a** (LIPS-ZIF-8 membrane) and **Figure 3.10b** (SG-ZIF-8 membrane). Impressively, even after 120 hours of continuous exposure to the C4 mixture, the membranes exhibited robust separation performance. Specifically, the 1,3-butadiene concentration in the permeate side remained at an impressive 97.1% for the LIPS-ZIF-8 membrane and 97.7% for the SG-ZIF-8 membrane. Furthermore, we employed XRD (**Figure 3.10c**) and SEM

(**Figure 3.10d-g**) to examine both the crystalline structure and surface morphology of the membranes before and after the long-term stability testing. Our analysis revealed that there were no discernible effects of long-term operation on the stability of the membranes. The XRD patterns before and after exposure showed no significant changes in the membrane's crystalline structure. The SEM images indicated that the surface morphology of the membranes remained largely unchanged, with no notable cracks or holes. Therefore, the long-term exposure to the C4 mixture did not induce any adverse impacts on the structure, morphology, or performance of the membranes. Regarding the comparison between the two types of membranes, our findings indicate that there is no substantial difference in their long-term stability. Both the LIPS-ZIF-8 and SG-ZIF-8 membranes demonstrated similar resilience to the extended exposure, confirming the robustness of our membrane performance.

3.4 Conclusions

In conclusion, we have uncovered high performance in two distinct ZIF-8 membranes, synthesized via different methods and exhibiting varied crystallinity, in purifying 1,3-butadiene from other C4 hydrocarbons that have similar kinetic diameters. For both membrane types, 1,3-butadiene permeance exceeded that of 1-butene, isobutene, and n-butane by one to two orders of magnitudes. In mixed gas separation, a single membrane separation step could increase the molar percentage of 1,3-butadiene from 50% in four-component C4 mixtures to approximately 96–98% in the permeate. Analysis of gas permeances with a mathematical model revealed significant differences in C4 diffusivities that contributed to the effective separation of the C4 molecules. These findings underscore the high efficacy of ZIF-8 membranes in 1,3-butadiene purification and the potential of molecular sieve membranes for challenging and complex gas separations.

Chapter 4 Three-dimensional Covalent Organic Frameworks for Membrane Separation: Literature Review

A large number of nanoporous materials have been widely studied in recent years owing to their excellent and specific properties such as large and permanent porosity [135-139]. The development of nanoporous materials has made great contributions to various applications, including adsorption, catalysis, energy storage [140], optics, electronics [141], and the field of membrane separation [142-145]. Membrane separation has made leaps and bounds in the past few decades due to its low energy consumption and pollution, easy operation, which is in line with the current sustainable development background, and it can meet the challenges of energy and environmental eco-friendliness [145].

The nanoporous materials, which include those based on inorganic building blocks such as zeolites [120, 146, 147] and hybrid materials containing organic components, have gained significant popularity in research [135, 139, 148]. For example, uniform amorphous nanoporous organic polymers composed of multifunctional structural units linked by covalent bonds have been synthesized [139, 148, 149]. In contrast, as a typical representative, metal-organic frameworks (MOFs) with high crystallinity, composed of metal ions or clusters connected by organic ligands through coordination bonds, have been extensively investigated [143, 150, 151]. Furthermore, covalent organic frameworks (COFs) have attracted great attention, which were first created by Yaghi and co-workers in 2005 [152].

4.1 COFs and 3D COFs

Covalent organic frameworks (COFs) are a class of crystalline porous polymers that were first reported by Yaghi and co-workers in 2005 [152]. COFs are composed of organic building blocks periodically connected by covalent bonds [152-155]. They have the advantages of structural diversity, large surface area, tunable pore size and structure, thermal stability, and low density [156, 157], and they have been studied for many applications such as adsorption, catalysis, separation, sensor, and energy storage [141, 145]. The structure and properties of COFs can be adjusted by using different combinations of monomers and/or introducing various functional sites on the organic linker, making them a promising materials platform for the design and construction of membranes [145]. Based on the dimensions of the connection, COFs can be classified into two-dimensional (2D) COFs and three-dimensional (3D) COFs [157]. Most of the current research is focused on 2D COFs that are constructed from planar monomers with a relatively large pore size (>8 Å) [158, 159]. In contrast, 3D COFs are built from 3D building blocks and can have more complex structures [157]. In addition to possessing high surface area and structural tunability, 3D COFs also feature a distinctive characteristic: the interpenetration of channels and cages. As a result, their effective pore size can be reduced, thereby achieving more effective separation [159, 160].

The design and synthesis of 3D COFs require careful consideration of several important factors, including topology, linkage, and building blocks. Topology directly determines the pore structures, properties, and potential applications of 3D COFs. Some common topologies in 3D COFs include ctn topology represented by COF-102, COF-103 and COF-105, bor topology with COF-108 as a typical representative [158], dia-c5 in COF-300 [41], and some other topologies

such as pts, rra, srs, ffc and lon, etc. (The topology structures are shown in **Figure 4.1.**reproduced from ref. [157]).

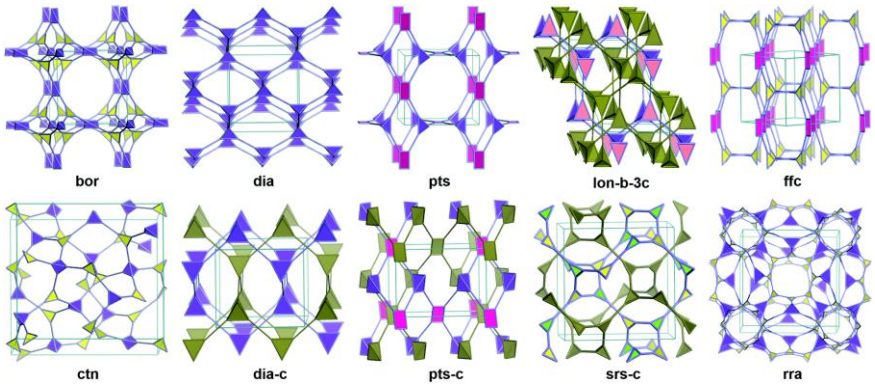

Figure 4.1 Topologies in 3D COFs (reproduced from ref. [157] with permission from Chemical Society Reviews, Copyright 2020).

Table 4.1 Synthesis Methods and Structures Information of 3D COFs.

3D COFs	**Topologies**	**Linkages**	**Building Blocks**	**Synthesis Methods**	**Structure Information**	**Ref.**
COF-300	dia	Imine	Tetrahedral TAPM	Solvothermal	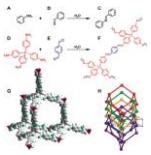	[41, 161-163]
COF-320	dia	Imine	Tetrahedral TAPM	Solvothermal		[164, 165]

3D-Por-COF	pts	Imine	Tetrahedral and square TAPM	Solvothermal	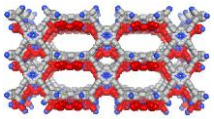	[166]
3D-CuPor-COF	pts	Imine	Tetrahedral and square TAPM	Solvothermal	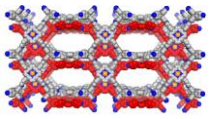	[166]
3D-OH-COF	dia	Imine	Tetrahedral TFPM	Solvothermal	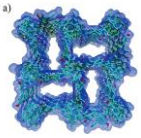	[155, 167, 168]
3D-COOH-COF	dia	Imine	Tetrahedral TFPM	Solvothermal	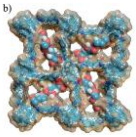	[155, 168]
3D-IL-COFS	dia	Imine	Tetrahedral TFPM	Ionothermal	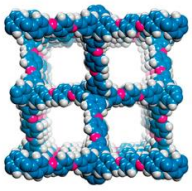	[169]
3D-TPB-COF-OMe	pts	Imine	Tetrahedra and quadrilateral TAPM	Solvothermal	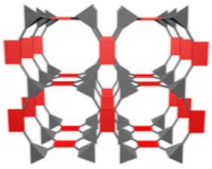	[170]

3D-TPB-COF-Ph	ljh	Imine	Tetrahedra and quadrilateral TAPM	Solvothermal	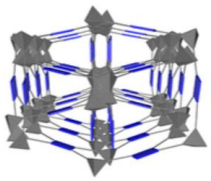	[170]

The linkage is the crucial factor determining whether the reaction can happen. In the beginning, two linkages mainly used in 3D COFs are B-O linkages, including boroxine (COF-102 and COF-103) and boronate ester rings (COF-105 and COF-108), which were first proposed by Yaghi and co-workers [158]. Compared with B-O linkages, the imine linkage (C=N) is more stable and has become the most frequently used linkage in 3D COFs reported in the literature.

The tetrahedral building blocks, which are composed of a tetrahedral core and four identical functional groups, are widely used in 3D COFs (**Table 4.1**). Tetraphenylmethane (TAPM) with various functional groups, such as amino (COF-300 and COF-320), aldehyde (3D-OH-COF and 3D-COOH-COF), is the most common knot in 3D COFs. COF-300, a representative 3D COF using amino as the functional group of TAPM, was designed using the tetrahedral building block tetra-(4-anilyl) methane and terephthaldehyde as a linear linker [41]. The single-crystal structure of COF-320, formed by linking the tetrahedral building blocks (Tetra-(4-anilyl) methane) and biphenyl linkers (4,4′-Biphenyldicarboxaldehyd) through imine bonds, showed a three-dimensional organic framework with a diamond net [165]. The 3D porphyrin-based COFs, namely 3D-Por-COF and 3D-CuPor-COF, were successfully synthesized using tetrahedral (3D-Td) and square (2D-C4) precursors interconnected through [4 + 4] condensation reactions. These COFs are suggested to exhibit a 2-fold interpenetrated pts topology within the *Pmc2₁* space group [166].

Additionally, two highly crystalline 3D COFs, 3D-TPB-COF-Ome, and 3D-TPB-COF-Ph, were synthesized through the polycondensation of TAPM and methoxy- or phenyl-substituted 1,2,4,5-tetrakis(4-formylphenyl)benzene. The structural analysis revealed that 3D-TPB-COF-Ome features a 5-fold interpenetrated structure with a pts net. In contrast, 3D-TPB-COF-Ph adopts an unprecedented self-penetrated ljh topology [170].

Another type of 3D COFs were prepared by using tetrakis(4-formylphenyl)methane (TFPM) aldehyde as the functional group; for example, in 3D-OH-COF and 3D-COOH-COOF, the tetrakis (4-formylphenyl)-methane (TFPM) is used as the tetrahedral monomer with a linear linker (3,3′-dihydroxybenzidine ($BD(OH)_2$)) to produce 3D framework structure [155]. Furthermore, a series of 3D ionic liquid (IL)-containing COFs, denoted as 3D-IL-COFs, were synthesized with multifold interpenetrated diamondoid (dia) nets. The synthesis involved using IL as a green solvent. The tetrahedral building blocks TFPM were reacted with linear links of increasing size, namely p-phenylenediamine (PDA), 4,4′-diaminobiphenyl (DABP), or 4,4″-diamino-p-terphenyl (DATP), resulting in the formation of extended 3D interpenetrated dia structures [169].

4.2 3D COF Membranes

The attractive properties of 3D COFs, such as rich open channels and sites, large internal surface area, and good stability, make them promising materials for membrane application. **Table 4.2.** lists some typical 3D COFs used for membrane fabrication. To date, only a few works on 3D COF membranes have been reported. Here, we provide a review of the synthesis methods and applications of 3D COF membranes.

Table 4.2 3D COFs used in membrane separation.

3D COFs	Linkages	Organic linkers	Pore size (Å)	Surface area ($m^2 \cdot g^{-1}$)	Application	Ref.
COF-300	Imine	Tetra-(4-anilyl) methane; Terephthaldehyde	7.2	1360	Gas separation; Proton conduction; dye separation	[41, 161 - 163]
COF-320	Imine	4,4′-Biphenyldicarboxaldehyd; Tetra-(4-anilyl) methane	~8	2400	Gas separation	[164, 165]
3D-OH-COF	Imine	Tetrakis(4-formylphenyl)-methane；3,3′-Dihydroxybenzidine	~8.8	~843.4	Molecular Separation (water, organic solvents)	[155]
3D-COOH-COF	Imine	Tetrakis(4-formylphenyl)-methane；3,3′-Dihydroxybenzidine	~8	~121.6	Molecular Separation (water, organic solvents); Ion capture	[155]

3D SNW-1	Imine	Melamine; Terephthalaldehyde	~5	858	Gas separation; OSN; pervaporation; Fuel cell;	[171, 172]
3D COF-1	Imine	P-phenylenediamine; Tetrakis(4-formylphenyl)-methane	~8.3	Powder ~486 Membrane <10	Precise separation of ions and fine molecules	[173]
3D SCOF	Imine	Tetra-(4-anilyl)-methane; Sulfonic acid-functionalized aldehyde	9.7	Membrane 49	Ion transport	[174]

4.3 Synthesis Methods of 3D COF Membranes

Since Yaghi and co-workers first used the solvothermal method to synthesize 3D COFs (COF-102 and COF-103) in 2007 [158], the solvothermal method has become the most popular and widely used method to synthesize COF powders, including 3D COFs. This method includes adding the monomers into a mixture of solvents and catalysts and heating the system in autoclaves or sealed tubes at 80-160°C for several days [157]. The COFs obtained are usually in the form of insoluble and difficult-to-process powders, which are challenging to be directly translated into membranes [168, 169, 175, 176]. Therefore, other membrane fabrication methods have been developed.

Several reviews have summarized the synthesis strategies and different applications of 2D COF membranes [144, 145, 177]. Some of these synthesis methods have been applied to the preparation of 3D COF membranes. So far, the most common approaches are based on solvothermal synthesis and interfacial polymerization, and the selection of suitable synthesis methods needs to consider the choice of substrates. Due to the high thermal and chemical stability, inorganic supports such as porous α-Al_2O_3 or SiO_2 allow for the use of solvothermal synthesis to prepare COF membranes. Interfacial polymerization has been adopted to prepare free-standing membranes, which are then transferred to porous substrates. Another approach to take advantage of the unique properties of 3D COFs is to fabricate mixed matrix membranes (MMM), in which COFs powders are embedded inside a polymer matrix to form a composite membrane structure. The following section will review the synthesis of 3D COF membranes on different substrates.

4.3.1 3D COF membranes grown on solid substrates

Yanan et al. successfully fabricated a 3D COF-320 membrane on porous ceramic α-Al_2O_3 substrates modified with 3-aminopropyltriethoxysilane (APTES) [164]. The COF-320 membrane was formed in the presence of tetrakis(4-aminophenyl)methane (TAPM) and biphenyl-4,4′-dicarbaldehyde (BPDA) under solvothermal conditions. The synthesized COF-320 membrane has a thickness of 4 μm and does not contain large defects that could be observed by scanning electron microscopy (SEM). The X-ray diffraction (XRD) of the membrane is in accordance with that of 3D COF-320 powders obtained from solvothermal synthesis, confirming the formation of the desired 3D COF structure. In another work, COF-300 membrane was synthesized on polyaniline (PANI)-modified porous SiO_2 disk. The solution used contained 36.00 mg terephthalaldehyde (TPA), 60.00 mg tetra-(4-anilyl)-methane, 3.00 mL anhydrous 1,4-dioxane, and 0.60 mL of 3.00

M aqueous solution of acetic acid as the catalyst. The synthesis was conducted at 100 °C for 3 days [162]. SEM images showed that the thickness of the COF-300 membrane was about 40 μm, and the diffraction peaks for the COF-300 layer were observed by XRD.

COF-300 membrane has also been prepared on an amino-modified porous Al_2O_3 tube by in-situ growth method [163]. The amino-modified porous Al_2O_3 was placed vertically in the solution (140 mg TAPM, 100 mg TPA, acetic acid (3 M in 6 ml distilled water), and 40 ml dioxane) and kept at 100 °C for 72 h. The Al_2O_3 tube has a smooth and uniform top surface, the color of which became yellow from white after solvothermal synthesis, indicating the formation of COF-300 materials on the ceramic substrate.

In addition, two 3D COF membranes, 3D-OH-COF and 3D-COOH-COF membranes, were fabricated on mesoporous cross-linked polyimide (CPI) and silicon wafers under solvothermal conditions [155]. The 3D-COOH-COF membrane was obtained by the chemical conversion of 3D-OH-COF through the ring-opening reaction. For the 3D-COOH-COF membrane, in a typical procedure, the CPI supports were loaded into a 100-mL PTFE lining with a mother solution containing 21.6 mg tetrakis(4-formylphenyl)-methane (TFPM), 21.6 mg 3,3′-dihydroxybenzidine ($BD(OH)_2$), and 20 mL 1,4-dioxane. Then 500 μL glacial acetic acid was added to the solution. The container was sealed into a steel reaction kettle and heated at 85 °C for 24 h. To carry out the chemical conversion, the 3D-OH-COF membranes were synthesized for 24 h and extended another 24 h to retain the membrane integrity during the ring-opening reaction. The 3D-OH-COF membranes were immersed in acetone, transferred to the succinic anhydride solution, and heated at 50 °C for 12 h. The thickness of films and membranes increased with extending the reaction

time. A 24 h growth produced a continuous 3D-OH-COF layer with a thickness of ~400 nm and the thickness of the 3D-COOH-COF layer was measured to be ~480 nm.

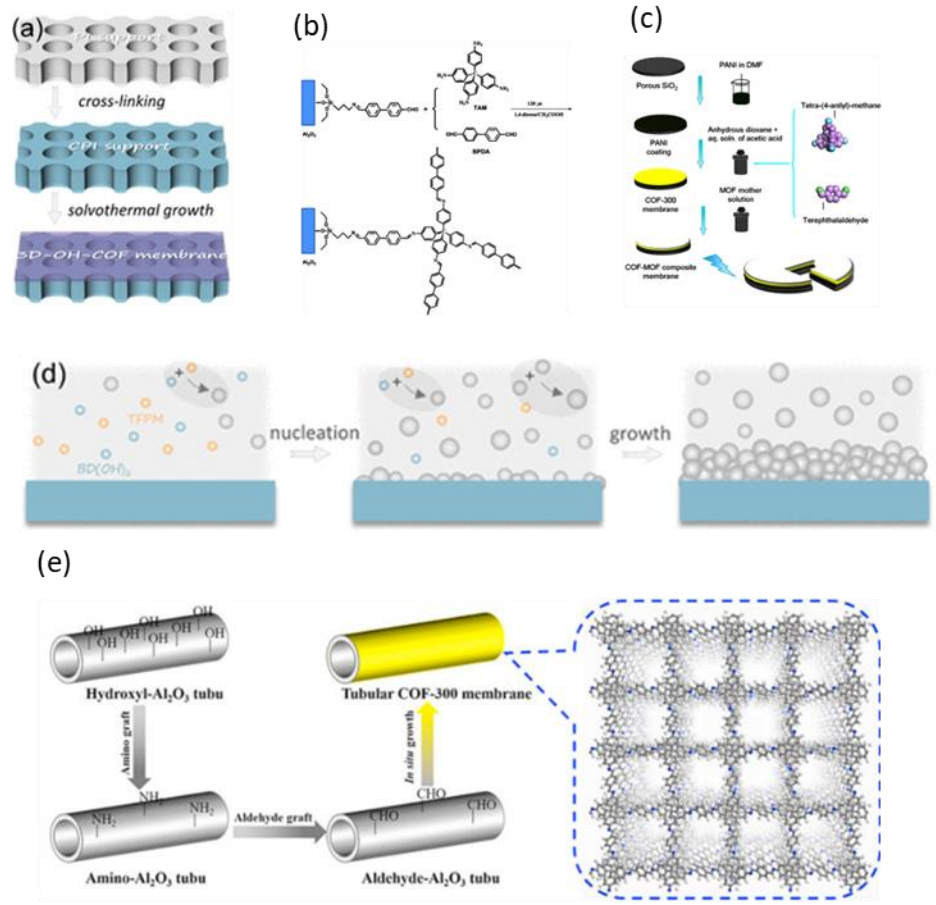

Figure 4.2 (a) Schematic diagram of the 3D-OH-COF membrane preparation (reproduced from ref. [155] with permission from American Chemical Society, Copyright 2021). (b) Fabrication of the COF-320 membrane on modified porous Al_2O_3 (reproduced from ref. [162]with permission from Royal Society of Chemistry, Copyright 2015). (c) Fabrication of the COF-300 membrane on modified porous SiO_2 (reproduced from ref. [163] with permission from American Chemical Society, Copyright 2016). (d) Schematic diagram of the 3D-OH-COF film formation (reproduced from ref. [155] with permission from American Chemical Society, Copyright 2021). (e)

Fabrication of the COF-300 membrane on a modified porous Al_2O_3 tube (reproduced from ref. [163] with permission from Elsevier, Copyright 2016).

4.3.2 Free-standing 3D COF membrane

Jiang et al. fabricated free-standing uniform 3D COF-300 membranes with interconnected nanochannels using interfacial polymerization. In this method, a mesitylene solution containing p-phthalaldehyde monomers was placed on top of an aqueous solution that contained TAPM monomer and acetic acid. The beaker was sealed and heated at 65 °C for 24 h [161]. The crystal structure of the COF-300 membrane was studied by PXRD and TEM, and a continuous, defect-free, and uniform morphology was observed by SEM. The COF-300 membrane was observed to demonstrate favorable characteristics, including good swelling resistance, excellent mechanical strength, and dynamic behavior similar to its powder counterpart. Furthermore, the membrane displayed high conductivity, leading to efficient proton conduction. In addition, Jiang et al. reported the fabrication of a 3D sulfonic acid-functionalized COF membrane (3D SCOF) designed for efficient and selective ion transport [174]. This was achieved through a dual acid-mediated interfacial polymerization strategy. By carefully controlling the assembly of sulfonic acid-functionalized aldehyde monomers and tetra-(4-anilyl)methane monomers with the mediation of octanoic acid in the organic phase and acetic acid in the aqueous phase, they successfully produced tight and defect-free 3D SCOF membranes. These membranes exhibit highly interconnected ion transport channels, ultramicroporous pore sizes (0.97 nm), and abundant sulfonate groups, resulting in high proton conductivity.

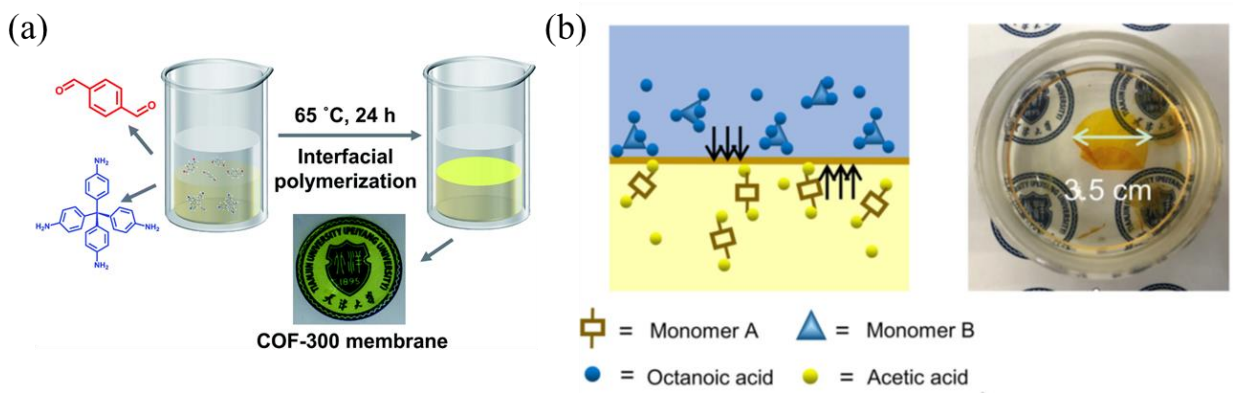

Figure 4.3 (a) Fabrication of the COF-300 membrane (reproduced from ref. [161] with permission from Royal Society of Chemistry, Copyright 2021), (b) preparation of the 3D SCOF membrane (reproduced from ref. [174]with permission from Springer Nature, Copyright 2023).

4.3.3 Mixed matrix membranes (MMMs)

The formation of MMMs was another method for preparing 3D COFs-based separation membranes. Bae and co-workers fabricated 10 wt%_3D-COF@6FDA-DAM and 15 wt%_3D-COF@6FDA-DAM membranes by dispersing different amounts of the 3D-COF in anhydrous chloroform, after which the 6FDA-DAM polymer was added stepwise [178]. Then, the dope solutions were used for membranes casting on a glass plate in a glove bag saturated with chloroform vapor. Subsequently, after drying at room temperature for 5 h, the casted membranes were heated in a vacuum oven at 180 °C for 24 h. In another work, Zhao et al. added COF-300 and COF-300 functionalized with poly(ethyleneimine) (PEI) as fillers in glassy 6FDA-DAM and rubbery Pebax polymer matrixes to construct MMMs for CO_2 capture (**Figure 4.4.**) [159]. The optimum filler content of 10 wt% in Pebax polymer matrixes was slightly higher than that of the glassy 6FDA-DAM system (7 wt%).

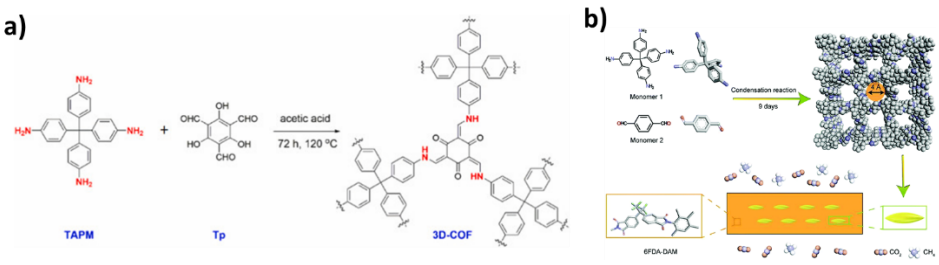

Figure 4.4 (a) Synthesis of the 3D-COF (reproduced from ref. [178] with permission from Elsevier, Copyright 2019). (b) Preparation of the COF-300/6FDA-DAM MMMs (reproduced from ref. [159] with permission from Royal Society of Chemistry, Copyright 2019).

4.3.4 COF@MOF composite membranes

Recently, there was an interesting development in that MOF can be grown on the COF membrane to fabricate COF-MOF composite membranes, as first proved by Qiu et al.[162]. In their work, they fabricated COF-300 on a PANI-modified porous SiO_2 disk; subsequently, this support with COF-300 membrane was placed horizontally in the Teflon-lined autoclave containing $Zn_2(bdc)_2(dabco)$ mother solution, with the COF layer facing up. The growth of MOF was carried out at 120 °C for 2 days. The resulting [COF-300]-[$Zn_2(bdc)_2(dabco)$] composite membrane was washed with DMF, immersed in anhydrous methanol overnight, and finally dried in air at room temperature. The fabrication procedure of the [COF-300]-[ZIF-8] composite membrane was similar to the one used for the [COF-300]-[$Zn_2(bdc)_2(dabco)$] composite membrane but with a different reaction time (120 °C for 4 h). The uniformity and thickness of different layers of composite membranes were evident from the cross-sectional SEM images. The thicknesses of the COF layer and the MOF layer were similar in both [COF-300]-[$Zn_2(bdc)_2(dabco)$] and [COF-300]-

[ZIF-8] composite membranes. The XRD showed the expected diffraction peaks of MOF and COF-300.

Another work about COF-MOF composite membranes was [COF-300]-[UiO-66] composite membrane reported by Ben and Das [179]. The UiO-66 membrane was firstly fabricated on the polyaniline-coated SiO_2 disk and subsequently inserted into the Teflon chamber with the COF-300 mother solution (40 mg TAPM, 24 mg TPA and 2 mL 1,4-dioxane) and dropped 0.40 mL of a 3.00 M aqueous solution of acetic acid inside the Teflon chamber and heated at 100 °C for 3 days. The obtained composite membrane was immersed in 15.00 mL THF for 12 h and finally degassed at 100 °C for 10 h after drying overnight in the air at room temperature. The XRD of COF-300 formed in the composite membrane matched the simulated XRD pattern. A continuous layer of COF-300 comprising closely packed rice-shaped COF-300 crystals was observed, and the thicknesses of the COF-300 and UiO-66 layers were about 40 and 60 μm, respectively. These results show that better-performing membranes can be obtained by integrating COFs and MOFs into a composite membrane structure.

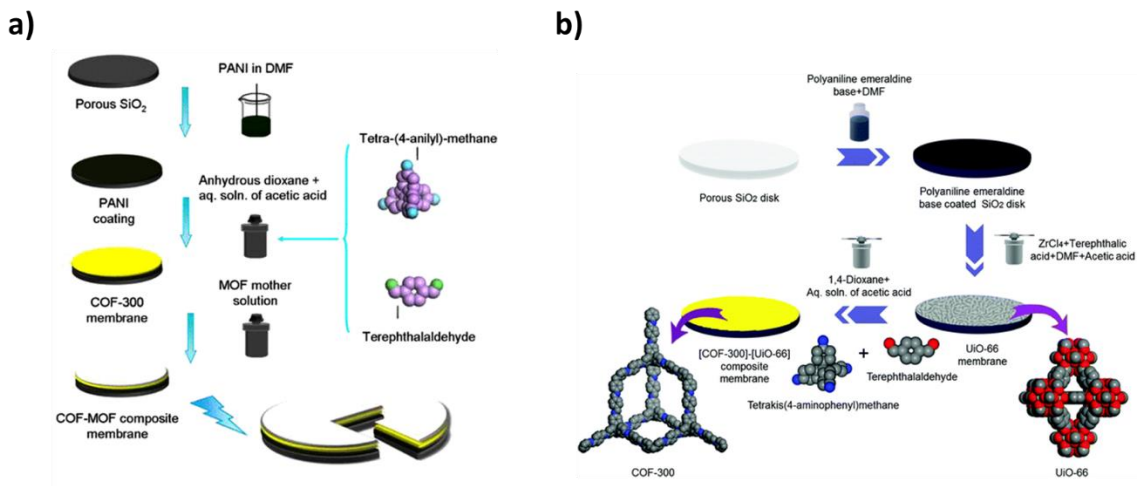

Figure 4.5 (a) Fabrication of the COF-MOF composite membranes (reproduced from ref. [162] with permission from American Chemical Society, Copyright 2016). (b) Preparation of the [COF-300]-[UiO-66] composite membrane (reproduced from ref. [179] with permission from Royal Society of Chemistry, Copyright 2018).

4.4 Separation Performance of 3D-COF Membranes

Up to now, studies on COF-based membranes cover a broad range of topics including gas separation membranes, separation membranes for liquid phase and proton exchange membranes in fuel cells, etc.

4.4.1 Gas Separation

COFs with abundant pores and large internal surface area are particularly promising in realizing ultrafast and highly selective molecular sieving. Therefore, COF-based membranes for gas separation have been fabricated. 2D COF membranes were very popular in the early years and many of them were successfully fabricated and used for CO_2 capture and storage (CCS) and its

separation from H_2 or CH_4. Gas permeation and permselectivity can directly reflect the performance of membranes, and 3D COF membranes are no exception. For the 3D COF membrane (COF-320) synthesized by Gao and co-workers for the first time, its performance was proved by carrying out gas permeation experiments [164]. The hydrogen permeation flux is higher than CH_4 and N_2, indicating that the COF-320 membrane is hydrogen-selective. The permselectivity for H_2/CH_4 and H_2/N_2 is about 2.5 and 3.5, which is similar to the Knudsen diffusion due to its larger pore size (~0.8 nm) than the kinetic diameters of gas molecules. However, the most popular 3D COF is COF-300, which has been fabricated as composite membranes and used as filler in MMMs. Qiu et al. synthesized the COF-300 membrane with a 6.0 mixture separation factor of the H_2/CO_2 gas pair, and combined it with MOFs to prepare composite membranes [162]. The resultant COF-MOF composite membranes demonstrated higher separation selectivity of H_2/CO_2 gas mixtures than the individual COF-300 and MOF membranes, which surpass the Robeson upper bound of polymer membranes. The same conclusions were reported in another work by Ben et al., where they made a continuous and uniform layer of COF-300 grown on a UiO-66 membrane to develop the [COF-300]-[UiO-66] composite membrane that exhibits high permeability together with excellent H_2/CO_2 separation selectivity [179]. The mixture-gas selectivities of H_2/CO_2 for the [COF-300]-[UiO-66] composite membrane is 17.2, which is higher than those of the individual UiO-66 (9.2) and COF-300 (6.0) membranes even the COF-MOF composite membranes (the [COF-300]-[$Zn_2(bdc)_2(dabco)$] composite membrane is 12.6 and the [COF-300]-[ZIF-8] composite membrane is 13.5) reported in work by Qiu et al. [162].

For 3D-COF@6FDA-DAM membrane, the performances were assessed using a CO_2/CH_4 1:1 mixture. At 10 wt% loading of the 3D-COF, compared with the pure 6FDA-DAM membrane.the

CO_2 permeability and CO_2/CH_4 selectivity of 850 barrer and 29.0, creating enhancements in the CO_2 permeability and CO_2/CH_4 selectivity of 57% and 18%, respectively, which elevate the MMM's performance beyond the 2008 Robeson upper limit [178]. The gas separation performance of the other two mixed matrix membranes was evaluated with the feed of an equal molar mixture of CO_2/CH_4 or CO_2/N_2. They find that with the incorporation of suitable amounts of COF-300 fillers, both 6FDA-DAM and Pebax systems demonstrate a concurrent increase in gas permeability and selectivity. They pointed out that the well-defined pores of COF-300 fillers can build fast gas permeation channels, thereby improving the gas permeability of the membranes. Simultaneously, the rigidified polymer chains on the surface of filler and the ultrasmall pores of COF-300 can lead to increased gas pair selectivity, greatly advancing the separation performance of pure polymeric membranes, which has even exceeded the 2008 Robeson upper limit. Furthermore, COF-300-based MMMs exhibited good anti-pressure and anti-moisture performance, accompanied by decent long-term stability originating from the excellent chemical stability of both polymer matrixes and COF-300 fillers [159].

4.4.2 Water treatment

It has been proved that membrane separation is an energy-efficient and environmentally sustainable method and is widely used in wastewater recycling and desalination. For instance, nanofiltration can be used to remove dyes, salts and other organics from water. The nanofiltration performance of COF-300 membrane was studied in different dye solutions by Qin and co-workers [163]. The tubular COF-300 membrane has a rejection of 97.41% of Chrome black T solution with a pure water permeance of 152.5 L m^{-2} h^{-1} bar^{-1}. It also has excellent rejections of 99.5%, 99.0%, 98.7%, 97.4% and 91.7% for rose bengal, methyl blue, congo red, chrome black T, and acid blue

25, respectively. Moreover, for small-size dyes such as methyl orange, the COF-300 membrane has a rejection of 78.3%. They demonstrated that the molecular weight cut-off (MWCO) of the COF-300 membrane is 410 g mol^{-1} (90%). The tubular COF-300 membrane also shows outstanding stable performance during 90 h of continuous operation, indicating its high potential for use as nanofiltration membranes for dye removal.

3D-COOH-COF was prepared by chemically converting 3D-OH-COF membrane with abundant hydroxyl groups into the carboxyl-functionalized COF through a ring-opening reaction by Wang and co-workers [155]. They used a homemade diffusion cell to test the dye/salt separation capability of 3D-COOH-COF membranes. The 3D-COOH-COF membrane shows a largely reduced diffusion rate of Cu^{2+} and exhibits exceptional selectivities of up to ~766, ~634, and ~490 for K^{+}/Cu^{2+}, Na^{+}/Cu^{2+}, and Li^{+}/Cu^{2+}.

4.4.3 Organic solvent nanofiltration

Organic solvent nanofiltration (OSN) has received extensive attention in the chemical industries as a promising separation technology. This technology relies on membranes to exchange, purify, and recycle organic solvents, as well as concentrate solutes. The membranes used in OSN need to have a high level of resistance and stability in solvents [145]. It was found that COFs are stable in organic solvents and are suitable for use as materials for the preparation of OSN membranes on account of their robust linking groups, such as imine, hydrazine, and ketoenamine. Currently, a lot of COF-based membranes for OSN have been proposed, and 3D COF is growing rapidly. For example, the performance of the 3D-OH-COF membrane synthesized on mesoporous CPI supports via solvothermal growth was assessed by Wang et al. They explored the permeance and selectivity in water and organic solvents by dead-end filtration. The 3D-OH-COF powders

were firstly soaked in various solvents including acetone and N,N-dimethylformamide (DMF) to test stability, thereby providing the feasibility of 3D-OH-COF membrane for liquid separation. Then, they measured the pure solvent permeance of the 3D-OH-COF membrane in water, ethanol, and methanol and estimated the molecular weight cutoff (MWCO) of the membrane by testing the rejections to various molecules. It was found that the 3D-OH-COF membrane showed a low MWCO (220 g mol^{-1}) with high rejections to most of dye molecules in methanol, implying the good rejection of 3D-OH-COF.

4.4.4 Fuel cells

Fuel cells are an indispensable energy source in our daily life. As a crucial part of a fuel cell, the proton exchange membranes conduct protons and act as an electronic insulator and reactant barrier to oxygen and hydrogen gas [145]. COFs can provide space for proton carriers because of their well-defined nanochannels, especially for 3D COFs with intrinsically interconnected nanochannels. They have emerged as promising candidates for next-generation proton-conducting materials in redox flow batteries, electrochemical sensors, fuel cells, etc. The performance of proton exchange membranes can be reflected by the proton conductivity. In a recent work, Jiang and co-workers fabricated defect-free uniform COF-300 membranes with a good swelling resistance and mechanical strength via a well-defined interfacial polymerization method [161]. At the same time, by embedding etidronic acid as proton carriers, they obtained etidronic acid@COF-300 membrane with a proton conductivity level of 0.236 S cm^{-1} at 30 °C, 100% relative humidity (RH) and 0.650 S cm^{-1} at 90 °C, 100% RH, which is significantly higher than that of the membrane without the etidronic acid as proton carriers.

4.5 Conclusions and Outlook

In conclusion, although 3D-COF-based membranes are still in their infant period, the unique properties of 3D COFs, such as high and permanent porosity, well-defined pores, large surface area, and various available building units, make them a promising material platform in membrane design for molecular separations. This review first briefly introduced the structure of 3D COF-based membranes and then focused on the various preparation methods of 3D COF membranes and the substrates used. In addition, the application of 3D COF membranes in gas separation, water treatment, organic solvent nanofiltration, and proton exchange shows great potential. The design of novel 3D COF structures is anticipated to accelerate the development of 3D COF membranes. However, some challenges remain to be addressed, including the relatively high cost of 3D COFs and the complicated and time-consuming fabrication methods. Therefore, the strategy of seeking low-cost and large-scale preparation of 3D COF-based membranes remains to be developed.

Chapter 5 Interfacial Synthesis of 3D Covalent Organic Framework Membranes for Organic Solvent Nanofiltration

5.1 Introduction

Organic liquid mixture separation is critical in the petroleum industry and was previously accomplished on a large scale using thermally driven, energy-intensive distillation processes. Membrane separations such as organic solvent nanofiltration (OSN) have been developed as an energy-efficient process compared with thermal processes. Initially, conventional polymer membranes were explored to separate organic liquid mixtures, but they undergo plasticization or swelling under certain solvents. Therefore, there is still a significant need for the development of new membrane materials that are stable, effective, and scalable for use in organic solvent nanofiltration. A variety of advanced inorganic and polymeric materials such as ceramics [180], polymers of intrinsic microporosity (PIM) [181, 182], graphene oxides [183-185], etc., have been studied to enhance separation performance and solvent stability.

Covalent organic frameworks (COFs), as a class of novel crystalline porous materials, are comprised of two-dimensional (2D) and three-dimensional (3D) frameworks constructed by linking organic building blocks through covalent bonds, attracting extensive interest in various fields. Recently, they have been extensively studied for membrane separations because of their structural diversity, large surface area, tunable pore size and structure, and good thermal stability. 2D COF membranes with a molecular weight cutoff (MWCO) in the range of 800-1200 g/mol have been fabricated for OSN [47, 48]. In contrast to 2D COFs, 3D COFs represented by COF-300 with a small pore size of less than 1 nm are fully covalent and more sensitive to the synthesis

conditions [41]. In addition, the interpenetrations of 3D COFs lead to shrunk channels, allowing them to have highly porous structures and smaller pore sizes, which is more promising for nanofiltration applications in terms of the separation of small molecular weight solutes/solvents. It is worth noting that some 2D and 3D COFs membranes can be synthesized on some polymeric or low-cost substrates by the scalable interfacial polymerization method, which increases the possibility of commercialization compared to other membrane materials [42-46].

However, reports on 3D COF membranes are still scarce. Although some 3D COF membranes were synthesized under solvothermal conditions and used for gas separation and water filtration, only several works were related to OSN [162, 163, 186]. In our work, COF-300 membranes were synthesized on lab-made porous ceramic supports with a pore size of ~500 nm by interfacial polymerization and studied for organic solvent nanofiltration.

5.2 Experimental Section

5.2.1 Raw materials

High purity alumina powder CR6 (Baikalox 1.0CR) from Baikowski International Corporation and nitric acid 1.0 N standardized solution (HNO_3, Alfa Aesar) were the main raw materials for the lab made ceramic supports. Tetrakis(4-aminophenyl) methane (TAPM, 98%, TCI) and terephthaldehyde (PDA, 98%, Alfa Aesar) are the monomers for the COF synthesis. P-Toluenesulfonic acid monohydrate (PTSA, ≥98.5%, Sigma-Aldrich) and acetic acid (glacial, ≥99%, Sigma-Aldrich) were used as catalysts. Mesitylene (98%, Sigma-Aldrich), hexane, chloroform (≥99%, Sigma-Aldrich) and ethyl acetate are the main solvents used to dissolve aldehyde monomers as organic phase. The performance of the membranes was assessed using

polar and nonpolar organic solvents, including 2-propanol (>99.7%, Fisher Scientific), ethyl alcohol (200 proof, Sigma-Aldrich), acetone (>99.5%, Fisher Scientific), acetonitrile (≥99.9%, Sigma-Aldrich), toluene (99.8%, Sigma-Aldrich) and deionized water (DI water) were used for the membrane washing. To measure dye rejection in ethanol, the following dyes were used: Rose Bengal (MW=1017.64 g/mol, Sigma-Aldrich), Fast Green (MW=808.85 g/mol, Fisher chemical), Congo Red (MW=696.65 g/mol, LabChem), Calcein (MW=622.5 g/mol, MP Biomedicals), Eriochrome Black T (MW=461.38 g/mol, Acros Organics), Methyl Orange (MW=327 g/mol, Sigma-Aldrich), and Disperse Orange 3 (MW=242.23 g/mol, Sigma-Aldrich). All chemicals were commercially obtained and used without further processing.

5.2.2 Preparation of COF-300 thin films and membranes

5.2.2.1 Preparation of free-standing COF-300 thin films

Freestanding COF-300 thin films were synthesized at the liquid-liquid interface via interfacial polymerization using beakers or glass vials shown in **Figure 5.1**. The amine monomer (TAPM) and catalyst (Acetic acid or PTSA) were dissolved in water and the aldehyde was dissolved in several low polarities and immiscible with the aqueous amine solution solvents, such as mesitylene, hexane, and chloroform. To allow the Schiff-base condensation reaction between aldehydes and amines to occur, the entire reaction was carried out at room temperature and under static conditions for 30 seconds to 72 hours. After the reaction, the thin film was taken out and washed with THF and acetone.

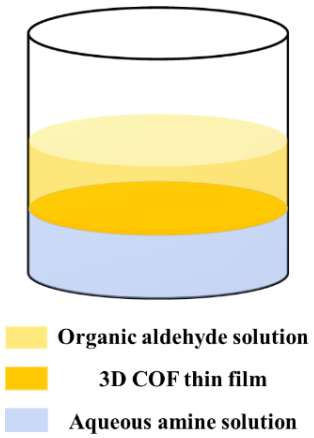

Figure 5.1 Schematic diagram of the interfacial polymerization of free-standing 3D COF thin films.

5.2.2.2 Preparation of COF-300 membranes

The 3D COF membranes were synthesized on the lad made ceramic supports sealed in a homemade synthesis tube as shown in **Figure 5.2**. The ceramic supports fabricated in the lab described in Chapter 2 were soaked in DI water prior to the synthesis of COF membranes. Typically, an aqueous amine solution with the catalyst was added to the home-made synthesis tube for 30 min, then the surface aqueous solution was completely removed, followed by an organic aldehyde solution was added and held for a period of time to allow the reaction to take place. Finally, the resulting 3D COF membranes were soaked in ethanol before testing.

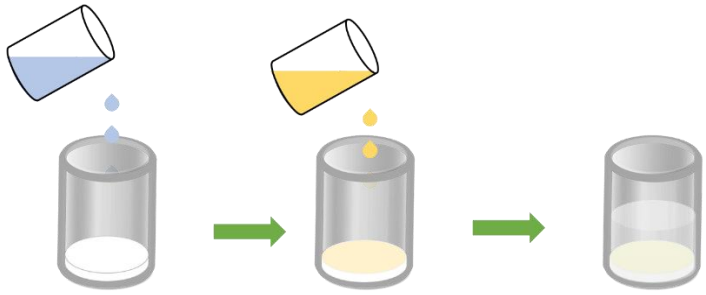

Figure 5.2 Schematic diagram of the interfacial polymerization of 3D COF membranes on lab-made ceramic support.

5.2.3 Organic solvent nanofiltration (OSN) measurements

The as-synthesized COF membranes were sealed into stainless steel cells with an effective membrane area of ~2.2×10^{-4} m^2. The dyes rejection in ethanol, including Rose Bengal (MW 1017.64 g/mol), Fast green (MW 808.85 g/mol), Congo red (MW 696.65 g/mol), Eriochrome black T (MW 461.38 g/mol), Methyl orange (MW 327 g/mol) and Disperse orange 3 (MW 242.23 g/mol), were first tested. All measurements were conducted at room temperature with a cross-flow permeation system, and the feed pressure was set at 40 psi with a flow rate of 40 ml/min. The solvent permeance (P) was calculated by the equation:

$$P = \frac{V}{A\times\Delta t\times\Delta p} \tag{5.1}$$

where V is the solvent volume (L) collected from permeate side during a time period of t (h), A is the effective membrane area (m^2), and Δp is the trans-membrane pressure drop (bar). A feed concentration of dye solutions of 10 ppm solutions was used in dye rejection measurements in two organic solvents, ethanol and THF, respectively. The rejection rate (R) of the dyes was calculated by the following equation:

$$R = \left(1 - \frac{C_P}{C_F}\right) \times 100\% \quad (5.2)$$

where C_P and C_F represent dye concentrations in the permeate side and feed side, which was measured by UV-vis spectroscopy. To exclude the effect of adsorption, all samples were collected after 30 minutes of stabilization. In addition, the permeance of the various pure solvents was measured and plotted as a function of the inverse of solvent viscosity.

5.2.4 Characterizations

A powder X-ray diffractometer using a Bruker D8 Discover A25 diffractometer equipped with a Cu K X-ray radiation source was used to examine the X-ray diffraction patterns (XRD) of all thin films and COF membranes. The morphologies of synthesized samples were observed by scanning electron microscope (SEM, Hitachi Model S4800) coupled with energy dispersive X-ray analysis (EDS). The surface functionality of the materials was investigated using Shimadzu IRTracer-100 Fourier transform infrared spectroscopy (FTIR).

5.3 Results and Discussion

5.3.1 Synthesis and structure characterization of freestanding COF thin films

The effects of the organic solvents, catalysts, monomer concentrations (0.5-9 mM) and reaction time (30 s-72 h) were systematically studied for 3D COF thin films.

5.3.1.1 The effect of solvents

In the literature, different solvents have been used to synthesize COF membranes. For example, mesitylene was used by Jiang et al. to fabricate 3D COF membranes for proton conduction [161]. Dinesh Shetty et al. studied the solvent effect of fragmentations in free-standing 3D COF membranes by using chloroform and ethyl acetate as organic solvents [187]. In addition, hexane has been widely used for the formation of an interface with an aqueous-phase solution to synthesize COF and other membranes [43, 188].

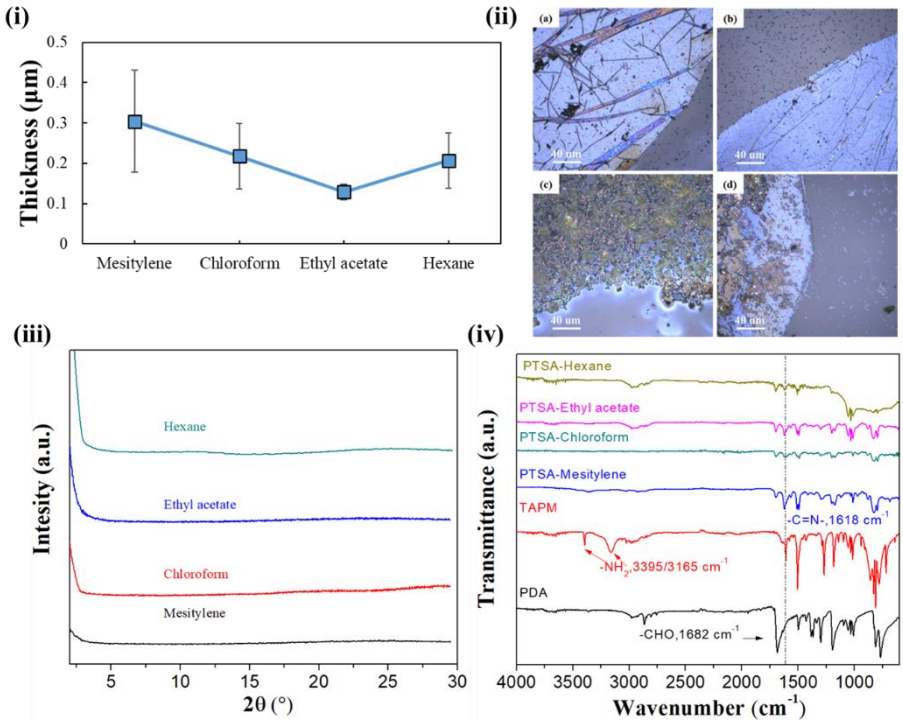

Figure 5.3 Characterization of 3D COF thin films synthesized with different solvents. (i) Thickness of 3D COF thin films. (ii) Confocal images of thin films: (a) mesitylene, (b) chloroform, (c) ethyl acetate and (d) hexane. (iii) XRD patterns and (iv) FT-IR spectra of 3D COF thin films.

Herein, four solvents were selected to prepare 3D COF thin films, including mesitylene, chloroform, ethyl acetate, and hexane. As shown in **Figure 5.3 (i)**, using mesitylene as the organic solvent resulted in the thickest thin film with a thickness of 300 nm, followed by the thin films

with a thickness of about 200 nm prepared using chloroform and hexane, while the thin film fabricated by using ethyl acetate is the thinnest, with a thickness of around 100 nm. These results were obtained while maintaining all other reaction conditions constant. The corresponding Confocal images are shown in **Figure 5.3 (ii)**. We can see that the continuous thin films were formed using mesitylene, chloroform, and hexane as solvents, and the thin film made by hexane appears especially thin compared to the others. However, when ethyl acetate was used as the solvent, the thin film appeared non-continuous. This is likely because the thin film was too thin compared to the others, which is also consistent with the measured thickness of thin films under various solvents. We also characterized these films using XRD to determine whether they were crystalline, and the results were shown in **Figure 5.3 (iii)**. We found that they were all amorphous without any XRD peaks, which could be attributed to all of the films being prepared at room temperature. There were hardly any reports of COF-300 thin films made at ambient temperature that contained crystalline structures. Furthermore, the FT-IR spectra of the 3D-COF thin films confirmed that monomers had reacted (**Figure 5.3 (iv)**). In the IR spectra of the membranes, there were no amine (N-H) vibration bands at 3165 and 3395 cm^{-1}, which was a sign that the tetratopic imine condensation on the TAPM moieties was complete. In addition, imine (C=N) stretching vibration was present at 1618 cm^{-1} in all COF films, suggesting the formation of imine linkages in the structure. Notably, the C=N stretching vibration of the film made using mesitylene as the solvent was the strongest of all membranes, possibly due to the relatively large film thickness.

5.3.1.2 The effect of catalysts

It was reported by Banerjee et al. that p-toluene sulfonic acid (PTSA) not only increases the solubility of amine but also acts as the catalyst during the organic Schiff base reaction [42]. When

PTSA was added to the amine solution, they formed H bonding with amines to slow down their diffusion rate to the liquid-liquid interface, driving the reaction toward thermodynamically controlled crystallization [42]. Furthermore, acetic acid has been identified as a critical component for membrane formation, as there is no obvious interface formation between the two miscible organic solvents in the absence of acetic acid [189].

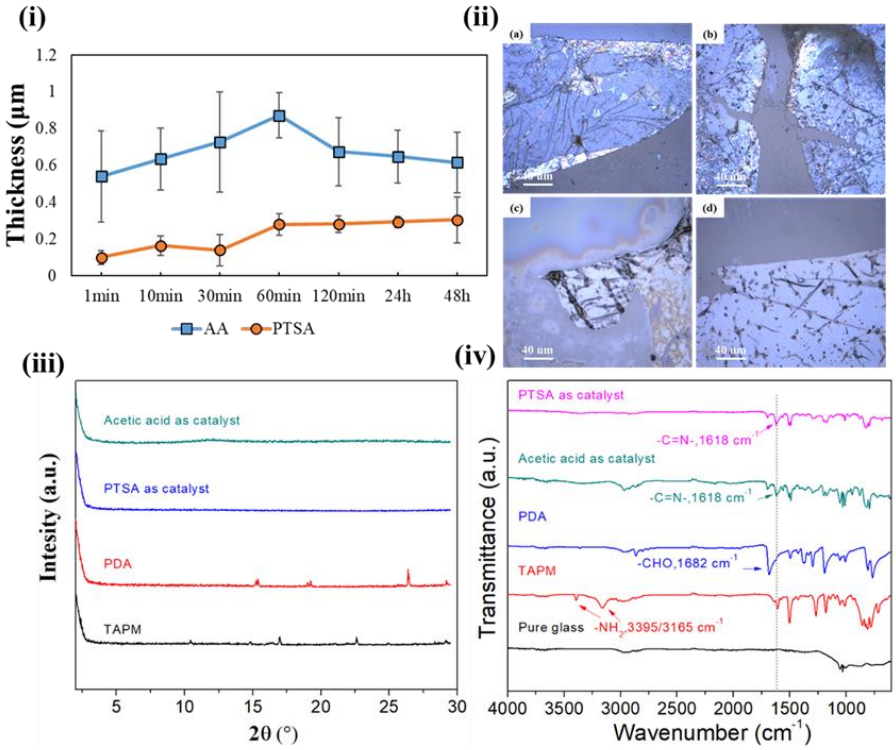

Figure 5.4 Characterization of 3D COF thin films. (i) Thickness of 3D COF thin films synthesized using different catalysts for different reaction times. (ii) Confocal images of 3D COF thin films under different catalysts: (a) acetic acid for 30 min, (b) acetic acid for 48 h, (c) PTSA for 30 min, and (d) PTSA for 48 h. (iii) XRD patterns of 3D COF thin films. (iv) FT-IR spectra of 3D COF thin films.

In our work, we used acetic acid and PTSA as catalysts to fabricate 3D COF thin films to observe the differences between them. As shown in **Figure 5.4 (i)**, there are two obvious trends from the thickness results. One observation is that, as the reaction time extends, regardless of the catalyst used, the thickness of the thin films initially increases and then stabilizes. The other obvious trend is that the thin films (500-800 nm) synthesized by acetic acid as the catalyst are thicker than the thin films (100-400 nm) prepared using PTSA as the catalyst. Those trends also can be observed intuitively in confocal images (**Figure 5.4 (ii)**). Thin films made with acetic acid as catalyst (**Figure 5.4 (ii) a and b**) are indeed thicker than those made with PTSA as catalyst (**Figure 5.4 (ii) a and b**). However, regardless of the catalyst, we were unable to obtain 3D COF thin films showing the XRD patterns displayed in (**Figure 5.4.Figure 5.4 (iii)**), especially under room temperature and with a short synthesis time. This result is consistent with the results demonstrated by Banerjee et al. that for 2D COF membranes, polymeric membrane was formed after 24 hours, but significant crystallinity was observed only after 72 hours [42]. Moreover, the 3D COF thin films are very thin, so there might not be enough material to produce XRD peaks. As presented in **Figure 5.4 (iv)**, the formation of 3D structure was confirmed by the imine (C=N) stretching vibration at 1618 cm^{-1} in all COF membranes, regardless of the catalyst used in thin film synthesis.

5.3.1.3 The effect of reaction time

COF membranes have a regular framework structure and require a certain degree of crystallinity after initial polymerization to achieve an ordered and regular alignment of pores, making it a time-consuming process [190]. Short reaction times may lead to inadequate mechanical properties of the resulting COF thin films so that it is not suitable for separation, but long reaction

time allows water-soluble monomers to diffuse into the organic phase, resulting in a thicker membrane with large polymeric particles on the surface [191]. Therefore, it is critical to investigate the effect of reaction time on COF films.

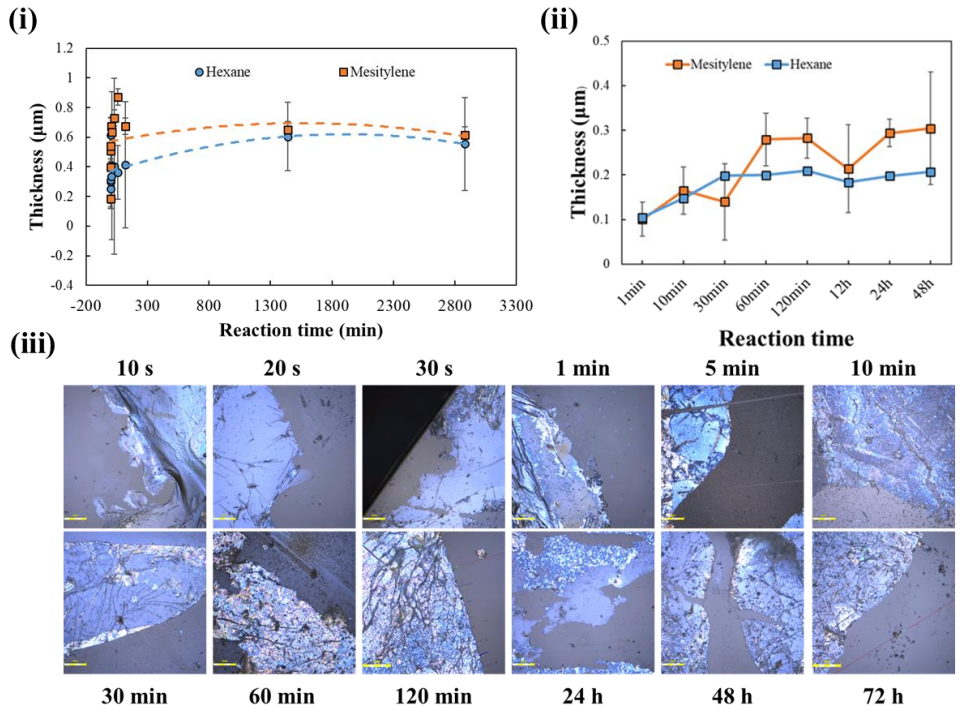

Figure 5.5 Characterization of 3D COF thin films under different reaction times. (i) Thickness of 3D COF thin films obtained for different reaction times using acetic acid as catalyst. (ii) Thickness of 3D COF thin films obtained for different reaction times using PTSA as the catalyst. (iii) Confocal images of 3D COF thin films under different reaction times.

Two solvents, mesitylene and hexane, were selected to explore the effect of reaction time on 3D COF thin films, and firstly, acetic acid was used as a catalyst because acetic acid can accelerate the reaction speed and form a film in a short time. **Figure 5.5 (i)** shows that the thickness of the thin films increases rapidly as the reaction time increased at the beginning, and when the reaction

time reached 120 min, the thickness appeared to stabilize. Furthermore, thin films made with mesitylene as a solvent were still thicker than those made with hexane, consistent with the results of previous solvents' effect on the thin films. At the same time, we tried to use PTSA as a catalyst to investigate the effect of reaction time to verify whether PTSA can produce thinner films in a short time. It was found that despite the use of PTSA as the catalyst, a thickness of 100 nm was obtained within 1 min, and the thickness of thin films increased with reaction time **Figure 5.5 (ii)**. Additionally, the resulting films (less than 400 nm) were thinner than those made using acetic acid at the same reaction time. **Figure 5.5 (iii)** depicts the thin films synthesized at various reaction times with the mesitylene as the organic solvent and acetic acid as the catalyst. It can be seen that as the reaction time increased, the thin films became more continuous and visually thicker.

5.3.1.4 The effect of monomer concentration

It was reported that the reaction time and monomer concentrations have a significant impact on the separation performance of the resulting membranes [43, 192]. The effect of amine (TAPM) and aldehyde (PDA) concentrations were separately investigated, and the results are shown in **Figure 5.6**.

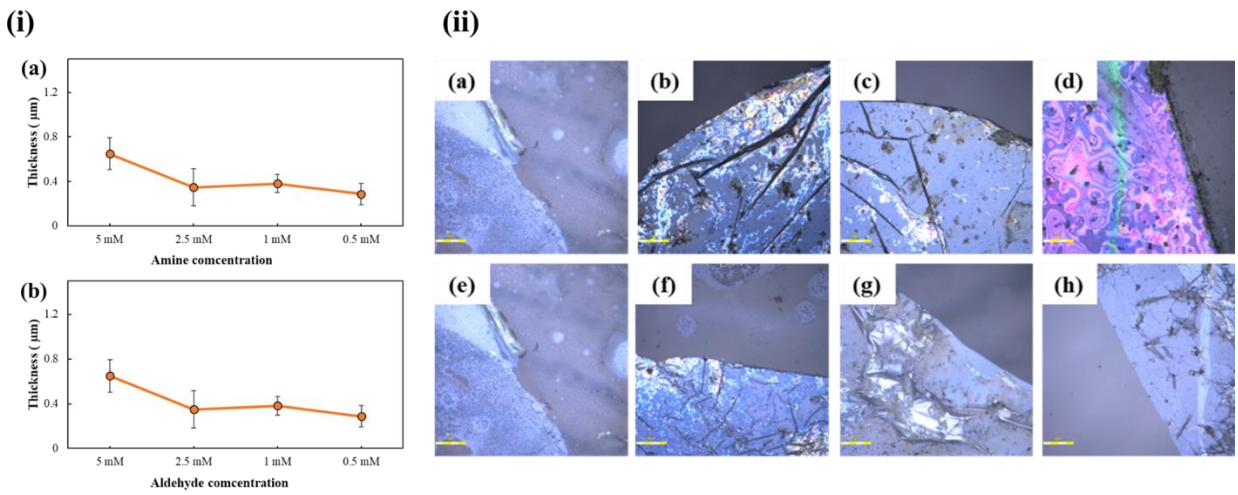

Figure 5.6 Effects of the monomer concentrations on the 3D COF thin films. (i) Thickness of 3D COF thin films made from different amine concentrations ((a) and aldehyde concentration (b). (ii) Confocal images of 3D COF thin films; different amine concentration: (a) 5 mM, (b) 2.5 mM, (c) 1 mM and (d) 0.5 mM; different aldehyde concentration: (e) 5 mM, (f) 2.5 mM, (g) 1 mM and (h) 0.5 mM.

In our work, the monomer concentration of the synthesized powder is 50 mM, and the original concentration of the thin film is 5 mM. The concentration of TAPM and PDA is then gradually reduced to 2.5 mM, 1 mM, and 0.5 mM, respectively. As shown in **Figure 5.6 (i)**, as the concentrations of TAPM (**Figure 5.6 (i-a)**) and PDA (**Figure 5.6 (i-b)**) decreased, the thickness of the thin films became thinner. However, when the concentration of TAPM decreased, the corresponding decrease in thickness was smaller compared to the change of thickness with decreasing PDA concentrations. The thickness of the thin film was around 300 nm when the PDA concentration was reduced to 1%, which is consistent with the confocal images shown in **Figure 5.6 (ii)**. The confocal images show that the continuous thin films could still form even when the concentrations were reduced to 0.5 mM.

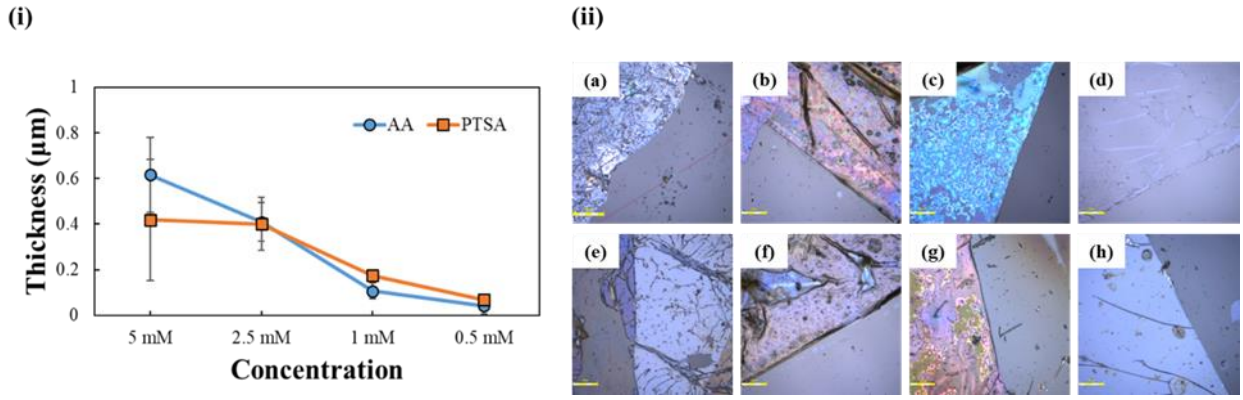

Figure 5.7 Characterization of 3D COF thin films under various monomer concentrations. (i) Thickness of 3D COF thin films obtained for different monomer concentrations. (ii) Confocal images of 3D COF thin films; acetic acid as catalyst: (a) 5 mM, (b) 2.5 mM, (c) 1 mM and (d) 0.5 mM; PTSA as catalyst: (e) 5 mM, (f) 2.5 mM, (g) 1 mM and (h) 0.5 mM.

The effect of simultaneously decreasing the concentrations of both reactants on film thickness was further investigated. Meanwhile, two catalysts were used again to study the effect of catalysts on the films at lower concentrations. As seen from Figure 5.7 (i), the 600 nm thick acetic acid thin film was thicker than the PTSA thin film under the 5 mM concentration, which was the highest concentration we used to synthesize thin films and membranes. The same result can be seen in the confocal images (**Figure 5.7 (ii a** and **e**)). Interestingly, when the reaction concentration was reduced to 2.5 mM, the thicknesses of the films produced by the two catalysts were comparable. As the reaction concentration kept decreasing, the thin films synthesized with PTSA as the catalyst became slightly thicker than those synthesized using acetic acid. At a concentration of 0.5 mM, the thin film synthesized using acetic acid has a thickness of less than 50 nm and is still of high quality and continuous, as shown in **Figure 5.7 (ii d** and **h**).

5.3.2 Synthesis and structure characterization of supported COF membranes

The supported 3D COF membranes were synthesized and characterized using XRD, FTIR and SEM, and the results are shown in **Figure 5.8**. Firstly, the 3D COF membranes synthesized at room temperature in a short time were amorphous, which was verified by XRD as shown in **Figure 5.8 (a)**. In comparison to 3D COF powders synthesized under hydrothermal conditions (**Figure 5.8 (b)**), there was no obvious peak at 2θ of 9°, indicating that the crystallinity of the membrane was relatively low and even amorphous. FT-IR was used to demonstrate the formation of the 3D COF membrane (**Figure 5.8 (c)**). The presence of amine and aldehyde groups in TAPM and PDA monomers was confirmed by the peaks at 3395 and 3165 cm^{-1} (N-H) and 1682 cm^{-1} (C=O), respectively. However, the stretching vibrations between 1615 and 1625 cm^{-1} associated with C=N bond were not obvious in the spectra of the membrane, which can be attributed to the fact that the membrane we synthesized was too thin to produce the C=N peaks in FTIR spectra.

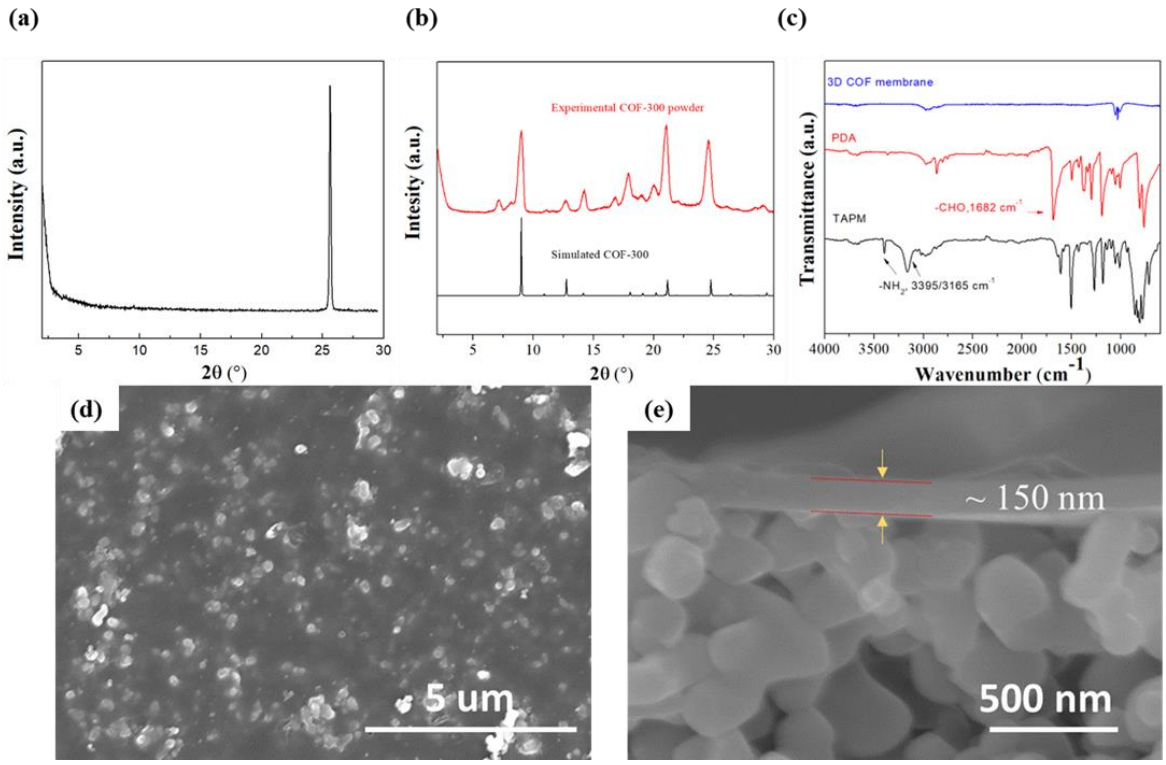

Figure 5.8 Characterization of 3D COF membrane on lab made ceramic support. (a) XRD pattern of 3D COF membrane on ceramic support, (b) XRD pattern of experimental and simulated 3D COF powders, (c) FT-IR spectra of monomers and 3D COF membrane, surface (d) and cross-section (e) SEM images of 3D COF membrane.

SEM was performed on the synthesized membrane to observe its surface and cross-section (**Figure 5.8 (d** and **e)**). From the SEM surface image of the 3D COF membrane, we can see that the very thin and continuous film covers the underlying substrate and vaguely see some alumina particles underneath the film. The SEM cross-section image revealed a membrane thickness of ~150 nm. These results suggested that our 3D COF membrane synthesized in a short time and at room temperature was extremely thin.

5.3.3 Organic solvent nanofiltration measurements of COF membranes

After that, we conducted a series of studies on the correlations between membrane synthesis parameters and membrane properties. The same synthesis conditions used for thin film synthesis were examined for membranes. During organic solvent nanofiltration (OSN) testing, the ceramic supported 3D COF membranes were sealed in a homemade stainless-steel cell with an active membrane area of ~2 cm^2 and tested in a cross-flow permeation system.

5.3.3.1 The effect of solvents

OSN performances of the 3D COF membrane synthesized using different solvents were investigated by a crossflow permeation system at a feed pressure of 40 psi. The ethanol permeance and dye rejection of membranes made with several solvents are shown in **Figure 5.9 (a).** The rejection of all membranes was greater than 90%, and the membrane synthesized with mesitylene had the lowest permeance (about 20 LMHB) but the highest Rose Bengal and Methyl orange rejection, whereas the membrane with the highest permeance and lowest rejection was produced with hexane. We then tested several dyes with varying molecular weights with two types of membranes prepared with mesitylene and hexane and determined their molecular weight cut-off (MWCO), as illustrated in **Figure 5.9 (b)**. The membranes exhibited exceptional separation performances for dyes, and similar MWCO values (~287 Da) were determined from both membranes.

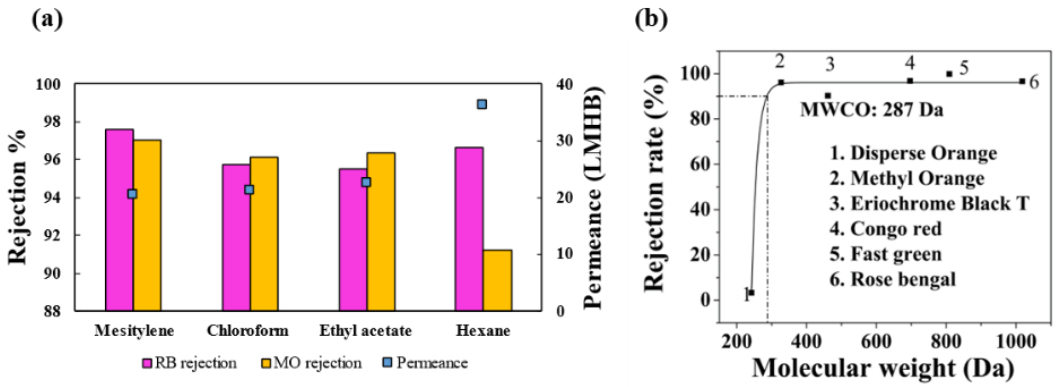

Figure 5.9 OSN performance of 3D COF membrane on lab-made ceramic support. (a) Ethanol permeance and dye rejection of 3D COF membranes, (b) MWCO of 3D COF membrane prepared using mesitylene as the organic solvent.

5.3.3.2 The effect of catalysts

Second, the effect of catalyst was explored using mesitylene as a solvent, PTSA and acetic acid were used as catalysts to prepare membranes, and other synthesis conditions were kept constant. Meanwhile, the OSN performance of the membrane was tested, and the results were shown in **Figure 5.10**.

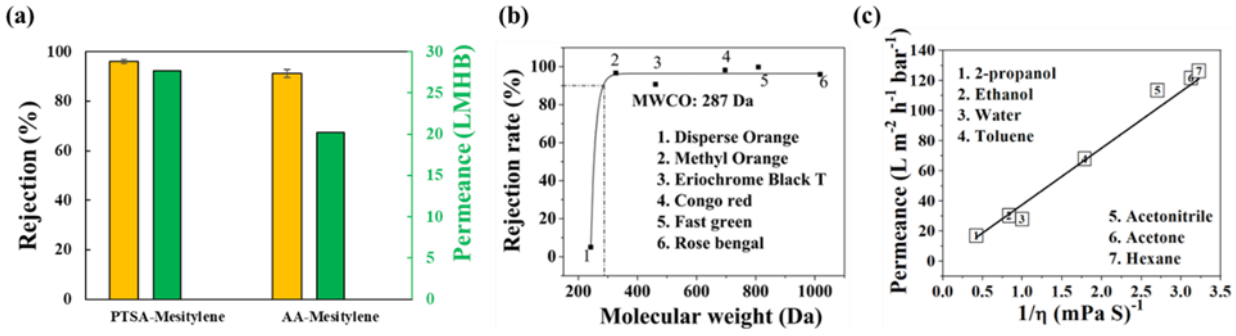

Figure 5.10 OSN performance of 3D COF membrane on lab-made ceramic support. (a) Ethanol permeance and Methyl orange rejection of 3D COF membrane, (b) MWCO of 3D COF membrane

and (c) Pure solvent permeance as a function of the inverse of solvent viscosity of 3D COF membrane using PTSA.

As shown in **Figure 5.10 (a)**, all membranes had high methyl orange rejection (> 95%), but when compared to acetic acid, the PTSA membrane had higher ethanol permeance, which is likely due to the thickness of the obtained membranes. This is consistent with previous thin film results, where the acetic acid catalyst produced thicker films than the PTSA catalyst at higher monomer concentrations, resulting in lower membrane permeance in the COF membrane made with acetic acid. **Figure 5.10 (c)** depicted the permeances of a variety of organic solvents and water at room temperature. It was found that the 3D membranes exhibit high permeance to most of the tested solvents, owing to the 3D interconnected porosity [193, 194]. Moreover, a good linear relationship between the permeance and the inverse of viscosity can be observed for both membranes, and the solvent permeance value is primarily dominated by the viscosity of solvents, which can be explained by the Hagen-Poiseuille equation [47, 185, 195].

5.3.3.3 The effect of reaction time

The effect of reaction time on COF membranes was studied in the next step. **Figure 5.11** revealed that the OSN performance of COF membranes obtained under different reaction times with different catalysts. In the beginning, we tried to synthesize membranes using acetic acid as the catalyst because the thickness and the reaction speed obtained from acetic acid were beneficial for the observation of the membrane's formation. As shown in **Figure 5.11 (a)**, when the reaction time is 30s, the membrane permeance decreased compared with the pure support (blank), but the dye rejection was improved. Interestingly, when the reaction time was increased to 1 min, the membrane permeance decreased, but the rejection of Rose Bengal and Methyl orange remained

above 90%, and with the increase of the reaction time, the membrane rejection was still above 90%. The membrane permeance fluctuated up and down, which can be attributed to the non-ideal uniformity of lab-made ceramic supports.

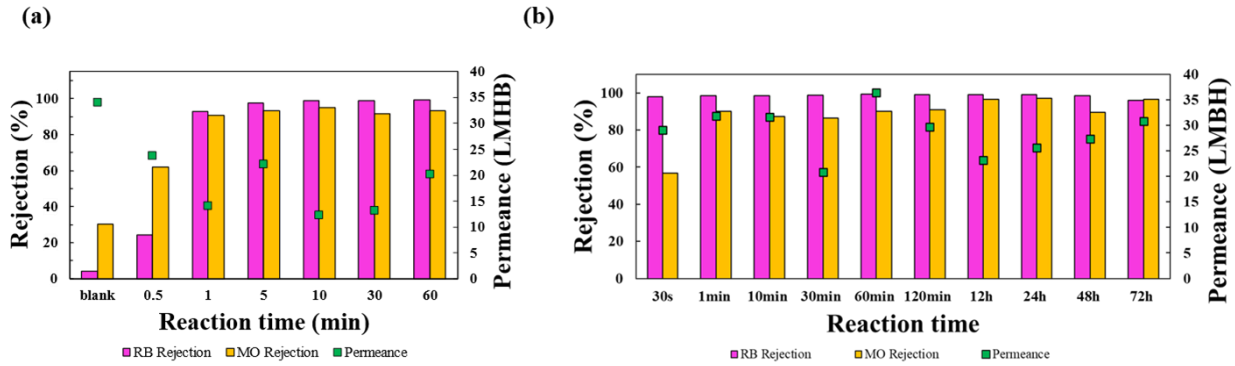

Figure 5.11 OSN performance of 3D COF membrane on lab made ceramic support. (a) acetic acid as catalyst, (b) PTSA as catalyst.

Simultaneously, we used PTSA as a catalyst to investigate the rejection and permeance of membranes made from 30 seconds to 48 hours. As illustrated by **Figure 5.11 (b)**, the extension of reaction time had no significant effect on the rejection and permeance of membranes. In addition, even membranes prepared in 30 s retained Rose Bengal dyes efficiently and the ethanol permeance of membranes did not drop noticeably over reaction time. However, for Methyl orange, the rejection increased as the reaction time increased, suggesting that the defects were repaired as the reaction time increased.

5.3.3.4 The effect of monomer concentration

It is critical to explore the relationship between monomer concentration and membrane performance. Therefore, the effect of monomer concentration was conducted in this part, and two

monomer concentrations were changed at the same time to see how they affected the membrane's OSN performance. Regardless of whether the reaction time was 1 hour or 30 s, there was still a high Rose Bengal rejection when the concentration was reduced to 0.25 mM When the reaction time was controlled at 30 s as shown in **Figure 5.12 (a)**, the rejections to Rose Bengal were above 90% except for the membrane with a lot of defects synthesized with the concentration of 0.05 mM However, the rejections to Methyl orange were much lower (less than 60%), and when the concentration was less than 2.5 mM, there were no rejections to Methyl orange. As the concentration of the monomer was further reduced, the methyl orange rejection dropped dramatically, especially when the reaction time was 1 minute and the concentration was reduced below 1 mM, where there was almost no methyl orange rejection (**Figure 5.12 (b)**).

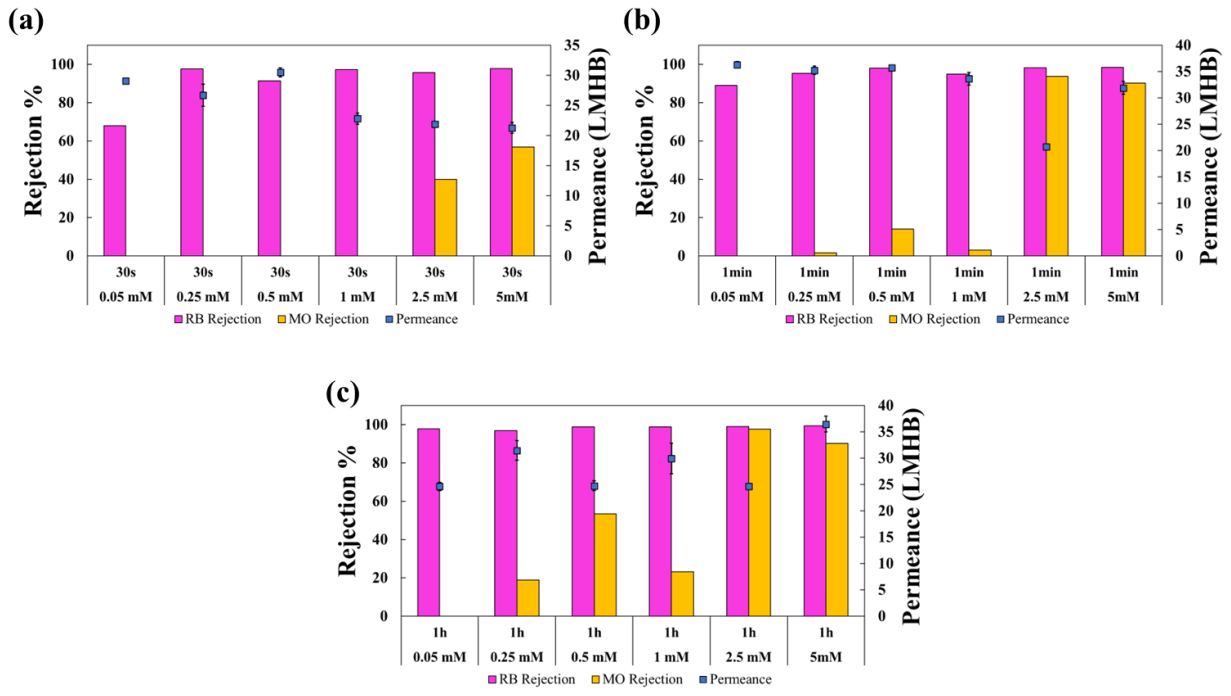

Figure 5.12 OSN Performance of 3D COF membrane on lab-made ceramic support. (a) 30 s of reaction time, (b) 1 min of reaction time and (c) 1 h of reaction time.

5.4 Mass transport modeling

Pore-flow model and solution-diffusion model are two popular models for OSN system modeling. In our study, pore-flow model was used to analyze the experimental solvent permeance data for the COF-300 membrane to investigate the mechanisms of mass transport through the 3D COF membrane. The model proposed by Dagan was employed, considering solvent viscosity and the geometric properties of the COF membrane [196]. Stable pores are assumed to be present inside the membrane, and the driving force for the transport is the pressure gradient across the membrane. This model combines Sampson's pore entrance resistance and Poiseuille's pore passage resistance in a linear superposition [196-198].

The analysis utilized Dagan's model to quantify the relative contributions of entrance and passage resistances to permeate flux (J) through a COF-300 membrane with specified structural parameters. Tortuosity (τ) was introduced as the fitting parameter in the equation to align predicted flux values with experimentally measured fluxes.

$$J \approx \frac{1}{\eta}\frac{1}{A_{mem}}\left\{\frac{R^3}{3}\left[1 - G\left(\frac{R}{L}\right)^3\right]^{-1} + \frac{n\pi R^4}{8t\tau}\right\}\Delta P \tag{5.3}$$

The equation accounts for solvent viscosity (η), effective membrane area (A_{mem}), pore tortuosity (τ), a constant for hexagonal pore array (G), estimated areal pore density (n), and applied hydraulic pressure (ΔP). Hydrodynamic corrections, G and L, were incorporated for the hexagonal pattern of the pore array and the distance between pores in the upper bound flow regime. The determination of tortuosity ($\tau = 2.7$) was derived from an analysis of various solvent flux data, known parameters, and modeling outcomes.

To gain deeper insights into the nature of fluid transport dominated by pore passages in the COF membrane nanochannels, we normalized the flux of diverse polar and nonpolar solvents across the COF-300 membrane by multiplying the flux by the COF thickness (J × t). The resulting thickness-normalized fluxes exhibited a linear correlation with inverse solvent viscosities, as illustrated in **Figure 5.13**. This correlation suggests a manifestation of Poiseuille's pore flow behavior in the COF membrane, providing further understanding of the passage-dominated fluid transport in its nanochannels.

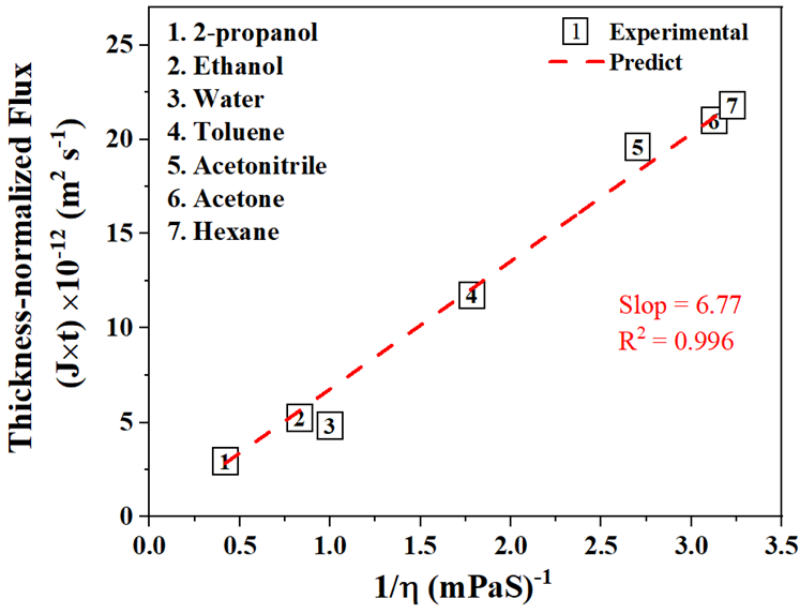

Figure 5.13 Linear correlation between thickness-normalized flux across COF-300 and inverse solvent viscosity.

5.5 Conclusion

In summary, the interfacial polymerization method has proven to be a successful approach for synthesizing 3D COF membranes, showcasing outstanding performance in organic solvent

nanofiltration (OSN). A comprehensive exploration into the impact of solvents, catalysts, reaction time, and monomer concentration on 3D thin films and membranes was conducted, revealing valuable insights into the synthesis process. In addition, our investigations unveiled the sensitivity of 3D thin film thickness to synthesis conditions, with variations observed based on factors such as the choice of solvents and catalysts. The use of acetic acid as a catalyst, higher monomer concentrations, and extended reaction times resulted in thicker films. Subsequently, the mesitylene/water system was chosen for the synthesis of 3D COF thin films and membranes due to its good OSN performance. The OSN performance evaluation further indicated that, even with lower monomer concentrations and shorter reaction times, the rejection rate for Rose Bengal exceeded 90%, except for the membrane prepared in 30 seconds with 0.1% monomer concentration. This underscores the rapid and energy-efficient synthesis capabilities of 3D COF membranes. Moreover, the characterizations employing FT-IR, XRD, and SEM techniques confirmed the successful formation of “amorphous” imine-linked 3D COF in the resultant membrane, featuring a thickness of 150 nm and a molecular weight cut-off (MWCO) of less than 300 Da. Furthermore, initial modeling results based on Dagan's model and the derived tortuosity of $\tau = 2.7$ provide valuable insights into the mechanisms of mass transport through the membrane nanochannels. The correlation of thickness-normalized fluxes with inverse solvent viscosities, aligns with Poiseuille’s pore flow behavior, suggesting the passage-dominated fluid transport in the 3D COF membrane.

Chapter 6 Conclusions and Recommendations

6.1 Conclusions

This study introduces a range of MOF and COF membranes with outstanding performance achieved through scalable synthesis methods on cost-effective supports. These membranes exhibit exceptional capabilities in various molecular separations.

In task 1, the effectiveness of the vapor phase seeding approach, which relies on ALD and ligand vapor treatment, was demonstrated in creating uniform and compact ZIF-8 seeds that can be readily grown into high-performing ZIF-8 membranes. The ALD cycle number and precursor pulse time were found to influence membrane microstructure strongly, and varying these parameters can be used to tune the membrane performance. Moreover, the vapor seeding approach can produce thin, high-quality ZIF-8 membranes on mesoporous TiO_2 support, achieving superior performance with a propylene/propane separation factor of up to 152. Additionally, we have demonstrated the versatility of this approach by combining it with epitaxial growth to synthesize polycrystalline ZIF membranes with different structures, including ZIF-67 and ZIF-90. Moreover, it was discovered that a ZIF-8 membrane exhibiting a high separation factor can be synthesized directly on a macroporous support through all-vapor-phase synthesis, eliminating the need for secondary growth. This achievement involves incorporating a heat treatment under vacuum and extending the pulse time. Our findings highlight the potential of vapor-phase processing as a robust and versatile method for the fabrication of high-quality ZIF membranes for gas separation applications. A relatively high temperature (~125 °C) was used in our work for the ALD and ligand vapor treatment steps, necessitating the utilization of thermally stable support. Further improving

the vapor-phase seeding method to lower the processing temperature would be highly beneficial, potentially enabling membrane fabrication on more cost-effective supports, such as polymer substrates. In addition, extending the vapor-seeding approach to supports with a tubular or hollow fiber geometry is vital for the scale-up of ZIF membranes.

In task 2, we have uncovered high performance in two distinct ZIF-8 membranes, synthesized via different methods and exhibiting varied crystallinity, in purifying 1,3-butadiene from other C4 hydrocarbons that have similar kinetic diameters. For both membrane types, 1,3-butadiene permeance exceeded that of 1-butene, isobutene, and n-butane by one to two orders of magnitudes. In mixed gas separation, a single membrane separation step could increase the molar percentage of 1,3-butadiene from 50% in four-component C4 mixtures to approximately 96–98% in the permeate. Analysis of gas permeances with a mathematical model revealed significant differences in C4 diffusivities that contributed to the effective separation of the C4 molecules. These findings underscore the high efficacy of ZIF-8 membranes in 1,3-butadiene purification and the potential of molecular sieve membranes for challenging and complex gas separations.

Task 3 presented a summary of recent advances on the development and application of 3D COFs and 3D COF membranes. Although 3D-COF-based membranes are still in their infant period, the unique properties of 3D COFs, such as high and permanent porosity, well-defined pore, large surface area, and various available building units, make them promising for membrane design. This review first briefly introduced the structure of 3D COF-based membranes, then focused on the various preparation methods of 3D COF membranes and the substrates used for the synthesis of 3D COF membranes. In addition, the application of 3D COF membranes in gas separation, water treatment, organic solvent nanofiltration, and fuel cells were discussed. The relatively high

cost of 3D COFs and time-consuming fabrication methods may hinder the large-scale fabrication of 3D COF-based membranes. Therefore, the strategy of seeking low-cost and large-scale preparation of 3D COF-based membranes remains to be developed.

In task 4, the interfacial polymerization method was successfully employed to synthesize 3D COF membranes that exhibit exceptional performance in organic solvent nanofiltration. The influence of solvents, catalysts, reaction time, and monomer concentration on 3D thin films and membranes was systematically investigated. It was discovered that the thickness of 3D thin films varied depending on the synthesis conditions (such as different solvents, catalysts, etc.) and that the thin films got thicker when acetic acid was used as a catalyst, the monomer concentration was increased, and the reaction time was extended. Combined with 3D COF membrane OSN performance, the mesitylene/water system was chosen for the subsequent synthesis of 3D COF thin films and membranes. The OSN performance also revealed that, even with a lower monomer concentration and a shorter reaction time, the rejection to Rose Bengal was still higher than 90% with the exception of the membrane prepared in 30s with 0.1% monomer concentration, indicating that 3D COF membrane can be synthesized very quickly and with a low concentration to reduce energy consumption. The FT-IR, XRD, and SEM characterizations demonstrated that the formation of 3D COF and the resultant membrane with a thickness of 150 nm had an MWCO of less than 300 Da.

6.2 Recommendations for Future Work

To promote the synthesis and application of MOF and COF membranes in molecular separations, several directions worth further and detailed research.

(1) Systematically study the influence of ALD conditions, synthesis parameters (such as the amount of ligands, vapor treatment temperature, vapor treatment time, etc.) and post-synthetic heat treatment conditions on membrane structures and gas separation performances. In addition, fully characterize the crystal structure and microstructure of ZIF membranes to understand the membrane formation and defects repair processes.

(2) Examine the viability of vapor-phase processing of MOF membranes on polymer supports as a means to expedite the entire membrane production process. This approach aims to save time and reduce cost by eliminating the need to fabricate ceramic supports and, consequently, advance the scale-up and practical application of MOF membranes.

(3) Employ innovative linker exchange techniques to modify MOF and COF membranes, subsequently exploring both the structural modifications and their impact on membrane performance.

(4) Develop and synthesize new types of MOF membranes for the separation of diverse C4 hydrocarbons.

(5) Further investigate the synthesis-structure-OSN properties of 3D COF membranes and understand the solvent transport mechanism through defect-free 3D COF membranes using different transport models, such as the pore-flow model and solution-diffusion model.

References

[1] M.S. Vassiliou, Historical dictionary of the petroleum industry, Rowman & Littlefield2018.

[2] R. Wei, X. Liu, Z. Lai, MOF or COF membranes for olefin/paraffin separation: Current status and future research directions, Advanced Membranes 2 (2022) 100035.

[3] J.M. Prausnitz, R.N. Lichtenthaler, E.G. De Azevedo, Molecular thermodynamics of fluid-phase equilibria, Pearson Education1998.

[4] S.-J. Kim, Y. Kwon, D. Kim, H. Park, Y.H. Cho, S.-E. Nam, Y.-I. Park, A review on polymer precursors of carbon molecular sieve membranes for olefin/paraffin separation, Membranes 11(7) (2021) 482.

[5] J.-W. Chang, T. Marrero, H. Yasuda, Continuous process for propylene/propane separation by use of silver nitrate carrier and zirconia porous membrane, J. Membr. Sci. 205(1-2) (2002) 91-102.

[6] R.B. Eldridge, Olefin/paraffin separation technology: a review, Ind. Eng. Chem. Res. 32(10) (1993) 2208-2212.

[7] Y. Ren, X. Liang, H. Dou, C. Ye, Z. Guo, J. Wang, Y. Pan, H. Wu, M.D. Guiver, Z. Jiang, Membrane-based olefin/paraffin separations, Advanced Science 7(19) (2020) 2001398.

[8] D.S. Sholl, R.P. Lively, Seven chemical separations to change the world, Nature 532(7600) (2016) 435-437.

[9] D.M.V.d. Miranda, L.d.S. Dutra, D. Way, N. Amaral, F. Wegenast, M.C. Scaldaferri, N. Jesus, J.C. Pinto, A bibliometric survey of Paraffin/Olefin separation using membranes, Membranes 9(12) (2019) 157.

[10] M. Yoshino, S. Nakamura, H. Kita, K.-i. Okamoto, N. Tanihara, Y. Kusuki, Olefin/paraffin separation performance of asymmetric hollow fiber membrane of 6FDA/BPDA–DDBT copolyimide, J. Membr. Sci. 212(1-2) (2003) 13-27.

[11] M.L. Jue, V. Breedveld, R.P. Lively, Defect-free PIM-1 hollow fiber membranes, J. Membr. Sci. 530 (2017) 33-41.

[12] M. Rungta, C. Zhang, W.J. Koros, L. Xu, Membrane-based ethylene/ethane separation: The upper bound and beyond, AlChE J. 59(9) (2013) 3475-3489.

[13] R.L. Burns, W.J. Koros, Defining the challenges for C3H6/C3H8 separation using polymeric membranes, J. Membr. Sci. 211(2) (2003) 299-309.

[14] A. Roy, S.R. Venna, G. Rogers, L. Tang, T.C. Fitzgibbons, J. Liu, H. McCurry, D.J. Vickery, D. Flick, B. Fish, Membranes for olefin–paraffin separation: An industrial perspective, Proceedings of the National Academy of Sciences 118(37) (2021) e2022194118.

[15] A.C.C. Campos, R.A. dos Reis, A. Ortiz, D. Gorri, I. Ortiz, A perspective of solutions for membrane instabilities in olefin/paraffin separations: a review, Ind. Eng. Chem. Res. 57(31) (2018) 10071-10085.

[16] X. Ma, P. Kumar, N. Mittal, A. Khlyustova, P. Daoutidis, K.A. Mkhoyan, M. Tsapatsis, Zeolitic imidazolate framework membranes made by ligand-induced permselectivation, Science 361(6406) (2018) 1008-1011.

[17] R. Bo, M. Taheri, B. Liu, R. Ricco, H. Chen, H. Amenitsch, Z. Fusco, T. Tsuzuki, G. Yu, R. Ameloot, Hierarchical metal-organic framework films with controllable meso/macroporosity, Advanced Science 7(24) (2020) 2002368.

[18] R.-B. Lin, L. Li, H.-L. Zhou, H. Wu, C. He, S. Li, R. Krishna, J. Li, W. Zhou, B. Chen, Molecular sieving of ethylene from ethane using a rigid metal–organic framework, Nat. Mater. 17(12) (2018) 1128-1133.

[19] X.C. Huang, Y.Y. Lin, J.P. Zhang, X.M. Chen, Ligand-directed strategy for zeolite-type metal–organic frameworks: zinc (II) imidazolates with unusual zeolitic topologies, Angew. Chem. Int. Ed. 45(10) (2006) 1557-1559.

[20] K.S. Park, Z. Ni, A.P. Côté, J.Y. Choi, R. Huang, F.J. Uribe-Romo, H.K. Chae, M. O'Keeffe, O.M. Yaghi, Exceptional chemical and thermal stability of zeolitic imidazolate frameworks, Proceedings of the National Academy of Sciences 103(27) (2006) 10186-10191.

[21] L. Mu, B. Liu, H. Liu, Y. Yang, C. Sun, G. Chen, A novel method to improve the gas storage capacity of ZIF-8, J. Mater. Chem. 22(24) (2012) 12246-12252.

[22] Y. Zhao, Y. Wei, L. Lyu, Q. Hou, J.r. Caro, H. Wang, Flexible polypropylene-supported ZIF-8 membranes for highly efficient propene/propane separation, J. Am. Chem. Soc. 142(50) (2020) 20915-20919.

[23] W. Xue, Q. Zhou, F. Li, B.S. Ondon, Zeolitic imidazolate framework-8 (ZIF-8) as robust catalyst for oxygen reduction reaction in microbial fuel cells, J. Power Sources 423 (2019) 9-17.

[24] Q. Wang, Y. Sun, S. Li, P. Zhang, Q. Yao, Synthesis and modification of ZIF-8 and its application in drug delivery and tumor therapy, RSC advances 10(62) (2020) 37600-37620.

[25] G. Lu, J.T. Hupp, Metal− organic frameworks as sensors: a ZIF-8 based Fabry− Pérot device as a selective sensor for chemical vapors and gases, J. Am. Chem. Soc. 132(23) (2010) 7832-7833.

[26] Y.-R. Lee, M.-S. Jang, H.-Y. Cho, H.-J. Kwon, S. Kim, W.-S. Ahn, ZIF-8: A comparison of synthesis methods, Chem. Eng. J. 271 (2015) 276-280.

[27] K. Li, D.H. Olson, J. Seidel, T.J. Emge, H. Gong, H. Zeng, J. Li, Zeolitic imidazolate frameworks for kinetic separation of propane and propene, J. Am. Chem. Soc. 131(30) (2009) 10368-10369.

[28] C. Zhang, R.P. Lively, K. Zhang, J.R. Johnson, O. Karvan, W.J. Koros, Unexpected molecular sieving properties of zeolitic imidazolate framework-8, J. Phys. Chem. Lett. 3(16) (2012) 2130-2134.

[29] U. Böhme, B. Barth, C. Paula, A. Kuhnt, W. Schwieger, A. Mundstock, J.r. Caro, M. Hartmann, Ethene/ethane and propene/propane separation via the olefin and paraffin selective metal–organic framework adsorbents CPO-27 and ZIF-8, Langmuir 29(27) (2013) 8592-8600.

[30] B. Kaewruksa, V. Vchirawongkwin, V. Ruangpornvisuti, Adsorption of propane and propylene in zeolitic imidazolate framework ZIF-8 pore: periodic SCC-DFTB method, Adsorption 24(7) (2018) 691-701.

[31] Y. Pan, Z. Lai, Sharp separation of C2/C3 hydrocarbon mixtures by zeolitic imidazolate framework-8 (ZIF-8) membranes synthesized in aqueous solutions, Chem. Commun. 47(37) (2011) 10275-10277.

[32] Y. Pan, T. Li, G. Lestari, Z. Lai, Effective separation of propylene/propane binary mixtures by ZIF-8 membranes, J. Membr. Sci. 390 (2012) 93-98.

[33] H.T. Kwon, H.-K. Jeong, Highly propylene-selective supported zeolite-imidazolate framework (ZIF-8) membranes synthesized by rapid microwave-assisted seeding and secondary growth, Chem. Commun. 49(37) (2013) 3854-3856.

[34] Y. Pan, W. Liu, Y. Zhao, C. Wang, Z. Lai, Improved ZIF-8 membrane: Effect of activation procedure and determination of diffusivities of light hydrocarbons, J. Membr. Sci. 493 (2015) 88-96.

[35] R. Wei, H.Y. Chi, X. Li, D. Lu, Y. Wan, C.W. Yang, Z. Lai, Aqueously cathodic deposition of ZIF-8 membranes for superior propylene/propane separation, Adv. Funct. Mater. 30(7) (2020) 1907089.

[36] D. Li, Y. Yan, H. Wang, Recent advances in polymer and polymer composite membranes for reverse and forward osmosis processes, Prog. Polym. Sci. 61 (2016) 104-155.

[37] J. Micovic, K. Werth, P. Lutze, Hybrid separations combining distillation and organic solvent nanofiltration for separation of wide boiling mixtures, Chem. Eng. Res. Des. 92(11) (2014) 2131-2147.

[38] K. Werth, P. Kaupenjohann, M. Skiborowski, The potential of organic solvent nanofiltration processes for oleochemical industry, Sep. Purif. Technol. 182 (2017) 185-196.

[39] R.P. Lively, D.S. Sholl, From water to organics in membrane separations, Nat. Mater. 16(3) (2017) 276-279.

[40] B. Liang, X. He, J. Hou, L. Li, Z. Tang, Membrane separation in organic liquid: technologies, achievements, and opportunities, Adv. Mater. 31(45) (2019) 1806090.

[41] F.J. Uribe-Romo, J.R. Hunt, H. Furukawa, C. Klock, M. O'Keeffe, O.M. Yaghi, A crystalline imine-linked 3-D porous covalent organic framework, J. Am. Chem. Soc. 131(13) (2009) 4570-4571.

[42] K. Dey, M. Pal, K.C. Rout, S. Kunjattu H, A. Das, R. Mukherjee, U.K. Kharul, R. Banerjee, Selective molecular separation by interfacially crystallized covalent organic framework thin films, J. Am. Chem. Soc. 139(37) (2017) 13083-13091.

[43] R. Wang, X. Shi, A. Xiao, W. Zhou, Y. Wang, Interfacial polymerization of covalent organic frameworks (COFs) on polymeric substrates for molecular separations, J. Membr. Sci. 566 (2018) 197-204.

[44] Y. Wu, Y. Wang, F. Xu, K. Qu, L. Dai, H. Cao, Y. Xia, L. Lei, K. Huang, Z. Xu, Solvent-induced interfacial polymerization enables highly crystalline covalent organic framework membranes, J. Membr. Sci. 659 (2022). https://doi.org/10.1016/j.memsci.2022.120799.

[45] Y. Qu, Y. Zha, X. Du, S. Xu, M. Zhang, L. Xu, H. Jia, Interfacial Polymerization of Self-Standing Covalent Organic Framework Membranes at Alkane/Ionic Liquid Interfaces for Dye Separation, ACS Applied Polymer Materials 4(10) (2022) 7528-7536.

[46] S. Li, F. Yang, S. Liu, H. Li, B. Su, L. Han, X. Gao, C. Gao, Effective regulating interfacial polymerization process of OSN membrane via in-situ constructed nano-porous interlayer of 2D TpHz covalent organic frameworks, J. Membr. Sci. 665 (2023) 121101.

[47] D.B. Shinde, G. Sheng, X. Li, M. Ostwal, A.-H. Emwas, K.-W. Huang, Z. Lai, Crystalline 2D covalent organic framework membranes for high-flux organic solvent nanofiltration, J. Am. Chem. Soc. 140(43) (2018) 14342-14349.

[48] D.B. Shinde, L. Cao, A.D. Wonanke, X. Li, S. Kumar, X. Liu, M.N. Hedhili, A.-H. Emwas, M. Addicoat, K.-W. Huang, Pore engineering of ultrathin covalent organic framework membranes for organic solvent nanofiltration and molecular sieving, Chemical science 11(21) (2020) 5434-5440.

[49] J.-R. Li, J. Sculley, H.-C. Zhou, Metal–organic frameworks for separations, Chem. Rev. 112(2) (2012) 869-932.

[50] X. Zhao, Y. Wang, D.S. Li, X. Bu, P. Feng, Metal–organic frameworks for separation, Adv. Mater. 30(37) (2018) 1705189.

[51] Q.M. Wang, D. Shen, M. Bülow, M.L. Lau, S. Deng, F.R. Fitch, N.O. Lemcoff, J. Semanscin, Metallo-organic molecular sieve for gas separation and purification, Microporous Mesoporous Mater. 55(2) (2002) 217-230.

[52] J.-W. Yoon, I.-T. Jang, K.-Y. Lee, Y.-K. Hwang, J.-S. Chang, Adsorptive separation of propylene and propane on a porous metal-organic framework, copper trimesate, Bull. Korean Chem. Soc. 31(1) (2010) 220-223.

[53] C. Gucuyener, J. van den Bergh, J. Gascon, F. Kapteijn, Ethane/ethene separation turned on its head: selective ethane adsorption on the metal− organic framework ZIF-7 through a gate-opening mechanism, J. Am. Chem. Soc. 132(50) (2010) 17704-17706.

[54] Y. Lin, Inorganic membranes for process intensification: Challenges and perspective, Ind. Eng. Chem. Res. 58(15) (2018) 5787-5796.

[55] M.R.A. Hamid, T.C.S. Yaw, M.Z.M. Tohir, W.A.W.A.K. Ghani, P.D. Sutrisna, H.-K. Jeong, Zeolitic imidazolate framework membranes for gas separations: Current state-of-the-art, challenges, and opportunities, Journal of Industrial and Engineering Chemistry 98 (2021) 17-41.

[56] H.T. Kwon, H.-K. Jeong, A.S. Lee, H.S. An, J.S. Lee, Heteroepitaxially grown zeolitic imidazolate framework membranes with unprecedented propylene/propane separation performances, J. Am. Chem. Soc. 137(38) (2015) 12304-12311.

[57] C. Wang, F. Yang, L. Sheng, J. Yu, K. Yao, L. Zhang, Y. Pan, Zinc-substituted ZIF-67 nanocrystals and polycrystalline membranes for propylene/propane separation, Chem. Commun. 52(85) (2016) 12578-12581.

[58] F. Hillman, J.M. Zimmerman, S.-M. Paek, M.R. Hamid, W.T. Lim, H.-K. Jeong, Rapid microwave-assisted synthesis of hybrid zeolitic–imidazolate frameworks with mixed metals and mixed linkers, J. Mater. Chem. A 5(13) (2017) 6090-6099.

[59] N.T. Tran, J. Kim, M.R. Othman, Microporous ZIF-8 and ZIF-67 membranes grown on mesoporous alumina substrate for selective propylene transport, Sep. Purif. Technol. 233 (2020) 116026.

[60] Q. Hou, S. Zhou, Y. Wei, J.r. Caro, H. Wang, Balancing the grain boundary structure and the framework flexibility through bimetallic Metal–Organic Framework (MOF) membranes for gas separation, J. Am. Chem. Soc. 142(21) (2020) 9582-9586.

[61] H. Bux, F. Liang, Y. Li, J. Cravillon, M. Wiebcke, J.r. Caro, Zeolitic imidazolate framework membrane with molecular sieving properties by microwave-assisted solvothermal synthesis, J. Am. Chem. Soc. 131(44) (2009) 16000-16001.

[62] H.T. Kwon, H.-K. Jeong, In situ synthesis of thin zeolitic–imidazolate framework ZIF-8 membranes exhibiting exceptionally high propylene/propane separation, J. Am. Chem. Soc. 135(29) (2013) 10763-10768.

[63] F. Hillman, J. Brito, H.-K. Jeong, Rapid one-pot microwave synthesis of mixed-linker hybrid zeolitic-imidazolate framework membranes for tunable gas separations, ACS Appl. Mater. 10(6) (2018) 5586-5593.

[64] J. Yao, D. Dong, D. Li, L. He, G. Xu, H. Wang, Contra-diffusion synthesis of ZIF-8 films on a polymer substrate, Chem. Commun. 47(9) (2011) 2559-2561.

[65] V.M.A. Melgar, J. Kim, Preparation of crack-free ZIF-7 thin films by electrospray deposition, Membrane Journal 23(4) (2013) 278-282.

[66] V.M.A. Melgar, H.T. Kwon, J. Kim, Direct spraying approach for synthesis of ZIF-7 membranes by electrospray deposition, J. Membr. Sci. 459 (2014) 190-196.

[67] V.M.A. Melgar, H. Ahn, J. Kim, M.R. Othman, Highly selective micro-porous ZIF-8 membranes prepared by rapid electrospray deposition, Journal of Industrial and Engineering Chemistry 21 (2015) 575-579.

[68] D.J. Babu, G. He, L.F. Villalobos, K.V. Agrawal, Crystal engineering of metal–organic framework thin films for gas separations, ACS Sustainable Chemistry & Engineering 7(1) (2018) 49-69.

[69] M.C. Lovallo, A. Gouzinis, M. Tsapatsis, Synthesis and characterization of oriented MFI membranes prepared by secondary growth, AlChE J. 44(8) (1998) 1903-1913.

[70] K. Tao, C. Kong, L. Chen, High performance ZIF-8 molecular sieve membrane on hollow ceramic fiber via crystallizing-rubbing seed deposition, Chem. Eng. J. 220 (2013) 1-5.

[71] J.B. James, L. Lang, L. Meng, J.Y. Lin, Postsynthetic modification of ZIF-8 membranes via membrane surface ligand exchange for light hydrocarbon gas separation enhancement, ACS Appl. Mater. 12(3) (2019) 3893-3902.

[72] H. Chang, Y. Wang, L. Xiang, D. Liu, C. Wang, Y. Pan, Improved H_2/CO_2 separation performance on mixed-linker ZIF-7 polycrystalline membranes, Chem. Eng. Sci. 192 (2018) 85-93.

[73] C. Zhang, J. Yan, T. Ji, D. Du, Y. Sun, L. Liu, X. Zhang, Y. Liu, Fabrication of highly (110)-Oriented ZIF-8 membrane at low temperature using nanosheet seed layer, J. Membr. Sci. 641 (2022) 119915.

[74] M.R. Abdul Hamid, S. Park, J.S. Kim, Y.M. Lee, H.-K. Jeong, Synthesis of ultrathin zeolitic imidazolate framework ZIF-8 membranes on polymer hollow fibers using a polymer modification strategy for propylene/propane separation, Ind. Eng. Chem. Res. 58(32) (2019) 14947-14953.

[75] G. Ramu, M. Lee, H.-K. Jeong, Effects of zinc salts on the microstructure and performance of zeolitic-imidazolate framework ZIF-8 membranes for propylene/propane separation, Microporous Mesoporous Mater. 259 (2018) 155-162.

[76] P. Nian, H. Liu, X. Zhang, Bottom-up fabrication of two-dimensional Co-based zeolitic imidazolate framework tubular membranes consisting of nanosheets by vapor phase transformation of Co-based gel for H2/CO2 separation, J. Membr. Sci. 573 (2019) 200-209.

[77] W. Li, P. Su, Z. Li, Z. Xu, F. Wang, H. Ou, J. Zhang, G. Zhang, E. Zeng, Ultrathin metal–organic framework membrane production by gel–vapour deposition, Nat. Commun. 8(1) (2017) 1-8.

[78] M. Drobek, M. Bechelany, C. Vallicari, A. Abou Chaaya, C. Charmette, C. Salvador-Levehang, P. Miele, A. Julbe, An innovative approach for the preparation of confined ZIF-8 membranes by conversion of ZnO ALD layers, J. Membr. Sci. 475 (2015) 39-46.

[79] C.-H. Chang, R. Gopalan, Y. Lin, A comparative study on thermal and hydrothermal stability of alumina, titania and zirconia membranes, J. Membr. Sci. 91(1-2) (1994) 27-45.

[80] Y. Pan, X. Yu, Preparation of Zeolitic Imidazolate Framework-91 and its modeling for pervaporation separation of water/ethanol mixtures, Sep. Purif. Technol. 237 (2020) 116330.

[81] I. Stassen, M. Styles, G. Grenci, H.V. Gorp, W. Vanderlinden, S.D. Feyter, P. Falcaro, D.D. Vos, P. Vereecken, R. Ameloot, Chemical vapour deposition of zeolitic imidazolate framework thin films, Nat. Mater. 15(3) (2016) 304-310.

[82] D. Liu, X. Ma, H. Xi, Y. Lin, Gas transport properties and propylene/propane separation characteristics of ZIF-8 membranes, J. Membr. Sci. 451 (2014) 85-93.

[83] Q. Ma, K. Mo, S. Gao, Y. Xie, J. Wang, H. Jin, A. Feldhoff, S. Xu, J.Y. Lin, Y. Li, Ultrafast semi-solid processing of highly durable ZIF-8 membranes for propylene/propane separation, Angew. Chem. 132(49) (2020) 22093-22098.

[84] J. Yu, Y. Pan, C. Wang, Z. Lai, ZIF-8 membranes with improved reproducibility fabricated from sputter-coated ZnO/alumina supports, Chem. Eng. Sci. 141 (2016) 119-124.

[85] N. Hara, M. Yoshimune, H. Negishi, K. Haraya, S. Hara, T. Yamaguchi, Diffusive separation of propylene/propane with ZIF-8 membranes, J. Membr. Sci. 450 (2014) 215-223.

[86] N. Hara, M. Yoshimune, H. Negishi, K. Haraya, S. Hara, T. Yamaguchi, ZIF-8 membranes prepared at miscible and immiscible liquid–liquid interfaces, Microporous Mesoporous Mater. 206 (2015) 75-80.

[87] N. Hara, M. Yoshimune, H. Negishi, K. Haraya, S. Hara, T. Yamaguchi, Effect of temperature on synthesis of ZIF-8 membranes for propylene/propane separation by counter diffusion method, Journal of the Japan Petroleum Institute 58(4) (2015) 237-244.

[88] N. Hara, M. Yoshimune, H. Negishi, K. Haraya, S. Hara, T. Yamaguchi, Effect of solution concentration on structure and permeation properties of ZIF-8 membranes for propylene/propane separation, J. Chem. Eng. Jpn. 49(2) (2018) 97-103.

[89] H.T. Kwon, H.-K. Jeong, A.S. Lee, H.S. An, T. Lee, E. Jang, J.S. Lee, J. Choi, Defect-induced ripening of zeolitic-imidazolate framework ZIF-8 and its implication to vapor-phase membrane synthesis, Chem. Commun. 52(78) (2016) 11669-11672.

[90] H.T. Kwon, H.-K. Jeong, Improving propylene/propane separation performance of Zeolitic-Imidazolate framework ZIF-8 Membranes, Chem. Eng. Sci. 124 (2015) 20-26.

[91] M.J. Lee, H.T. Kwon, H.K. Jeong, High-flux zeolitic imidazolate framework membranes for propylene/propane separation by postsynthetic linker exchange, Angew. Chem. Int. Ed. 57(1) (2018) 156-161.

[92] T. Kim, Y.J. Kim, C. Yu, J. Kim, K. Eum, Facile Fabrication of α-Alumina Hollow Fiber-Supported ZIF-8 Membrane Module and Impurity Effects on Propylene Separation Performance, Membranes 12(10) (2022) 1015.

[93] H. Lian, Y. Yang, J. Chen, B. Bao, W. Yang, R. Hou, S. Ju, Y. Pan, Highly durable ZIF-8 tubular membranes via precursor-assisted processing for propylene/propane separation, J. Membr. Sci. 660 (2022) 120813.

[94] E. Song, K. Wei, H. Lian, J. Hua, H. Tao, T. Wu, Y. Pan, W. Xing, Improved propylene/propane separation performance under high temperature and pressures on in-situ ligand-doped ZIF-8 membranes, J. Membr. Sci. 617 (2021) 118655.

[95] H. Lian, B. Bao, J. Chen, W. Yang, Y. Yang, R. Hou, S. Ju, Y. Pan, Controllable synthesis of ZIF-8 interlocked membranes for propylene/propane separation, Sep. Purif. Technol. 300 (2022) 121811.

[96] M. Gehre, Z. Guo, G. Rothenberg, S. Tanase, Sustainable Separations of C4-Hydrocarbons by Using Microporous Materials, ChemSusChem 10(20) (2017) 3947-3963.

[97] M. Bender, An overview of industrial processes for the production of olefins–C4 hydrocarbons, ChemBioEng Reviews 1(4) (2014) 136-147.

[98] V. Zacharopoulou, A.A. Lemonidou, Olefins from biomass intermediates: a review, Catalysts 8(1) (2017) 2.

[99] G. Meyer, G. Kaibel, G. Bohner, K. Kindler, T. Adrian, K. Pickenaecker, M. Pahl, T. Hill, Method and device for treating a c4 fraction, Google Patents. 2003.

[100] P.-Q. Liao, N.-Y. Huang, W.-X. Zhang, J.-P. Zhang, X.-M. Chen, Controlling guest conformation for efficient purification of butadiene, Science 356(6343) (2017) 1193-1196.

[101] X. Tian, X. Zhang, L. Wei, S. Zeng, L. Huang, S. Zhang, Multi-scale simulation of the 1, 3-butadiene extraction separation process with an ionic liquid additive, Green Chemistry 12(7) (2010) 1263-1273.

[102] W.C. White, Butadiene production process overview, Chem. Biol. Interact. 166(1-3) (2007) 10-14.

[103] T.A. Agbaje, L.F. Vega, M. Khaleel, K. Wang, G.N. Karanikolos, Membranes and adsorbents in separation of C4 hydrocarbons: A review and the definition of the current upper bounds, Sep. Purif. Technol. 278 (2021). https://doi.org/10.1016/j.seppur.2021.119530.

[104] A. Motelica, O.S. Bruinsma, R. Kreiter, M. den Exter, J.F. Vente, Membrane Retrofit Option for Paraffin/Olefin Separation-A Technoeconomic Evaluation, Ind. Eng. Chem. Res. 51(19) (2012) 6977-6986.

[105] P. Kostetskyy, G. Mpourmpakis, Computational insights into adsorption of C4 hydrocarbons in cation-exchanged ZSM-12 zeolites, Ind. Eng. Chem. Res. 56(24) (2017) 7062-7069.

[106] C. Gücüyener, J. Van Den Bergh, A.M. Joaristi, P.C. Magusin, E.J. Hensen, J. Gascon, F. Kapteijn, Facile synthesis of the DD3R zeolite: performance in the adsorptive separation of buta-1, 3-diene and but-2-ene isomers, J. Mater. Chem. 21(45) (2011) 18386-18397.

[107] A.H. Assen, T. Virdis, W. De Moor, A. Moussa, M. Eddaoudi, G. Baron, J.F.M. Denayer, Y. Belmabkhout, Kinetic separation of C4 olefins using Y-fum-fcu-MOF with ultra-fine-tuned aperture size, Chem. Eng. J. 413 (2021). https://doi.org/10.1016/j.cej.2020.127388.

[108] K. Kishida, Y. Okumura, Y. Watanabe, M. Mukoyoshi, S. Bracco, A. Comotti, P. Sozzani, S. Horike, S. Kitagawa, Recognition of 1, 3-butadiene by a porous coordination polymer, Angew. Chem. Int. Ed. 55(44) (2016) 13784-13788.

[109] P. Mukherjee, P.K. Ghorai, Separation of trans-1, 3-butadiene from C4 hydrocarbons mixtures by metal organic framework: A molecular dynamics simulation investigation, Chem. Phys. 566 (2023) 111790.

[110] C.Y. Chuah, T.-H. Bae, Polyimide-derived carbon molecular sieve membranes for advanced gas separation: from membrane development to pilot-scale operations, Sep. Purif. Technol. (2023) 124114.

[111] D.A. Kang, H.-K. Jeong, Enhancing the C3 separation performances of polycrystalline ZIF-8 membranes by additive-assisted secondary growth, J. Membr. Sci. (2023) 121593.

[112] M.M. Rahman, Multiblock copolymers containing polyether segments for separation of C4 hydrocarbons, J. Membr. Sci. 666 (2023) 121176.

[113] K. Okamoto, K. Noborio, J. Hao, K. Tanaka, H. Kita, Permeation and separation properties of polyimide membranes to 1, 3-butadiene and n-butane, J. Membr. Sci. 134(2) (1997) 171-179.

[114] H.S. Kim, J.Y. Bae, S.J. Park, H. Lee, H.W. Bae, S.O. Kang, S.D. Lee, D.K. Choi, Separation of olefin/paraffin mixtures using zwitterionic silver complexes as transport carriers, Chemistry–A European Journal 13(9) (2007) 2655-2660.

[115] I.U. Haq, T. Wang, A.S. Zhang, H. Mao, R. Khan, L.H. Xu, Z.P. Zhao, Fabrication of zeolitic imidazolate frameworks based mixed matrix membranes and mass transfer properties of C_4H_6 and N2 in membrane separation, AlChE J. 67(4) (2021) e17114.

[116] X. Cen, Y. Sun, C. Yu, Z. Qiao, C. Zhong, Metal confined in metal-organic framework-based mixed matrix membranes for efficient butadiene recognition separation, Aggregate (2023) e361.

[117] Q. Ma, S. Kim, Y. Jeong, E. Jang, J. Choi, Construction of a thermally stable ZIF-8 membrane embedded inside a porous support for H_2/CO_2 separation: Close interlocking between membrane grains and porous support grains, J. Membr. Sci. 677 (2023) 121654.

[118] X. Duan, P. Kaya, H.-Y. Chi, B. Topuz, K.V. Agrawal, Fabrication of ZIF-8 membranes by direct assembly of nanosheets from bottom-up synthesis growth solution, Journal of Membrane Science Letters 3(1) (2023) 100045.

[119] Y. Peng, Y. Li, Y. Ban, H. Jin, W. Jiao, X. Liu, W. Yang, Metal-organic framework nanosheets as building blocks for molecular sieving membranes, Science 346(6215) (2014) 1356-1359.

[120] S.R. Venna, M.A. Carreon, Highly permeable zeolite imidazolate framework-8 membranes for CO2/CH4 separation, J. Am. Chem. Soc. 132(1) (2010) 76-78.

[121] Q. Hou, Y. Wu, S. Zhou, Y. Wei, J. Caro, H. Wang, Ultra-Tuning of the Aperture Size in Stiffened ZIF-8_Cm Frameworks with Mixed-Linker Strategy for Enhanced CO2 /CH4 Separation, Angew. Chem. Int. Ed. Engl. 58(1) (2019) 327-331. https://doi.org/10.1002/anie.201811638.

[122] D.S. Chiou, H.J. Yu, T.H. Hung, Q. Lyu, C.K. Chang, J.S. Lee, L.C. Lin, D.Y. Kang, Highly CO2 selective metal–organic framework membranes with favorable coulombic effect, Adv. Funct. Mater. 31(4) (2021) 2006924.

[123] Y. Wang, H. Jin, Q. Ma, K. Mo, H. Mao, A. Feldhoff, X. Cao, Y. Li, F. Pan, Z. Jiang, A MOF glass membrane for gas separation, Angew. Chem. 132(11) (2020) 4395-4399.

[124] S.R. Venna, M.A. Carreon, Metal organic framework membranes for carbon dioxide separation, Chem. Eng. Sci. 124 (2015) 3-19.

[125] S. Zhou, O. Shekhah, T. Jin, J. Jia, S.J. Datta, P.M. Bhatt, M. Eddaoudi, A CO_2-recognition metal-organic framework membrane for continuous carbon capture, Chem 9(5) (2023) 1182-1194.

[126] J.B. James, J. Wang, L. Meng, Y. Lin, ZIF-8 membrane ethylene/ethane transport characteristics in single and binary gas mixtures, Ind. Eng. Chem. Res. 56(26) (2017) 7567-7575.

[127] R. Wei, X. Liu, Z. Zhou, C. Chen, Y. Yuan, Z. Li, X. Li, X. Dong, D. Lu, Y. Han, Carbon nanotube supported oriented metal organic framework membrane for effective ethylene/ethane separation, Sci. Adv. 8(7) (2022) eabm6741.

[128] K.S. Goh, Y. Chen, D.Y.F. Ng, J.W. Chew, R. Wang, Organic solvent forward osmosis membranes for pharmaceutical concentration, J. Membr. Sci. 642 (2022) 119965.

[129] T. Ji, J. Yan, Y. He, W. Hu, Y. Peng, W. Yang, Y. Liu, Towards ZIF-8 membranes with superb C3H6/C3H8 separation performances under varying conditions: Necessity of precise temperature control, J. Membr. Sci. 683 (2023) 121776.

[130] Z. Qiang, Z. Yi, J.-W. Wang, R.S. Khandge, X. Ma, Fabrication of Polycrystalline Zeolitic Imidazolate Framework Membranes by a Vapor-Phase Seeding Method, Membranes 13(9) (2023) 782.

[131] Z. Zhao, X. Ma, Z. Li, Y. Lin, Synthesis, characterization and gas transport properties of MOF-5 membranes, J. Membr. Sci. 382(1-2) (2011) 82-90.

[132] I.U. Haq, S.H. Li, H.-G. Zhen, R. Khan, A.-S. Zhang, Z.-P. Zhao, Highly efficient separation of 1, 3-butadiene from nitrogen mixture by adsorption on highly stable MOF, Chem. Eng. J. 402 (2020) 125980.

[133] K.-i. Okamoto, S. Kawamura, M. Yoshino, H. Kita, Y. Hirayama, N. Tanihara, Y. Kusuki, Olefin/paraffin separation through carbonized membranes derived from an asymmetric polyimide hollow fiber membrane, Ind. Eng. Chem. Res. 38(11) (1999) 4424-4432.

[134] T. Yamaguchi, C. Baertsch, C.A. Koval, R.D. Noble, C.N. Bowman, Olefin separation using silver impregnated ion-exchange membranes and silver salt/polymer blend membranes, J. Membr. Sci. 117(1-2) (1996) 151-161.

[135] N. Huang, P. Wang, D. Jiang, Covalent organic frameworks: a materials platform for structural and functional designs, Nature Reviews Materials 1(10) (2016). https://doi.org/10.1038/natrevmats.2016.68.

[136] M. Dogru, T. Bein, On the road towards electroactive covalent organic frameworks, Chem Commun (Camb) 50(42) (2014) 5531-46. https://doi.org/10.1039/c3cc46767h.

[137] X. Feng, X. Ding, D. Jiang, Covalent organic frameworks, Chem. Soc. Rev. 41(18) (2012) 6010-22. https://doi.org/10.1039/c2cs35157a.

[138] L. Zhu, Y.B. Zhang, Crystallization of Covalent Organic Frameworks for Gas Storage Applications, Molecules 22(7) (2017). https://doi.org/10.3390/molecules22071149.

[139] N.B. McKeown, P.M. Budd, Polymers of intrinsic microporosity (PIMs): organic materials for membrane separations, heterogeneous catalysis and hydrogen storage, Chem. Soc. Rev. 35(8) (2006) 675-83. https://doi.org/10.1039/b600349d.

[140] Y. Zhu, L. Peng, Z. Fang, C. Yan, X. Zhang, G. Yu, Structural Engineering of 2D Nanomaterials for Energy Storage and Catalysis, Adv. Mater. 30(15) (2018) e1706347. https://doi.org/10.1002/adma.201706347.

[141] M.S. Lohse, T. Bein, Covalent Organic Frameworks: Structures, Synthesis, and Applications, Adv. Funct. Mater. 28(33) (2018). https://doi.org/10.1002/adfm.201705553.

[142] H. Fan, A. Mundstock, A. Feldhoff, A. Knebel, J. Gu, H. Meng, J. Caro, Covalent Organic Framework-Covalent Organic Framework Bilayer Membranes for Highly Selective Gas Separation, J Am Chem Soc 140(32) (2018) 10094-10098. https://doi.org/10.1021/jacs.8b05136.

[143] B. Hosseini Monjezi, K. Kutonova, M. Tsotsalas, S. Henke, A. Knebel, Current Trends in Metal-Organic and Covalent Organic Framework Membrane Materials, Angew. Chem. Int. Ed. Engl. 60(28) (2021) 15153-15164. https://doi.org/10.1002/anie.202015790.

[144] J. Li, X. Zhou, J. Wang, X. Li, Two-Dimensional Covalent Organic Frameworks (COFs) for Membrane Separation: a Mini Review, Ind. Eng. Chem. Res. 58(34) (2019) 15394-15406. https://doi.org/10.1021/acs.iecr.9b02708.

[145] S. Yuan, X. Li, J. Zhu, G. Zhang, P. Van Puyvelde, B. Van der Bruggen, Covalent organic frameworks for membrane separation, Chem. Soc. Rev. 48(10) (2019) 2665-2681. https://doi.org/10.1039/c8cs00919h.

[146] M.E. Davis, Zeolites from a Materials Chemistry Perspective, Chem. Mater. 26(1) (2013) 239-245. https://doi.org/10.1021/cm401914u.

[147] Y. Li, J. Yu, New stories of zeolite structures: their descriptions, determinations, predictions, and evaluations, Chem Rev 114(14) (2014) 7268-316. https://doi.org/10.1021/cr500010r.

[148] N.B. McKeown, Polymers of Intrinsic Microporosity, ISRN Materials Science 2012 (2012) 1-16. https://doi.org/10.5402/2012/513986.

[149] D. Ramimoghadam, E.M. Gray, C.J. Webb, Review of polymers of intrinsic microporosity for hydrogen storage applications, Int. J. Hydrogen Energy 41(38) (2016) 16944-16965. https://doi.org/10.1016/j.ijhydene.2016.07.134.

[150] W. Lu, Z. Wei, Z.Y. Gu, T.F. Liu, J. Park, J. Park, J. Tian, M. Zhang, Q. Zhang, T. Gentle, 3rd, M. Bosch, H.C. Zhou, Tuning the structure and function of metal-organic frameworks via linker design, Chem. Soc. Rev. 43(16) (2014) 5561-93. https://doi.org/10.1039/c4cs00003j.

[151] G. Liu, A. Cadiau, Y. Liu, K. Adil, V. Chernikova, I.D. Carja, Y. Belmabkhout, M. Karunakaran, O. Shekhah, C. Zhang, A.K. Itta, S. Yi, M. Eddaoudi, W.J. Koros, Enabling Fluorinated MOF-Based Membranes for Simultaneous Removal of H_2 S and CO_2 from Natural Gas, Angew. Chem. Int. Ed. Engl. 57(45) (2018) 14811-14816. https://doi.org/10.1002/anie.201808991.

[152] A.P. Cote, A.I. Benin, N.W. Ockwig, M. O'Keeffe, A.J. Matzger, O.M. Yaghi, Porous, crystalline, covalent organic frameworks, Science 310(5751) (2005) 1166-1170.

[153] S. Kandambeth, K. Dey, R. Banerjee, Covalent organic frameworks: chemistry beyond the structure, J. Am. Chem. Soc. 141(5) (2018) 1807-1822.

[154] S.-Y. Ding, W. Wang, Covalent organic frameworks (COFs): from design to applications, Chem. Soc. Rev. 42(2) (2013) 548-568.

[155] X. Shi, Z. Zhang, S. Fang, J. Wang, Y. Zhang, Y. Wang, Flexible and Robust Three-Dimensional Covalent Organic Framework Membranes for Precise Separations under Extreme Conditions, Nano Lett. 21(19) (2021) 8355-8362. https://doi.org/10.1021/acs.nanolett.1c02919.

[156] H. Furukawa, O.M. Yaghi, Storage of hydrogen, methane, and carbon dioxide in highly porous covalent organic frameworks for clean energy applications, J. Am. Chem. Soc. 131(25) (2009) 8875-8883.

[157] X. Guan, F. Chen, Q. Fang, S. Qiu, Design and applications of three dimensional covalent organic frameworks, Chem. Soc. Rev. 49(5) (2020) 1357-1384. https://doi.org/10.1039/c9cs00911f.

[158] H.M. El-Kaderi, J.R. Hunt, J.L. Mendoza-Cortés, A.P. Côté, R.E. Taylor, M. O'Keeffe, O.M. Yaghi, Designed synthesis of 3D covalent organic frameworks, Science 316(5822) (2007) 268-272.

[159] Y. Cheng, L. Zhai, Y. Ying, Y. Wang, G. Liu, J. Dong, D.Z.L. Ng, S.A. Khan, D. Zhao, Highly efficient CO2 capture by mixed matrix membranes containing three-dimensional covalent organic framework fillers, J. Mater. Chem. A 7(9) (2019) 4549-4560. https://doi.org/10.1039/c8ta10333j.

[160] T. Ma, J. Li, J. Niu, L. Zhang, A.S. Etman, C. Lin, D. Shi, P. Chen, L.-H. Li, X. Du, Observation of interpenetration isomerism in covalent organic frameworks, J. Am. Chem. Soc. 140(22) (2018) 6763-6766.

[161] C. Fan, H. Geng, H. Wu, Q. Peng, X. Wang, B. Shi, Y. Kong, Z. Yin, Y. Liu, Z. Jiang, Three-dimensional covalent organic framework membrane for efficient proton conduction, J. Mater. Chem. A 9(33) (2021) 17720-17723. https://doi.org/10.1039/d1ta05005b.

[162] J. Fu, S. Das, G. Xing, T. Ben, V. Valtchev, S. Qiu, Fabrication of COF-MOF composite membranes and their highly selective separation of H_2/CO_2, J. Am. Chem. Soc. 138(24) (2016) 7673-7680.

[163] Z. Wang, Z. Si, D. Cai, G.L.S. Li, P. Qin, Synthesis of stable COF-300 nanofiltration membrane via in-situ growth with ultrahigh flux for selective dye separation, J. Membr. Sci. 615 (2020) 118466.

[164] H. Lu, C. Wang, J. Chen, R. Ge, W. Leng, B. Dong, J. Huang, Y. Gao, A novel 3D covalent organic framework membrane grown on a porous alpha-Al_2O_3 substrate under solvothermal conditions, Chem Commun (Camb) 51(85) (2015) 15562-5. https://doi.org/10.1039/c5cc06742a.

[165] Y.-B. Zhang, J. Su, H. Furukawa, Y. Yun, F. Gándara, A. Duong, X. Zou, O.M. Yaghi, Single-crystal structure of a covalent organic framework, J. Am. Chem. Soc. 135(44) (2013) 16336-16339.

[166] G. Lin, H. Ding, R. Chen, Z. Peng, B. Wang, C. Wang, 3D porphyrin-based covalent organic frameworks, J. Am. Chem. Soc. 139(25) (2017) 8705-8709.

[167] Y. Zhang, T. Fang, Q. Hou, Z. Li, Y. Yan, Water desalination of a new three-dimensional covalent organic framework: a molecular dynamics simulation study, Physical Chemistry Chemical Physics 22(29) (2020) 16978-16984.

[168] Q. Lu, Y. Ma, H. Li, X. Guan, Y. Yusran, M. Xue, Q. Fang, Y. Yan, S. Qiu, V. Valtchev, Postsynthetic functionalization of three-dimensional covalent organic frameworks for selective extraction of lanthanide ions, Angew. Chem. 130(21) (2018) 6150-6156.

[169] X. Guan, Y. Ma, H. Li, Y. Yusran, M. Xue, Q. Fang, Y. Yan, V. Valtchev, S. Qiu, Fast, ambient temperature and pressure ionothermal synthesis of three-dimensional covalent organic frameworks, J. Am. Chem. Soc. 140(13) (2018) 4494-4498.

[170] Y. Xie, J. Li, C. Lin, B. Gui, C. Ji, D. Yuan, J. Sun, C. Wang, Tuning the topology of three-dimensional covalent organic frameworks via steric control: from pts to unprecedented ljh, J. Am. Chem. Soc. 143(19) (2021) 7279-7284.

[171] H. Yang, H. Wu, F. Pan, Z. Li, H. Ding, G. Liu, Z. Jiang, P. Zhang, X. Cao, B. Wang, Highly water-permeable and stable hybrid membrane with asymmetric covalent organic framework distribution, J. Membr. Sci. 520 (2016) 583-595.

[172] Y. Yin, Z. Li, X. Yang, L. Cao, C. Wang, B. Zhang, H. Wu, Z. Jiang, Enhanced proton conductivity of Nafion composite membrane by incorporating phosphoric acid-loaded covalent organic framework, J. Power Sources 332 (2016) 265-273.

[173] X. Shi, Z. Zhang, M. Wei, X. Wang, J. Wang, Y. Zhang, Y. Wang, Three-Dimensional Covalent Organic Framework Membranes: Synthesis by Oligomer Interfacial Ripening and Application in Precise Separations, Macromolecules 55(8) (2022) 3259-3266.

[174] T. Zhu, Y. Kong, B. Lyu, L. Cao, B. Shi, X. Wang, X. Pang, C. Fan, C. Yang, H. Wu, 3D covalent organic framework membrane with fast and selective ion transport, Nat. Commun. 14(1) (2023) 5926.

[175] Z. Wang, S. Zhang, Y. Chen, Z. Zhang, S. Ma, Covalent organic frameworks for separation applications, Chem. Soc. Rev. 49(3) (2020) 708-735.

[176] D. Rodríguez-San-Miguel, F. Zamora, Processing of covalent organic frameworks: an ingredient for a material to succeed, Chem. Soc. Rev. 48(16) (2019) 4375-4386.

[177] X. Zhu, C. Tian, C.L. Do-Thanh, S. Dai, Two-Dimensional materials as prospective scaffolds for mixed-matrix membrane-based CO_2 separation, ChemSusChem 10(17) (2017) 3304-3316.

[178] Y. Yang, K. Goh, P. Weerachanchai, T.-H. Bae, 3D covalent organic framework for morphologically induced high-performance membranes with strong resistance toward physical aging, J. Membr. Sci. 574 (2019) 235-242. https://doi.org/10.1016/j.memsci.2018.12.078.

[179] S. Das, T. Ben, A [COF-300]-[UiO-66] composite membrane with remarkably high permeability and H 2/CO 2 separation selectivity, Dalton Transactions 47(21) (2018) 7206-7212.

[180] R.B. Merlet, M.-A. Pizzoccaro-Zilamy, A. Nijmeijer, L. Winnubst, Hybrid ceramic membranes for organic solvent nanofiltration: State-of-the-art and challenges, J. Membr. Sci. 599 (2020) 117839.

[181] M. Cook, P.R. Gaffney, L.G. Peeva, A.G. Livingston, Roll-to-roll dip coating of three different PIMs for Organic Solvent Nanofiltration, J. Membr. Sci. 558 (2018) 52-63.

[182] J. Li, M. Zhang, W. Feng, L. Zhu, L. Zhang, PIM-1 pore-filled thin film composite membranes for tunable organic solvent nanofiltration, J. Membr. Sci. 601 (2020) 117951.

[183] T. Gao, H. Wu, L. Tao, L. Qu, C. Li, Enhanced stability and separation efficiency of graphene oxide membranes in organic solvent nanofiltration, J. Mater. Chem. A 6(40) (2018) 19563-19569.

[184] D.K. Mahalingam, S. Wang, S.P. Nunes, Stable graphene oxide cross-linked membranes for organic solvent nanofiltration, Ind. Eng. Chem. Res. 58(51) (2019) 23106-23113.

[185] L. Nie, K. Goh, Y. Wang, J. Lee, Y. Huang, H.E. Karahan, K. Zhou, M.D. Guiver, T.-H. Bae, Realizing small-flake graphene oxide membranes for ultrafast size-dependent organic solvent nanofiltration, Sci. Adv. 6(17) (2020) eaaz9184.

[186] H. Lu, C. Wang, J. Chen, R. Ge, W. Leng, B. Dong, J. Huang, Y. Gao, A novel 3D covalent organic framework membrane grown on a porous α-Al 2 O 3 substrate under solvothermal conditions, Chem. Commun. 51(85) (2015) 15562-15565.

[187] A.K. Mohammed, A.A. Al Khoori, M.A. Addicoat, S. Varghese, I. Othman, M.A. Jaoude, K. Polychronopoulou, M. Baias, M.A. Haija, D. Shetty, Solvent-Influenced Fragmentations in Free-Standing Three-Dimensional Covalent Organic Framework Membranes for Hydrophobicity Switching, Angew. Chem. Int. Ed. 61(13) (2022) e202200905.

[188] I.C. Kim, J. Jegal, K.H. Lee, Effect of aqueous and organic solutions on the performance of polyamide thin-film-composite nanofiltration membranes, J. Polym. Sci., Part B: Polym. Phys. 40(19) (2002) 2151-2163.

[189] Y. Li, Q. Wu, X. Guo, M. Zhang, B. Chen, G. Wei, X. Li, X. Li, S. Li, L. Ma, Laminated self-standing covalent organic framework membrane with uniformly distributed subnanopores for ionic and molecular sieving, Nat. Commun. 11(1) (2020) 1-9.

[190] N.A. Khan, R. Zhang, H. Wu, J. Shen, J. Yuan, C. Fan, L. Cao, M.A. Olson, Z. Jiang, Solid–vapor interface engineered covalent organic framework membranes for molecular separation, J. Am. Chem. Soc. 142(31) (2020) 13450-13458.

[191] M. Matsumoto, L. Valentino, G.M. Stiehl, H.B. Balch, A.R. Corcos, F. Wang, D.C. Ralph, B.J. Mariñas, W.R. Dichtel, Lewis-acid-catalyzed interfacial polymerization of covalent organic framework films, Chem 4(2) (2018) 308-317.

[192] Y.-Y. Su, X. Yan, Y. Chen, X.-J. Guo, X.-F. Chen, W.-Z. Lang, Facile fabrication of COF-LZU1/PES composite membrane via interfacial polymerization on microfiltration substrate for dye/salt separation, J. Membr. Sci. 618 (2021) 118706.

[193] X. Shi, Z. Zhang, C. Yin, X. Zhang, J. Long, Z. Zhang, Y. Wang, Design of Three-Dimensional Covalent Organic Framework Membranes for Fast and Robust Organic Solvent Nanofiltration, Angew. Chem. Int. Ed. 61(36) (2022) e202207559.

[194] A. He, Z. Jiang, Y. Wu, H. Hussain, J. Rawle, M.E. Briggs, M.A. Little, A.G. Livingston, A.I. Cooper, A smart and responsive crystalline porous organic cage membrane with switchable pore apertures for graded molecular sieving, Nat. Mater. 21(4) (2022) 463-470.

[195] J.K. Holt, H.G. Park, Y. Wang, M. Stadermann, A.B. Artyukhin, C.P. Grigoropoulos, A. Noy, O. Bakajin, Fast mass transport through sub-2-nanometer carbon nanotubes, Science 312(5776) (2006) 1034-1037.

[196] R. Shevate, D.L. Shaffer, Large-Area 2D Covalent Organic Framework Membranes with Tunable Single-Digit Nanopores for Predictable Mass Transport, ACS nano 16(2) (2022) 2407-2418.

[197] K.H. Jensen, A.X. Valente, H.A. Stone, Flow rate through microfilters: Influence of the pore size distribution, hydrodynamic interactions, wall slip, and inertia, Phys. Fluids 26(5) (2014).

[198] J. Buchheim, K.-P. Schlichting, R.M. Wyss, H.G. Park, Assessing the thickness–permeation paradigm in nanoporous membranes, ACS nano 13(1) (2018) 134-142.